

T338



MICROWAVE ELECTRONICS

**DEVELOPMENT OF A NOVEL WIDEBAND CYLINDRICAL
DIELECTRIC RESONATOR ANTENNA**

A THESIS SUBMITTED TO THE



COCHIN UNIVERSITY OF SCIENCE AND TECHNOLOGY

IN PARTIAL FULFILLMENT OF THE REQUIREMENTS FOR

THE DEGREE OF

DOCTOR OF PHILOSOPHY

UNDER THE FACULTY OF TECHNOLOGY

BY

A.V. PRAVEEN KUMAR

MICROWAVE TOMOGRAPHY AND MATERIALS RESEARCH LAB

DEPARTMENT OF ELECTRONICS

COCHIN UNIVERSITY OF SCIENCE AND TECHNOLOGY

COCHIN - 682 022, INDIA

JANUARY 2008

CERTIFICATE

This is to certify that the thesis titled *Development of a Novel Wideband Cylindrical Dielectric Resonator Antenna* is a bona fide record of the research work carried out by *Mr. A.V. Praveen Kumar* under my supervision in the Microwave Tomography and Materials Research Laboratory, Department of Electronics, Cochin University of Science and Technology, Cochin, India and that no part of it has been presented for any other degree.

Cochin-22
17-01-2008



Dr. K.T. Mathew
(Supervising Guide)
Professor Emeritus
Department of Electronics
Cochin University of Science
and Technology, Cochin, India

DECLARATION

I hereby declare that the work presented in the thesis titled *Development of a Novel Wideband Cylindrical Dielectric Resonator Antenna* is based on the original research work carried out by me in the Microwave Tomography and Materials Research Laboratory, Department of Electronics, Cochin University of Science and Technology, Cochin, India, under the guidance of Dr. K. T. Mathew and that no part thereof has been presented for the award of any other degree.

Cochin-22
17-01-2008


A.V. Praveen Kumar

ACKNOWLEDGMENT

I deeply owe to Dr. K. T. Mathew, Professor Emeritus, Dept. of Electronics, Cochin University of Science and Technology, for his lectures which evoked my interest in electromagnetics as an M. Sc. student in the Dept. of Electronics, Cochin University of Science and Technology. Later, as his research student in the Microwave Tomography and Materials Research Laboratory in the same institution, I availed his invaluable guidance, continuous encouragement and ever memorable humanitarian considerations.

I heartfully acknowledge the helps and support provided by Dr. K. Vasudevan, Professor & Head, Dept. of Electronics, Cochin University of Science and Technology, for carrying out the academic and research works. Also the infrastructural facilities arranged by him for the research works are worth mentioning on this instance.

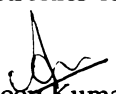
Dr. P. Mohanan, Professor and Dr. C. K. Anandan, Reader, Dept. of Electronics, Cochin University of Science and Technology have always been supporting me and I am deeply indebted to them for all these.

Dr. P. R. S. Pillai, Dr. Tesemma Thomas, Mr. James Kuriyan and Ms. Supriya M. H., Dept. of Electronics are also mentioned here with gratitude.

I am deeply indebted to Dr. Jaimon Yohannan, Research Associate, for being my senior colleague, for his guidance, motivation, assistance and a lot more.

The financial support provided by Kerala State Council for Science, Technology and Environment (KSCSTE) through the research fellowship is gratefully acknowledged here.

Mr. V. Hamsakutty, Mr. Vinu Thomas, Mr. Anil Lonappan, Mr. Anupam R. Chandran, Mr. Robin Augustine, Mr. Ullas G. Kalappura, Mr. Ashkar Ali and Mrs. Deepti Das Krishna, research scholars, Dept. of Electronics are mentioned here for their companionship and timely support. Mr. Gopi Krishna deserves a special mention here for designing the cover pages of this thesis and for his timely helps. I am grateful to Mr. Rohith K. Raj, Mr. Shynu S. V, Mr. Manoj Joseph, Mr. Gijo Augustine, Mr. Deepu V. and Miss. Suma M. N., research scholars, Dept. of Electronics for their help in carrying out the antenna measurements and also for the fruitful research related discussions. Technical discussions with Dr. Sreemoolanathan, VSSC, Thiruvanthapuram were helpful for clarifying a few concepts in my research. I also acknowledge Mr. Rajeev, Mr. Siraj, other teaching & non-teaching staffs, research scholars and project staffs of Dept. of Electronics for extending their assistance to me whenever needed.


A.V. Praveen Kumar

CONTENTS

CHAPTER 1

INTRODUCTION	1
1.1 Wireless and microwaves	1
1.2 Microwave antennas	5
1.3 Industrial, Scientific and Medical applications of microwaves	9
1.4 Microwave materials	9
1.5 Numerical methods in electromagnetics	11
1.6 Commercial electromagnetic simulation tools	16
1.7 Motivation for the research work	17
1.8 Organisation of the thesis	18
References	20

CHAPTER 2

LITERATURE REVIEW	23
2.1 Dielectric resonator antenna – the beginning	23
2.2 Wideband DRAs	24
2.3 Multi-band DRAs	26
2.4 Monopole/Conical beam DRAs	28
2.5 Circularly polarised DRAs	29
2.6 Compact DRAs	31
2.7 FDTD analysis of DRAs	33
Conclusion	35
References	36

CHAPTER 3

DIELECTRIC RESONATOR ANTENNAS – DESIGN, FABRICATION AND CHARACTERISATION	51
3.1 Introduction	51
3.2 Characteristics of a dielectric resonator	52
3.3 Fabrication of the dielectric resonator	58
3.4 Microwave characterisation of the dielectric resonator	62
3.5 Evolution of dielectric resonator as a radiator	68
3.6 Dielectric resonator geometries	69
3.7 Microwave power coupling techniques	71
3.8 Applications of dielectric resonators	75
3.9 Measurement setup	76
3.10 Measurement procedure	85

Conclusion	91
References	92

CHAPTER 4

EXPERIMENTAL ANALYSIS	99
4.1 Broadside mode operation of a cylindrical DRA	99
4.2 Results	100
4.3 Low Q_r / Wideband design: Design 1	103
4.4 Results	103
4.5 Modified design with a horizontal stub: Design 2	110
4.6 Results	110
4.7 Radiation from the antenna feed	128
4.8 Wideband design using other DRs - Results	130
4.9 Radiation efficiency	137
4.10 Wideband design using a different substrate	138
Conclusion	139
References	140

CHAPTER 5

NUMERICAL ANALYSIS USING FINITE DIFFERENCE TIME DOMAIN TECHNIQUE	141
5.1 Introduction	141
5.2 FDTD in electromagnetics	142
5.3 FDTD computations	143
5.4 The Yee algorithm	145
5.5 Cell size and time step	147
5.6 Antenna analysis	148
5.7 Results	164
Conclusion	177
References	178

CHAPTER 6

CONCLUSION	181
-------------------	------------

APPENDIX A

A Cylindrical Dielectric Resonator Antenna for
Dual-Frequency Operation 187

APPENDIX B

A Circularly Polarised Cylindrical Dielectric
Resonator Antenna 191

APPENDIX C

A Wideband Cylindrical Dielectric Resonator Antenna 197

APPENDIX D

A Half-Cylindrical Dielectric Resonator Antenna 201

LIST OF PUBLICATIONS 207

CURRICULUM VITAE 210

Modern age owes to the wireless technology for enjoying abundance of information, communication and entertainment (ICE). *Wireless*, the fastest growing segment of the communication industry is the generic term meaning *without using wires between points*. Many technologies such as wireless sensor networks, automated highways and factories, smart homes and appliances, intelligent transport systems, remote telemedicine etc. have been emerged from research ideas to physical systems. Hence, wireless communication has stolen the attention of the media and imagination of the public. The field of wireless communication was revolutionised with the advancements in microwave systems, comprising of microwave devices and circuits which led to small size and low cost communication systems.

1.1 WIRELESS AND MICROWAVES

The first wireless communication occurred in the pre-industrial age when transmission of information over line-of-sight distances were achieved using smoke signals, torch signaling, flashing mirrors, signal flares, or semaphore flags. Signal combinations were developed to convey complex messages with these basic signals. Observation stations were built on hilltops and along roads to relay these messages over large distances. These early communication networks were replaced first by the telegraph network invented by Samuel Morse, an American painter in 1838 and later by the telephone.

Introduction

The concept of radio began in 1865 with James Clerk Maxwell, a Scottish mathematician and theoretical physicist. Though Maxwell had never seen or experienced radio waves, he successfully anticipated most of the laws that govern their propagation, calculating their speed and noting their resemblance to light waves. These laws were later popularised as Maxwell's equations. Maxwell also showed how radio waves could be reflected, absorbed and focused like the beam from a torch and could change the very nature of the object on which they were focused.

Based on Maxwell's work, Heinrich Hertz, the German physicist invented the oscillator and created radio waves in 1887. In 1894, the British scientist Oliver Lodge succeeded in transmitting wireless signals over 150 yards. But it was with the Italian inventor, Guglielmo Marconi, who in 1895 sent a radio telegraph transmission across the English Channel and in 1901 a transmission across the Atlantic, the new era in wireless communication began. Public use of radio began in 1907 and over the years, the wireless technology, in every aspect became an inevitable part of human life. The term *microwave* seems to have first appeared in a writing by Nello Carrara in the first issue of an Italian journal *Alta Frequenza* in 1932. The term gained acceptance during the Second World War to describe wavelengths less than about 30 cm (1–300 GHz). Table 1 shows the band designations in the microwave frequency range.

Table 1: Microwave frequency band designations

Frequency Band	Designation (old)	Designation (new)
500–1000 MHz	UHF	C
1–2 GHz	L	D
2–3 GHz	S	E
3–4 GHz	S	F
4–6 GHz	C	G
4–8 GHz	C	H
8–10 GHz	X	I
10–12.4 GHz	X	J
12.4–18 GHz	Ku	J
18–20 GHz	K	J
20–26.5 GHz	K	K
26.5–40 GHz	Ka	K

Microwaves were much shorter than those normally used for communications at that time, but were being used in RADAR (Radio Detection and Ranging).

In the early 1920s, Marconi had noted the use of radio waves for detecting targets. The development of RADAR technology in the 1930s accelerated the production of high-power microwave generators and antennas. Microwave antennas tend to be smaller in size, with high directivity. The use of microwaves yields greater modulation bandwidth and these waves can pass through the ionospheric layers unlike the radio waves.

Table 2: Summary of the existing wireless communication services

Service	Frequency Band (MHz)
GSM (Global System for Mobiles)	880–960
GPS (Global Position System)	band1: 1227–1575 band2: 1565–1585
DCS (Digital Communication System)	1710–1880
PCS (Personal Communication System)	1850–1990
UMTS (Universal Mobile Telecommunication System)	1900–2200
IMTS (Improved Mobile Telephone System)	1920–2170
WiBro (Wireless Broadband)	2300–2390
ISM (Industrial Scientific and Medical)	band 1: 2400–2484 band 2: 5150–5350 band 3: 5725–5825
WiMAX (Worldwide Interoperability for Microwave Access)	band 1: 2495–2695 band 2: 3250–3850 band 3: 5250–5850

These features of microwaves enabled the satellite communication and with the launch of the International Telecommunications Satellite (INTELSAT III) – the first commercial geo-synchronous satellite of the US, in 1969, global communication, which was a dream until then became a reality.

At present, several wireless communication services are in use, a summary of which is given in Table 2.

1.2 MICROWAVE ANTENNAS

Antennas are the start and end nodes of a wireless link. Generally, they are metallic structures designed for radiating and receiving electromagnetic energy. According to the IEEE standard definition, an antenna is *a means for radiating or receiving radio waves* [1]. In practice, an antenna acts as a transitional structure or impedance transformer between the guiding device (e.g. waveguide, transmission line etc.) and the free space. In other words, antenna is an electromagnetic transducer.

A conducting wire radiates mainly because of time-varying current or an acceleration or deceleration of charges [1]. If there is no motion of charges in a wire, no radiation takes place, since no flow of current occurs. Radiation will not occur even if charges are moving with uniform velocity along a straight wire. However, charges moving with uniform velocity along a curved or bent wire will produce radiation. If the charge is oscillating with time, then radiation occurs even along a straight wire. In the antenna structure, the charges, accelerated by an external source sets up a charge flow. These charges reaching the discontinuity or transition in the structure get decelerated and their energy is radiated.

1.2.1 EARLY DEVELOPMENTS

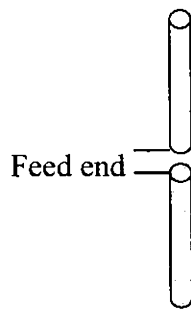
The first practical antenna was constructed by Heinrich Hertz in 1886. He used an *end loaded dipole* as transmitting antenna and a resonant *square loop* as the

Introduction

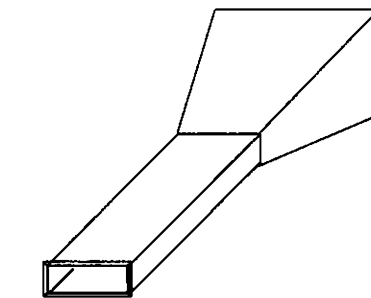
receiving antenna. In 1897, Jagadish Chandra Bose, the eminent Indian scientist constructed the first *horn antenna* for his studies using millimeter waves. He set up the first ever wireless link between his house and his workplace, much earlier than Marconi's transatlantic communication. The invention of microwave tubes during the Second World War launched the modern antenna technology and new antenna elements like aperture antennas, reflector antennas, leaky-wave antennas etc. were introduced.

In addition to metallic antennas, dielectric and dielectric loaded antennas were also proved to be useful candidates at microwave and millimeter wave frequencies. Earlier dielectric antennas were transmission type in nature where the electromagnetic energy is transmitted through structures like *dielectric lens* and *dielectric rods*. Use of dielectric material as part of the antenna started in 1944 with the invention of dielectric lens antennas. These act as secondary antennas, using a dielectric lens to change the cylindrical or spherical waves from a primary antenna into flat plane waves. Dielectric materials having refractive index greater than unity, like lucite or polystyrene are used for the fabrication of these antennas. Later, in 1947, the concept of dielectric rod antennas was introduced. These perform as dielectric waveguides that guide the energy from the feed-end and transforms it into radiated energy at the free-end. Low gain and high side lobe levels are the main characteristics of these antennas. However, loading metallic horn antennas with dielectric rod antennas has been shown to increase the gain and reduce the cross polar and side lobe levels. Dielectric antennas were also being used in the form of a solid or hollow dielectric horn antenna.

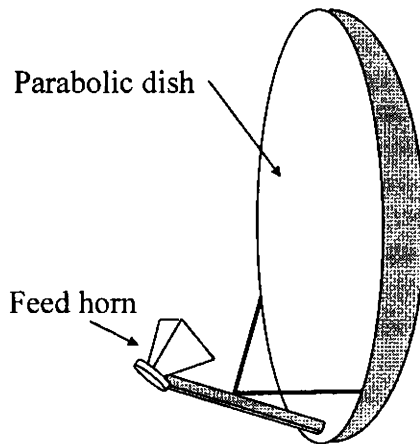
In the early 1950s the *microstrip patch* antenna (MPA) technology was introduced but the major advancements took place only in the 1970s. In the general form, an MPA is a planar metallic area formed on a dielectric substrate of appropriate thickness and material properties. MPAs are of easy fabrication, low-profile, conformable to planar and non-planar surfaces, mechanically robust, compatible with monolithic microwave integrated circuit (MMIC) designs and flexible in designs. However, they suffer from narrow bandwidth, low gain, low radiation efficiency, low power handling capacity and high surface wave losses.



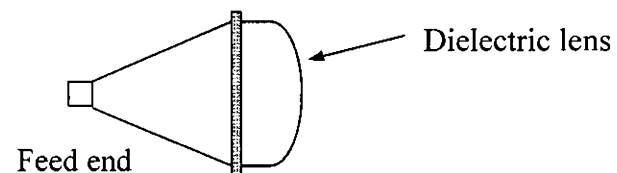
Wire dipole antenna



Metallic horn antenna



Parabolic reflector antenna



Dielectric lens antenna

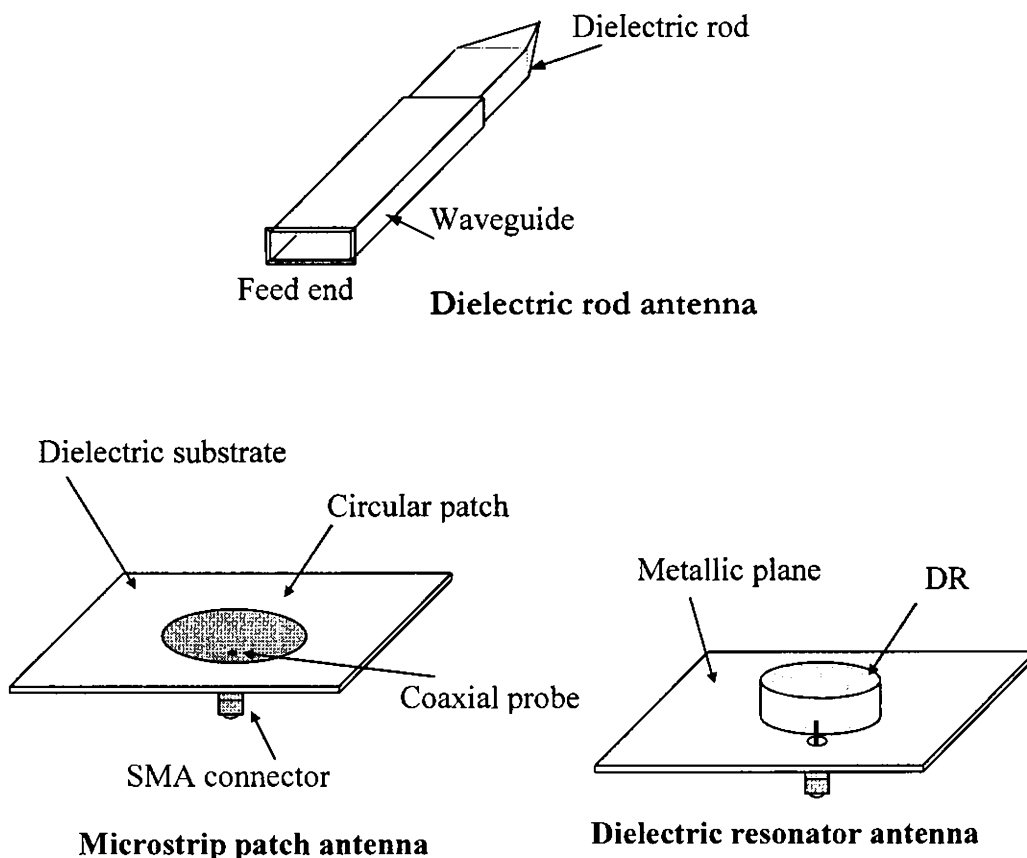


Figure 1: Different types of antennas

1.2.2 LATEST TREND

The antenna community had to wait until the early 1980s for a competitor to the MPA – the *dielectric resonator antenna* (DRA). A DRA contains a known volume of dielectric material or *puck*, called the dielectric resonator (DR), of appropriate characteristics especially a high dielectric constant and low loss. Like the MPA, the DRA also offers the advantages of low-profile, light-weight and flexible excitation schemes. Both antennas are candidates for numerous

applications, either as individual elements or as array elements. But the lack of metallic losses in DRAs assures higher radiation efficiency than MPAs, especially in the millimeter wave applications. Also the possibility of exciting low Q-radiating modes offers a higher operating bandwidth to them than the MPAs. A comparative study between the DRA and MPA [2] shows that the former is a real competitor to MPAs in terms of performance. Various aspects of DR and DRAs are described in detail in Chapter 3. Figure 1 shows the schematic diagrams of different types of antennas discussed above.

1.3 INDUSTRIAL, SCIENTIFIC AND MEDICAL APPLICATIONS OF MICROWAVES

Microwaves are useful not only for the transfer of information, communication and entertainment but also for the transfer of energy. This aspect describes the Industrial, Scientific and Medical (ISM) applications of microwaves [3]. Drying, cooking, irradiation, purification, liquification, sintering, enzymatic inactivation, sterilization, pasteurization, vulcanization etc. using microwaves come under the industrial applications. Microwave diathermy, hyperthermia, medical imaging etc. are the medical applications. Scientific field uses microwaves in particle accelerators, in semiconductor industry and for material characterisation.

1.4 MICROWAVE MATERIALS

Dielectric and magnetic materials are highly applicable in microwave devices, circuits and systems in the form of substrates, dielectric waveguides,

Introduction

resonators, phase shifters, tuning devices, radomes, radiation absorbers etc. Suitability of a material for any microwave application is determined by the microwave properties of that material. Permittivity and permeability are the major quantities representing the electromagnetic properties of a material.

Generally, material characterisation using microwaves falls in three classes namely (1) Resonance methods [4] (2) Guided wave methods [5] and (3) Freespace methods [6] developed in 1946, 1954 and 1986 respectively.

Resonance methods use cavity resonators, of either cylindrical or rectangular cross section. Measurement is done either by length tuning or by frequency tuning. In the former method, the length of the cavity with sample is tuned mechanically for a fixed frequency. From the measured changes of length and Q-factor of the cavity at resonance, the material parameters can be calculated. In the latter method, the cavity length is fixed, while the frequency is swept. Here the shift in the resonant frequency and the cavity-Q are measured.

Guided wave method is based on the two port measurement of the S-parameters (S_{11} or S_{21}) of a filled section of coaxial line or metallic waveguide. Comparing it with the S-parameters of the unfilled line, the dielectric and magnetic properties can be obtained. However this method requires the sample to be accurately machine-worked to perfectly fit the transmission line in order to have accurate measurements.

Freespace methods are based on the optical type measurement, generally suitable at the millimeter wave frequencies. Here also S_{11} or S_{21} is measured with

and without the sample placed between two antennas. This method is contactless as well as nondestructive. Large samples, preferably in the form of sheets are usually needed in order to avoid the edge diffraction effect of waves. The measurement uncertainties are attributed to the sample roughness, deformations and a spherical wavefront instead of the plane wave.

Design, evaluation and analysis of electromagnetic problems involving antennas, cavities, microwave circuits (MIC/MMIC) etc. have been simplified with the popularity of digital computers and computer simulation tools. Analytical or numerical techniques are mainly used for the above purpose. The former makes simplifying assumptions about the geometry of a problem in order to apply a closed-form solution, but is unsuitable for most problems that are quite unpredictable in nature. In such cases, numerical solution is the best alternative and the present day simulation tools are based on these techniques.

1.5 NUMERICAL METHODS IN ELECTROMAGNETICS

The area of computational electromagnetics involves evaluating the fundamental field quantities from the Maxwell's curl equations using numerical methods with a given set of initial or boundary values [7]. These solutions describe propagation of electromagnetic waves and their interactions with a material. There are many different methods which can be used to solve 3-dimensional electromagnetic problems. These methods can be classified into (1) integral equation and differential equation methods or (2) time domain and frequency domain methods. Integral equation method start with the selection of

an appropriate Green's function which is manipulated analytically so that it incorporates the boundary conditions and then a solution is sought. Differential equation methods exploit Maxwell's equations in differential form and require a minimum of analytical manipulation. Time domain methods typically obtain the impulse response (which contains information at all frequencies) and frequency domain methods obtain the transfer function at a specific frequency.

Method of moments [8], Finite element method [9], Finite difference time domain method [10] and Transmission line matrix method [11] are the most commonly used numerical techniques.

1.5.1 METHOD OF MOMENTS

The method of moments (MoM) was developed in the early 1920s by Galerkin and became popular in 1967 with the work of R.F. Harrington. MoM is a method for solving differential or integral equations numerically by transforming them into simultaneous equations. The equation solved by moment method techniques is generally a form of the electric field integral equation or the magnetic field integral equation. The form of the integral equation used determines which types of problems a moment-method technique is best suited to solve. The first step in the moment-method solution process is to expand the unknown quantity as a finite sum of basis (or expansion) functions. A set of linearly independent weighting (or testing) functions are defined and an inner product of each weighting function is formed with both sides of the equation being solved which yields a set of M equations in M unknowns. Now, these unknowns are solved by using the matrix inversion. For getting accurate results, a

large number of basis functions are required and the CPU time required to solve the simultaneous equations also increases. In order to solve this difficulty, many combinations of the basis and testing functions were evolved. In electromagnetic field analysis, MoM solution directly provides the surface current on a conductor or the polarization current in a dielectric. Arbitrary configurations with complex geometries or inhomogeneous dielectrics are difficult to analyze using MoM. They also are not well-suited for analyzing the interior of conductive enclosures or thin plates with wire attachments on both sides.

1.5.2 FINITE ELEMENT METHOD

Development of the finite element method (FEM) began in the middle to late 1950s for airframe and structural analysis and was popularised in the 1960s for use in civil engineering. The first step in finite element analysis is to divide the configuration into a number of small homogeneous pieces or elements. The model contains information about the device geometry, material constants, excitations, and boundary constraints. The corners of the elements are called nodes. The next step is to assign nodes to each element and then choose an interpolation function (polynomials) to represent the variation of the field variable over the element. The degree of the polynomial chosen depends on the number of nodes assigned to the element, the nature and number of unknowns at each node, and certain continuity requirements imposed at the nodes and along the element boundaries. The magnitudes of the field variable and their derivatives may be the unknowns at the nodes. Once the finite element model has been established, next is to determine the matrix equations expressing the properties of

the individual elements and hence to form the matrix equations expressing the behavior of the entire system. Application of the appropriate boundary conditions gives a set of simultaneous equations to be solved to obtain the unknown nodal values of the problem. The major advantage of the finite element method is that the electrical and geometric properties of each element can be defined independently. Thus it is possible to model configurations that have complicated geometries and many arbitrarily shaped dielectric regions in a relatively efficient manner.

1.5.3 FINITE DIFFERENCE TIME DOMAIN METHOD

The finite difference time domain (FDTD) method has been proved to be very versatile in analyzing complex geometries such as antennas and filters, microwave and optical waveguides, interaction between electromagnetic waves and the human body etc. The strength of FDTD lies in the fact that it provides an easy understanding on the temporal physical phenomena. This is because FDTD is a time domain computational technique. In this approach introduced by Yee in the mid 1960s, the computational volume is sampled in space and the field quantities are evaluated at discrete intervals of time. The time step and the spatial increment are so chosen as to avoid aliasing error and instability of the algorithm. Maxwell's curl equations are solved for each cell by a knowledge of the field quantity (E or H) at the previous time step and that (H or E) at the immediately neighboring cell. The field updating process is stopped when the field quantities over the computational volume reaches a steady state. Because of the limited computer resources, the computation volume is terminated by using appropriate

absorbing boundary conditions (ABCs). The primary advantage of FDTD is their great flexibility. The total memory storage and the computational time are directly related to the number of field unknowns in the problem space, which in turn depends on the electrical size of the problem space and the space resolution. Large objects with regions that contain small, complex geometries may require large, dense grids which in turn cause long computational times. Details of the FDTD method are provided in Chapter 5.

1.5.4 TRANSMISSION LINE MATRIX METHOD

The transmission line matrix (TLM) method was proposed by Johns *et al.* in 1971. According to TLM method, a continuous system is replaced by a network or an array of lumped elements. It requires division of the solution region into a rectangular mesh of the transmission lines. The basic TLM cell, known as the symmetrical condensed node is a twelve-port device characterised by a scattering matrix. Each node is connected to its neighboring nodes by a pair of orthogonally polarized transmission lines. Pulse voltages incident to appropriate nodes simulate the excitations. Scattering occur at those nodes that produce reflected voltages become incident voltages to neighboring nodes for the next iteration. Generally, dielectric loading is accomplished by loading nodes with reactive stubs. These stubs are usually half the length of the mesh spacing and have a characteristic impedance appropriate for the amount of loading desired. Absorbing boundaries are easily constructed in TLM meshes by terminating each boundary node transmission line with its characteristic impedance. Similar to FDTD, complex, nonlinear materials are readily modeled in TLM and also impulse responses and

the time-domain behavior of systems are determined explicitly. TLM fails in the same way as FDTD in terms of the computational time that is proportional to the volume and grid size required for accurate solution of the problem.

Each of the above method is well-suited to a particular structure so that when analyzing a complex, hybrid problem, two or more of them can be suitably combined.

1.6 COMMERCIAL ELECTROMAGNETIC SIMULATION TOOLS

Commercial electromagnetic simulators based on the aforesaid numerical methods, such as Zeland IE3D (MoM) [12], Ansoft HFSS (FEM) [13], Flomerics MicroStripes (TLM) [14] and Zeland FIDELITY (FDTD) [12] are popular among engineers and researchers.

HFSS™ is the tool used in this thesis, which is a high-performance FEM based full-wave electromagnetic field simulator for arbitrary 3-D volumetric passive device modeling [13]. It integrates simulation, visualization, solid modeling, and automation in a user-friendly and easy-to-learn environment. HFSS calculates the S, Y and Z-parameters, resonant frequency, Q-factors, near/far fields, smith chart, specific absorption rate (SAR), electric and magnetic fields in vector/magnitude forms and lot other parameters and displays them in high quality 2-D/3-D/animated plots. Integrated optimization/parametric solutions, geometry/material parameterization, sensitivity/statistical analysis etc. are added features of HFSS [15]. Applications of HFSS include package modeling, printed circuit board modeling, EMC/EMI, antennas/mobile communications,

connectors, waveguide, filters and biomedical devices. Basic mesh element of the HFSS is tetrahedron, which allows modeling and solving complex, arbitrary geometries.

1.7 MOTIVATION FOR THE RESEARCH WORK

A dielectric resonator (DR), as evident from the name itself, is a resonant structure. Hence a DR antenna (DRA) can be expected to have a limited bandwidth. Typical impedance bandwidth is of the order of 10 % for a dielectric constant of $\epsilon_r \sim 10$. To be suitable in modern communication applications, a single antenna needs to cover preferably two or more application bands. Thus, investigations on bandwidth enhancement of DRAs have been of main interest for the last several years. Well-known methods being adopted are (1) combining multiple resonators (2) use of additional impedance matching techniques or (3) reducing the radiation Q-factor of the DR. Lowering the Q-factor of a DR is a highly attractive method since it doesn't require additional components as in the other two methods. The Q-factor of a DR is directly proportional to the ratio of the stored energy to the dissipated (radiated) power. In most wideband designs, low-Q is achieved by lowering the amount of energy stored in the DR, by reshaping it into the form of a cylindrical (or rectangular) ring or cup, stacked geometry etc. This however, results in uneasy fabrication efforts compared to the basic geometries like simple cylinder or rectangular.

The work presented in this thesis is focused on the design of a cylindrical DRA for wideband operation, based on the low-Q method. Here, the radiated

power from the DR is increased rather than reducing the stored energy, thereby not demanding any geometrical modifications of the DR. Parameters like return loss, input impedance, radiation pattern, gain and radiation efficiency of the fabricated antennas are measured. High frequency structure simulator (HFSS™) is utilised to ease the design procedure. A numerical model of the DRA was developed using the technical language MATLAB®, based on the FDTD method, to compute the important antenna parameters in order to validate the measured results.

1.8 ORGANISATION OF THE THESIS

The thesis is organised into six chapters, the present chapter being **Chapter 1**.

Chapter 2 reviews the past research works carried out and the major research developments taken place in the area of dielectric resonator antennas.

Chapter 3 deals with the fabrication and characterisation of dielectric resonators. It also describes the evolution of DR antenna, emphasising various DR geometries and excitation techniques studied so far. The antenna design, basic measurement facilities and measurement procedure are also discussed.

Chapter 4 gives the details of the wideband DRA design, simulation and measurement results. Influence of various design parameters on the antenna performance is also discussed.

Chapter 5 explains the computational modeling and analysis of DRAs using the FDTD technique. Computed results are compared with the measured results.

Chapter 6 discusses the conclusions drawn from the work, and the scope for future work.

Four appendices A, B, C and D are included, which deal with the works done by the author in the field of DRAs.

REFERENCES

- [1] C. A. Balanis, Antennas, Chapter 1 - *Antenna Theory, Analysis and Design*, 3rd edition, Wiley, 2002
- [2] R. Chair, A. A. Kishk, K. F. Lee and D. Kajfez, Performance Comparisons Between Dielectric Resonator Antennas and Printed Microstrip Patch Antennas at X-Band, *Microwave Journal*, Vol. 49, pp. 90-104, January 2006
- [3] J. Thuery, *Microwaves: Industrial Scientific and Medical Applications*, Artech House, 1992
- [4] F. Horner, T. A. Taylor, R. Dunsmuir, J. Lamb and W. Jackson, Resonance Methods of Dielectric Measurement at Centimeter Wavelengths, *Journal Inst. Elec. Eng*, Vol. 93, pp. 53-68, January 1946
- [5] A. R. Von Hippel, *Dielectric materials and applications*, Wiley, 1954
- [6] J. Musil and F. Zacek, *Microwave measurements of complex permittivity by free space methods and their applications*, Elsevier, 1986
- [7] T. H. Hubing, Survey of Numerical Electromagnetic Modeling Techniques, available at <http://www.emclab.umn.edu/pdf/TR91-1-001.pdf>
- [8] M. M. Ney, Method of Moments applied as Applied to Electromagnetic Problems, *IEEE Trans. Microwave Theory Tech.*, Vol. 33, pp 972-980, October 1985
- [9] J. Cousty, S. Verdeyme, M. Aubourg and P. Guillon, Finite Elements for Microwave Device Simulation: Application to Microwave Dielectric Resonator Filters, *IEEE Trans. Microwave Theory. Tech*, Vol. 40, pp. 925-932, May 1992

- [10] K. S. Yee, Numerical Solution of Initial Boundary Value Problems Involving Maxwell's Equations in Isotropic Media, IEEE Tran. Antennas Propagat., Vol. 14, 302–307, May 1966
- [11] P. B. Johns and R. L. Beurle, Numerical Solution of Two-Dimensional Scattering Problems Using a Transmission-Line Matrix, Proc. IEEE, Vol. 118, pp. 1203-1209, 1971
- [12] Zeland website URL: <http://www.zeland.com/>
- [13] Ansoft website URL : <http://www.ansoft.com/products/hf/hfss/>
- [14] Flomerics website URL: <http://www.flomerics.com/products/microstripes/>
- [15] User's manual: High Frequency Structure Simulator (HFSS), Ansoft Corporation

This chapter reviews the evolution of dielectric resonator antenna (DRA) technology over the past 24 years from the first cylindrical DRA to the latest magneto DRA. An account of the existing design aspects for achieving wideband operation, multi-band operation, conical radiation patterns, circular polarisation and compactness for DRAs has been presented. Finally, a survey of the FDTD analysis of DRAs has been carried out.

2.1 DIELECTRIC RESONATOR ANTENNA - THE BEGINNING

Dielectric resonator (DR) is a ceramic puck characterised by a definite volume, shape, high dielectric constant and low loss. Radiation from open DRs was realized by Richtmyer in 1939 [1]. But the first theoretical and experimental analysis of a cylindrical DR antenna was carried out by Long *et al.* in 1983 [2]. Since then, DRAs transformed into a fast growing focus among the antenna researchers so that new DR geometries like rectangle, hemispherical, triangular, ring etc. were evolved and studied extensively [3-7], [9].

Kishk *et al.* presented a detailed numerical analysis of a dielectric disk antenna placed on a conducting surface based on surface integral equations to compute the resonant frequency and Q-factor [8]. Later, Mongia *et al.* published a comprehensive review of the modes and radiation properties of various DRs [10]. Accurate closed-form expressions for the resonant frequency, radiation Q-factors and the inside fields of a cylindrical DR were also described in the above work.

A detailed study of the fabrication imperfections of probe fed cylindrical DRAs was reported in [12]. It described that even thin air gaps between the DRA and the ground plane backing or between the probe and the DRA can notably modify its input impedance. An account of the various technological aspects of DRA research at the Communications Research Centre, Ottawa, Canada till year 1998 was published in [13]. This included novel DRA elements and arrays designed for wide bandwidth, compactness, circular polarisation, high gain and active antenna applications. All the existing feed mechanisms such as coaxial probe [2, 8], microstrip [5, 14, 15], coplanar waveguide [16, 17], slot-line [6, 11, 18], waveguide [19-21] etc are compatible with DRAs also.

2.2 WIDEBAND DRAs

In the early 90s when Junker *et al.* noted that the presence of an air gap between a cylindrical DRA and the ground plane, a kind of fabrication imperfection can cause broadening of the resonant curve of the DRA [12, 22]. This was the effect of reduced unloaded or radiation Q-factor (Q_u or Q_r) of the DRA due to an increased effective radiating area. Later, Ittipiboon *et al.* introduced an aperture fed rectangular DRA, with its centre portion removed. This DRA and its image formed a rectangular ring DRA to acquire a 28 % bandwidth [23]. This was motivated by the work of Verplanken *et al.* [24] which reported that the Q_r of certain modes of a cylindrical ring DR is lower than those of the corresponding cylindrical DR.

Use of multiple DRAs as part of the radiator provided an easy and straight forward way of exciting multiple radiating modes, which facilitated multi-band DRA design. By properly choosing the ϵ_r and dimension of individual DRAs, the resonant frequencies corresponding to the modes can be brought closer so as to enhance the bandwidth. Kishk *et al.* showed that a low ϵ_r DRA stacked on top of a high ϵ_r DRA could provide a bandwidth of 25 % [25]. Further studies on stacked DRA designs were carried out both experimentally and numerically [26-28]. Two rectangular DRAs separated by a metallic plate yielded a much broader bandwidth of 76.8 % [29]. Keeping the separate DR elements as a single entity in the above cases was tiresome and was avoided by fabricating single stacked DRA structures in the form of flipped staired pyramid [30], L and T shaped equilateral triangular [31, 32] which offered a maximum bandwidth in excess of 60%.

Special DRA shapes like split-cylinder [33] and conical [34] were also reported to have wide bandwidths. Such geometries however suffered from an increased antenna dimension, especially the DRA height, compared to an individual element. Embedding one DRA within another, in the form of an annular ring solved the above problem where the antenna dimensions are the same as that of the parent DRA [35, 36]. Later, a stacked-embedded DRA design improved the bandwidth to 68 % [37]. A detailed comparative study of the stacked and embedded wideband DRAs with the homogeneous DRA was also carried out [38].

Modification of the feed geometry proved to be a successful method for improving the impedance matching and bandwidth. Luk *et al.* used a vertical metallic stub extended from a microstripline [39] or a coaxial probe [40] enhanced the bandwidth to 19 % and 43 % respectively for cylindrical and rectangular DRAs. In addition, this was also shown to improve the impedance matching. A fork-like tuning stub [41] coupling energy from a microstrip through a circular aperture to the DRA also improved the bandwidth. Feeding techniques like L-shaped [42] and T shaped [43] microstrip also improved the impedance bandwidth. To be suitable with low- Q_r DRA shapes like cylindrical cup, novel feeds like L, hook and J shaped probes [44, 45] were also found suitable in addition to the probe or slot feed. An aperture feed which excites the DRA in addition to radiating itself [46, 47] was capable of producing two merged-resonances causing wide bandwidth operation.

Designs using a simple DRA is also presented for bandwidth enhancement [48, 49], where an aspect ratio greater than unity allowed excitation and merging of dual modes of similar radiation properties.

2.3 MULTI-BAND DRAs

A dual-band antenna can replace two single band antennas of suitable operating bands. The work [25] on stacked wideband DRA was an implication to the design of dual-band DRAs by choosing two DRAs of different dimensions, excited by a single feed.

A wideband antenna unless is operating over a useful application band, is useless. This suggests the design of independent application bands where the antenna radiates only over those bands. Z. Fan *et al.* introduced a slot excited double element rectangular DRA for dual or wideband application [50]. Stacking of two cylindrical DRAs excited by an annular ring excited by a probe has shown a three-band behavior [51]. In [52] dual frequency operation was achieved by incorporating additional DRA in a parent DRA, both cylindrical in shape, so that the volume of the structure remains unchanged. A cylindrical ring DRA is fed with two orthogonal microstrip feeds is reported [53] for dual resonance. This also has the effect of producing orthogonally polarised bands but with similar broadside radiation patterns. Special eye-shaped DRA is also shown to be effective in producing dual radiating modes [54].

By adding an additional radiator to the DRA also, dual-frequency operation can be achieved. This principle is implemented in [55] where a cylindrical DRA and a ring-slot are fed together by a circular slot thereby allowing radiation from the two at respective resonances. If the feed to the DRA is also radiating at a particular frequency, it will be advantageous in this context. This technique is explained in [56] where the rectangular slot-feed to the DRA is made radiating by adjusting its dimensions. The same team introduced another design [57] by using a T-shaped microstrip feed that radiates in addition to exciting the DRA. A ceramic loaded annular ring monopole antenna is found to resonate in the dual WLAN bands [58]. The principle is nothing but the inherent size reduction property of high ϵ_r DRs to be explained in the next chapter.

2.4 MONOPOLE/CONICAL BEAM DRAs

Most of the DRA designs discussed above produce broadside radiation where the pattern maximum occurs at the broadside or zenith ($\theta = 90^\circ$). This is achieved by properly exciting the magnetic dipole mode of the DRA [10]. But certain other applications like high performance radio local area network (HIPERLAN) [59] and vehicular communications need monopole-like or conical radiation patterns with the maximum radiation located at the elevation, most commonly in the range $30^\circ < \theta < 60^\circ$ and a null at the zenith. This is done in most cases by exciting the monopole-like modes of the DR with a center-fed coaxial probe.

In 1993, Kishk *et al.* noted that in the case of a probe fed cylindrical DRA, when the probe is positioned close to the centre of the antenna, a monopole TM_{0m8} mode is also excited with the same strength as the broadside HEM_{1m8} [8]. Mongia *et al.* demonstrated that a cylindrical ring DRA excited in the TM_{018} mode can produce near monopole-like radiation [9] over a small bandwidth. Later, this design was modified for size reduction and good mode separation by incorporating a metallic cylinder concentrically inside the ring DRA [61].

A combination of microstrip line and probe was used for exciting monopole mode of a cylindrical ring DRA [62]. Conical beam operation is also realized by the use of two cylindrical DRAs fed by a single probe [63]. This has the effect of a 35 % increase in antenna gain but a 0.7 % decrease in bandwidth compared to a single element.

Recently, Guha *et al.* showed that by using an array of four cylindrical DRAs surrounding a coaxial probe [64] a wider impedance bandwidth of 29 % can be achieved. Special geometries like stacked triangular DRA [32] or half-hemispherical DRAs [65] have also been reported to provide wideband conical-beam operation. Ultra wideband (UWB) monopole mode DRA was employed [66] by combining a quarter wave monopole and a ring DRA. The design details of the above antenna were given by Guha *et al.* [67]. In this, three resonances, resulted from the bare monopole, the ring DRA and the DR loaded effective monopole, combine to provide the UWB response.

2.5 CIRCULARLY POLARISED DRAs

Generally a DRA produce linearly polarised radiation when operated on any of the fundamental modes. The ability of DRAs to support multiple radiating modes simultaneously is well exploited in the design of circularly polarised (CP) antennas.

CP antenna design using DRAs started with [68] that propose a rectangular DR with two diagonally opposite corners truncated similar to the design implemented with rectangular patch antennas to produce CP. Later, Mongia *et al.* [69] produced CP by exciting the two orthogonal HE_{118} modes of a cylindrical ring DRA using a 3dB quadrature coupler. In [70] the orthogonal HE_{118} modes of a cylindrical dielectric resonator are excited by two probes fed in phase quadrature by a microstrip line. In [71] a slot-coupled rectangular DRA is used where the DRA position is adjusted 45° with respect to the slot to produce

CP from a cylindrical DRA over a bandwidth of 3.4 % and beam width of 110°. A cross-slot of unequal slot lengths in the ground plane of a microstrip line has been used [72] to produce CP from a cylindrical DRA over 3.91 % of bandwidth. A design with dual conformal strip feed [73] can also produce CP but over a wide bandwidth of 20 %. A cylindrical DRA is fed by a perturbed annular ring slot [74] to achieve an axial ratio bandwidth of 3.4 %. In this design, a backing cavity of hemispherical shape was used to block the back lobe radiation. Effect of parasitic conducting strip loading on the impedance characteristics of a cylindrical DRA has been studied [75] where CP is achieved by varying the angular position of the parasitic strip relative to the conformal feed.

A design similar to [71] is reported [76] where a parasitic strip is diagonally attached on top of a rectangular DRA and is fed through an aperture. The design is also shown suitable for a four element sequentially rotation DRA array. CP from a hemispherical DRA [77] has been produced by using an approach discussed in [75]. In the design, a slot aperture is used for coupling and the dual orthogonal modes for CP are generated by using a grounded parasitic strip attached to the DRA surface. A new geometry DRA in the form of a stair has been fed by a slot is also reported [78] for generating CP over a 10.6 % bandwidth. In [79] a 4.7 % axial ratio bandwidth has been achieved by using a cross-slot of unequal slot lengths for coupling to a cylindrical DRA. A cylindrical DRA with longitudinal slots of limited depth has been shown to produce CP over a 4 % bandwidth [80]. Compact CP design [88] is also reported using a half-split cylindrical DRA.

2.6 COMPACT DRAs

Design of compact DRAs has always been a challenging issue among antenna researchers. By using a high dielectric constant material, a small volume of DR can resonate at a lower resonant frequency as per Eq. (3.8) in Chapter 3. But this will increase the Q-factor and hence a lower bandwidth with the resonant frequency becoming highly temperature dependent [81].

Mongia *et al.* noted the existence of one or more planes of symmetry for isolated DR shapes. While this plane of symmetry serves as an electric wall for certain modes, it behaves as a magnetic wall for the other modes. This was the motivation for the work [82] where a half-split cylindrical DR was placed over a metallic ground plane, which was at the plane of symmetry ($\Phi = 0$). The particular antenna configuration was excited in TE_{018} (magnetic dipole) mode with a low Q_r thereby facilitating more than 8 % bandwidth. A similar split-DR with a slot feed was used for allowing integration with MICs [83]. Numerical analysis of a half-split cylindrical DRA on a ground plane excited in the low Q_r modes - TE_{018} and HEM_{128} is presented [84] using a method of moment approach for the coupling between a body of revolution (BOR) geometry and a non-BOR geometry.

M. T. K. Tam *et al.* reported a half-volume design [85] for the broadside modes of a cylindrical (HEM_{118}) and rectangular (TE_{118}) DRAs based on the aforesaid approach. But they used an additional metallic plate attached to the plane of symmetry of the DR which was oriented in the orthogonal plane of that in [82]. In the same paper, the above team put forward the thread for further size

reduction of the DRA by using a metallic post instead of the metallic plate. The FDTD analysis of the above design was carried out by Steven G. O'Keefe [86] additionally demonstrating a higher directivity for the half-volume DRA.

But a revolutionizing low-volume design was presented by Tam *et al.* in 1999 using circular and annular sector DRAs [87] where a 75 % reduction in volume is demonstrated. The design used different inner to outer radius ratios, sector angles and boundary conditions (metallic, open or mixed) for the sector DRA. A modification of the structure in [85] was used to produce circular polarisation [88]. Kishk *et al.* exhaustively studied the bandwidth enhancement property of split-cylinder DRAs numerically and experimentally [89]. Use of partial vertical and horizontal metallizations on a rectangular DRA has been proposed to reduce the overall dimensions of the DRA to be used at WLAN applications [90]. A thorough analysis of a reduced volume rectangular DRA based on the above principle has been presented [98] using FDTD and measurements.

For the enhanced miniaturization and a simultaneous increase in bandwidth, the new DRA trend was introduced by K. Sarabandi *et al.* utilising magneto-dielectric materials having both relative permittivity and permeability greater than unity [91]. The dimensions of the DR is thus proportional to the square root of the product of ϵ_r and μ_r . Recently, the experimental and theoretical aspects of a probe fed cylindrical DRA based on a magnetodielectric material have been studied [92].

2.7 FDTD ANALYSIS OF DRAs

Modeling of DR based structures using the FDTD method has been a major research area during the past few years. In 1991, Navarro *et al.* [93] theoretically obtained the resonant frequencies of a cylindrical DR enclosed in a metallic cavity, using FDTD combined with discrete Fourier transform (DFT). Kaneda *et al.* presented a modified contour-path integral FDTD [94] to analyze a shielded cylindrical DR, while maintaining the rectangular cells. In [95] Dey *et al.* discuss a conformal FDTD approach for cylindrical DR modeling based on weighted volume effective dielectric constant. An alternate and easier method was proposed by Yu *et al.* [96] based on a linear average effective dielectric constant concept. A fast and more accurate computation of resonant properties of axisymmetric DRs using FDTD was presented by Shi *et al.*, by using the Pade'-DFT technique [97].

Much works on the modeling and analysis of DRAs using FDTD are not available in the literature. In 1994, Shum *et al.* studied the effect of an air gap between the DRA and the ground plane on the resonant frequency of a coaxial fed cylindrical ring DRA using FDTD [98]. The FDTD coordinate system used was cylindrical (r , Φ and z) because of the axial symmetry of the structure. An absorbing boundary condition (ABC) based on a parabolic interpolation was used to terminate the boundary and was placed at distances three times the dimensions of the DRA. A Gaussian-modulated sinusoidal pulse was used for excitation. The same team also calculated the resonant frequency of an aperture coupled rectangular DRA using FDTD [99].

Later, Esselle [100] obtained the radiation patterns of an aperture coupled low-profile rectangular DRA using FDTD. Mur's ABC was used to terminate the volume. The patterns were obtained by using the equivalence principle over a fictitious surface enclosing the DRA.

But the fundamental probe fed cylindrical DRA structure of [2] was analyzed by S. M. Shum *et al* in 1995 [101] and in detail in 1998 [102]. Since their DRA is offset-fed, unlike the approach in [98], the rectangular coordinate system was used with the second order Liao's ABC at the boundary. Various feed models like Voltage gap, Jenson and Magnetic-frill for the coaxial probe have been compared. A simple Gaussian pulse excited the system. The equivalent sources just above the DRA are calculated by using the Goertzel algorithm and the far-fields are computed by using the fundamental integral equations, The effect of fabrication imperfections of the DRA on its performance has also been simulated.

The effect of ground plane thickness and coupling slot geometries on the field coupling to a cylindrical DRA has been studied using FDTD by Guo *et al.* [103]. Four layer perfectly matched layer (PML) ABC has been used. In 2002, O'Keefe *et al.* studied the radiation characteristics of reduced-size DRAs [86] using FDTD. A four layer PML ABC with parabolic conductivity profile and Gaussian pulse excitation were used. In the work, they also computed the return loss, in-field and radiation patterns of HEM_{118} , TE_{118} and TE_{018} modes.

Conformal FDTD was used by Farahat *et al.* [104] to analyze a circularly polarised cross-shaped DRA. It is shown that the conformal mapping offers a 2:1

advantage over staircase mapping, without compromising accuracy. FDTD was used to design the dimensions of a rectangular DRA, feed and parasitic elements for the design of a CP DRA [88]. Sernouchkina *et al.* presented a detailed analysis of the modes in a rectangular DRA fed by a microstrip line [105]. Additionally, the influence of DR dimensions, feed location and surface metallization on the modes was also presented. In [106], Lan *et al.* used FDTD to design both the radiator and feed sections a combination antenna using a rectangular DRA and an inverted L-plate. A complemented dispersive boundary condition has been implemented in order to reduce the computational domain.

CONCLUSION

In this chapter, a detailed survey of the past works carried out in the field of dielectric resonator antennas was presented. Various aspects such as bandwidth enhancement, multi-band operation, circular polarisation, pattern modification and compact designs for DRAs were discussed. In view of the above, a new DRA design for wideband conical beam applications is proposed and studied in the forthcoming chapters.

REFERENCES

- [1] R. D. Richtmyer, Dielectric Resonators, J. Appl. Phys, Vol. 10, pp. 391-398, June 1939
- [2] S. A. Long, M. McAllister and L. C. Shen, The Resonant Cylindrical Dielectric Cavity Antenna, IEEE Tran. Antennas Propagat., Vol. 31, pp. 406-412, 1983
- [3] M. W. McAllister, S. A. Long and G. L. Conway, Rectangular Dielectric Resonator Antenna, Electro. Lett., Vol. 19, pp. 219-220, March 1983
- [4] M. W. McAllister and S. A. Long, Resonant Hemispherical Dielectric Antenna, Electro. Lett., Vol.20, pp. 657-659, 1984
- [5] R. A. Kranenburg and S. A. Long, Microstrip Transmission Line Excitation of Dielectric Resonator Antennas, Electro. Lett., Vol. 24, pp. 1156-1157, January 1988
- [6] J. T. H St. Martin, Y. M. M. Antar, A. A. Kishk, A. Ittipiboon and M. Cuhaci, Dielectric Resonator Antenna using Aperture Coupling, Electro. Lett., Vol.26, pp. 2015-2016, 1990
- [7] A. Ittipiboon, R. K. Mongia, Y .M. M. Antar, P. Bhartia and M. Cuhaci, Aperture Fed Rectangular and Triangular Dipole Antennas Dielectric Resonators for Use as Magnetic Dipole Antennas, Electro. Lett., Vol.29, pp. 2001-2002, 1993
- [8] A. A. Kishk, M. R. Zunoubi and D. Kajfez, A Numerical Study of a Dielectric Disk Antenna above a Grounded Dielectric Substrate, IEEE Trans. on Antennas Propagat., Vol.41, pp. 813-821, June 1993

- [9] R. K. Mongia, A. Ittipiboon, P. Bhartia and M. Cuhaci, Electric-Monopole Antenna Using a Dielectric Ring Resonator, *Electron. Lett.*, Vol. 29, pp. 1530-1531, August 1993
- [10] R. K. Mongia and P. Bhartia, Dielectric Resonator Antennas-A Review and General Design Relations for Resonant Frequency and Bandwidth, *Inter. Journal of Microwave and Millimeter-Wave Computer-aided Engineering*, Vol. 4, pp. 230-247, July 1994
- [11] K. W. Leung, K. Y. A. Lai, K. M. Luk and D. Lin, Input Impedance of Aperture Coupled Hemispherical Dielectric Resonator Antenna, *Electron. Lett.*, Vol. 29, pp. 1165-1167., June 1993
- [12] G. P. Junker, A. A. Kishk, A. W. Glisson, and D. Kajfez, Effect of Fabrication Imperfections from Ground-Plane-Backed Dielectric Resonator Antennas, *IEEE Antennas Propagat. Mag.*, Vol. 37, pp. 40-47, February 1995
- [13] A. Petosa, A. Ittipiboon, Y. M. M. Antar, D. Roscoe and M. Cuhaci, Recent Advances in Dielectric Resonator Antenna Technology, *IEEE Antennas Propagat. Magazine*, Vol. 40, pp. 35-48, June 1998
- [14] K. W. Leung, K. Y. Chow, K. M. Luk and E. K. N. Yung, Low-Profile Circular Disk DR Antenna of Very High Permittivity Excited by a Microstrip Line, *Electron. Lett.*, Vol. 33, pp. 1004-1005, June 1997
- [15] A. Petosa, R. K. Mongia, A. Ittipiboon, and J. S. Wight, Design of Microstrip-Fed Series Array of Dielectric Resonator Antennas, *Electron. Lett.*, Vol. 31, pp. 1306-1307, August 1995

- [16] R. A. Kranenburg, S. A. Long and J. T. Williams, Coplanar Waveguide Excitation of Dielectric Resonator Antennas, *IEEE Trans. on Antennas Propagat.*, Vol. 39, pp. 119-122 , January 1990
- [17] M. S. Al Salameh, Y. M. M. Antar and G. Séguin, Coplanar-Waveguide-Fed Slot-Coupled Rectangular Dielectric Resonator Antenna, *IEEE Trans. on Antennas Propagat.*, Vol.50, pp. 1415-1419 , January 2002
- [18] A. A. Kishk, A. Ittipiboon, Y. M. M. Antar and M. Cuhaci, Slot Excitation of Dielectric Disk Radiator, *IEEE Trans. on Antennas Propagat.*, Vol. 43, pp. 198-201 , February 1995
- [19] K. W. Leung, H. Y. Lo, K. K. So, and K. M. Luk, High-Permittivity Dielectric Resonator Antenna Excited by a Rectangular Waveguide, *Microwave and Opt. Tech. Letters.*, Vol. 34, pp. 157–158 , August 2002
- [20] I. A. Eshrah, A. A. Kishk, A. B. Yakovlev, and A. W. Glisson, Excitation of Dielectric Resonator Antennas by a Waveguide Probe: Modeling Technique and Wide-Band Design, *IEEE Trans. on Antennas Propagat.*, Vol. 53, pp. 1028-1037, March 2005
- [21] I. A. Eshrah, A. A. Kishk, A. B. Yakovlev, and A. W. Glisson, Theory and Implementation of Dielectric Resonator Antenna Excited by a Waveguide Slot, *IEEE Trans. on Antennas Propagat.*, Vol. 53, pp. 483-494, January 2005
- [22] G. P. Junker, A. A. Kishk, A. W. Glisson, and D. Kajfez, Effect of An Air Gap on Cylindrical Dielectric Resonator Antenna Operating in TM_{01} Mode, *Electron Lett.*, Vol. 30, pp. 97-98 , January 1994

- [23] A. Ittipiboon, A. Petosa, D. Roscoe, and M. Cuhaci, An Investigation of a Novel Broadband Dielectric Resonator Antenna, IEEE Inter. Symp. on Ant. and Prop. Digest, Baltimore, MA, pp. 2038-2041, July 1996
- [24] M. Verplanken and J. V. Bladel, The Electric-Dipole Resonances of Ring Resonators of Very High Permittivity, IEEE Trans. Microwave Theory Tech., Vol. MTT, Vol. 24, pp.108-112, February 1976
- [25] A. A. Kishk, B. Ahn, D. Kajfez, Broadband Stacked Dielectric Resonator Antennas, Electron. Lett, Vol. 25, pp. 1232-1233, August 1989
- [26] K. W. Leung, K.M. Luk, K. Y. Cho and E. K. N. Yung, Bandwidth Enhancement of Dielectric Resonator Antenna by Loading a Low-Profile Dielectric Disk of Very High Permittivity, Electron. Lett, Vol. 33, pp. 725-726, April 1997
- [27] A. A. Kishk, X. Zhang, A. W. Glisson and D. Kajfez, Numerical Analysis of Stacked Dielectric Resonator Antennas Excited by a Coaxial Probe for Wideband Applications, IEEE Trans. on Antennas Propag, Vol. 51, pp. 1996-2006, December 2003
- [28] A. Rashidian, K. Forooraghi and M. T. Aligodarz, Investigations On Two-Segment Dielectric Resonator Antennas, Microwave and Opt. Tech. Letters., Vol. 45, pp. 533-537, June.2005
- [29] P. Rezaei, M. Hakkak, and K. Forooraghi, Design of Wide-Band Dielectric Resonator Antenna with a Two-Segment Structure, Progress In Electromagnetics Research, PIER 66, pp. 111–124, 2006

- [30] R. Chair, A. A. Kishk, K. F. Lee and C. E. Smith, Wideband Flipped Staired Pyramid Dielectric Resonator Antennas, *Electron. Lett*, Vol. 40, pp.581-582, May 2004
- [31] T. A. Denidni, Q. Rao, and A. R. Sebak, Broadband L-Shaped Dielectric Resonator Antenna, *IEEE Anten. Wireless Propagat. Lett.*, Vol.5, pp. 453-454, 2006
- [32] Q. Rao, T. A. Denidni and A. R. Sebak, Broadband Compact Stacked T-Shaped DRA with Equilateral-Triangle Cross Sections, *IEEE Microwave Wireless Comp. Lett*, Vol. 16,pp. 7-9, January 2006
- [33] A. A. Kishk , A. W. Glisson and G. P. Junkar, Bandwidth Enhancement for Split Cylindrical Dielectric Resonator Antennas, *Progress In Electromagnetics Research*, PIER 33, pp. 97–118, 2001
- [34] A. A. Kishk, Y. Yin, and A. W. Glisson, Conical Dielectric Resonator Antennas for Wide-Band applications, *IEEE Trans. on Antennas Propagat.*, Vol. 50, pp. 469-474, April 2002
- [35] A. Sangiovanni, J. Y. Dauvignac and C. Pichot, Embedded Dielectric Resonator Antenna for Bandwidth Enhancement, *Electron. Lett*, Vol. 33, pp.2090-2091,December 1997
- [36] A. A Kishk, Experimental Study of Broadband Embedded Dielectric Resonator Antennas Excited by a narrow slot, *IEEE Anten. and Wireless Propagat. Lett.*, Vol. 4, pp. 79-81, 2005
- [37] Y. F. Ruan, Y. X. Guo, and X. Q. Shi, Wideband Dielectric Resonator Antenna, *Microwave and Opt. Tech. Letters.*, Vol. 48, pp. 222-226, February 2006

- [38] A. G. Walsh, C. S. De Young, and S. A. Long, An Investigation of Stacked and Embedded Cylindrical Dielectric Resonator Antennas, *IEEE Anten. Wireless Propagat. Lett.*, Vol. 5, pp. 130-133, 2006
- [39] K. M. Luk, M. T. Lee, K. W. Leung and E. K. N. Yung, Technique for Improving Coupling Between Microstripline and Dielectric Resonator Antenna, *Electron. Lett.*, Vol. 35, pp. 357-358, March 1999
- [40] Bin Li and K.W. Leung, Strip-Fed Rectangular Dielectric Resonator Antennas with/without a Parasitic Patch, *IEEE Trans. on Antennas Propagat.*, 53, pp. 469-474, July 2005
- [41] K. W. Leung and C. K. Leung, Wideband Dielectric Resonator Antenna Excited by Cavity-Backed Circular Aperture with Microstrip Tuning Fork, *Electron. Lett.*, Vo 39, pp. 1033-1035, July 2003
- [42] S. K. Menon, B. Lethakumary, P. Mohanan, P. V. Bijumon and M. T. Sebastian, Wideband Cylindrical Dielectric Resonator Antenna Excited Using an L-Strip Feed, *Microwave and Opt. Tech. Letters.*, Vol. 42, pp.293-294, August 2004
- [43] P. V. Bijumon, S. K. Menon, M. N. Suma, M. T. Sebastian and P. Mohanan Broadband Cylindrical Dielectric Resonator Antenna Excited by Modified Microstripline, *Electron. Lett.*, Vol. 41, pp. 385-387, March 2005
- [44] A. A. Kishk, R. Chair, and K. F. Lee, Broadband Dielectric Resonator Antennas Excited by L-Shaped Probe, *IEEE Trans. on Antennas Propagat.*, Vol. 54, pp. 2182-2189, August 2006

- [45] R. Chair, A. A. Kishk and K-F. Lee, Hook- and 3-D J-shaped Probe Excited Dielectric Resonator Antenna for Dual Polarization Application, IEE Proc.-Microw. Antennas Propagat., Vol. 153, pp. 277-281, June 2006
- [46] A. Buerkle, K. Sarabandi, and H. Mosallaei, Compact Slot and Dielectric Resonator Antenna with Dual-Resonance, Broadband Characteristics, IEEE Trans. on Antennas Propagat. , Vol. 53 , pp. 1020-1027, March 2005
- [47] Y. Gao, B. L. Ooi, W. B. Ewe, and A. P. Popov, A Compact Wideband Hybrid Dielectric Resonator Antenna, IEEE Microwave Wireless Comp. Lett, Vol. 16, pp. 227-229, April 2006
- [48] R. Chair, A. A. Kishk and K -F. Lee, Wideband Simple Cylindrical Dielectric Resonator Antennas, IEEE Microwave Wireless Comp. Lett, Vol. 15, pp. 241-243, April 2005
- [49] C. S. De Young and S. A. Long, Wideband Cylindrical and Rectangular Dielectric Resonator Antennas, IEEE Anten. Wireless Propagat. Lett., Vol. 5, pp. 426-429, 2006
- [50] Z. Fan and Y. M. M. Antar, Slot coupled DR Antenna for Dual-frequency Operation, IEEE Trans. on Antennas Propagat., Vol. 45, pp. 306-308 , February 1997
- [51] A. Sangiovanni, J. Y. Dauvignac, Ch. Pichot , Stacked Dielectric Resonator Antenna for Multifrequency Operation, Microwave and Opt. Tech. Letters., Vol. 18, pp. 303-306, July 1998
- [52] C. Nannini, J. M. Ribero, J. Y. Dauvignac, and C. Pichot, A Dual-frequency Dielectric Resonator Antenna, Microwave and Opt. Tech. Letters., Vol. 38, pp. 9-10, July 2003

- [53] Y. Sung, C. S. Ahn and Y. S. Kim, Microstripline Fed Dual-frequency Dielectric Resonator Antenna, *Microwave and Opt. Tech. Letters.*, Vol. 42, pp. 388-390, September 2004
- [54] B. Paul, S. Mridula, P. Mohanan, P. V. Bijumon, and M. T. Sebastian, A Compact Very High Permittivity Dielectric-Eye Resonator Antenna for Multiband Wireless Applications, *Microwave and Opt. Tech. Letters.*, Vol. 43, pp. 118-121, October 2004
- [55] T. A. Denidni and Q. Rao, Hybrid Dielectric Resonator Antennas with Radiating Slot for Dual-Frequency Operation, *IEEE Anten. Wireless Propagat. Lett.*, Vol.3, pp. 321-323 , 2004
- [56] Q. Rao, T. A. Denidni and A. R. Sebak, A Hybrid Resonator Antenna Suitable for Wireless Communication Applications at 1.9 and 2.45 GHz, *IEEE Anten. Wireless Propagat. Lett.*, Vol.4, pp. 341-342 , 2005
- [57] Q. Rao, T. A. Denidni, A. R. Sebak and R. H. Johnston, Compact Independent Dual-Band Hybrid Resonator Antenna with Multi-functional Beams, *IEEE Anten. Wireless Propagat. Lett.*, Vol.5, pp. 239-242 , 2006
- [58] Y. F. Lin, C. H. Lin, H. M. Chen and P. S. Hall, A Miniature Dielectric Loaded Monopole Antenna for 2.4/5 GHz WLAN Applications, *IEEE Microwave Wireless Comp. Lett.*, Vol.16, pp. 591-593, November 2006
- [59] Y. J. Guo, A. Paez, R. A. Sadeghzadeh and S. K. Barton, A Circular Patch Antenna for Radio LANs, *IEEE Trans. on Antennas Propagat.*, Vol. 45, pp. 177-178 , February 1997

- [60] Zhi Ning Chen, K. Hirasawa, Kwok-Wa Leung, and Kwai-Man Luk, A New Inverted F Antenna with a Ring Dielectric Resonator, IEEE Trans. on Vehicular Tech., Vol. 48, pp. 1029-1032, May 1999
- [61] R. K. Mongia, Small Electric Monopole Mode Dielectric Resonator Antenna, Electron. Lett, Vol. 32, pp. 947-949, May 1996
- [62] K. W. Leung, K.Y. Chow, M. K. Luk and E. K. N. Yung, Excitation of Dielectric Resonator Antenna Using Soldered Through Probe, Electron. Lett, Vol. 33, pp. 349-350, February 1997
- [63] G. Drossos, Z. Wu and L. E. Davis, Two-element Endfire Dielectric Resonator Antenna Array, Electron. Lett, Vol. 32, pp. 618-619, March 1996
- [64] D. Guha and Y. M. M. Antar, Four-Element Cylindrical Dielectric Resonator Antenna for Wideband Monopole-Like Radiation, IEEE Trans. on Antennas Propagat. , Vol. 54, pp. 2657-2662, September 2006
- [65] D. Guha, and Y. M. M. Antar, New Half-Hemispherical Dielectric Resonator Antenna for Broadband Monopole-Type Radiation, IEEE Trans. on Antennas Propagat., Vol. 54, pp. 3621-3628 , December 2006
- [66] M. Lapierre, Y. M. M. Antar, A. Ittipiboon, and A. Petosa,, Ultra Wideband Monopole/Dielectric Resonator Antenna, IEEE Microwave Wireless Comp. Lett, Vol. 15, pp. 7-9, January 2005
- [67] D. Guha, Y. M. M. Antar, A. Ittipiboon, A. Petosa, and David Lee, Improved Design Guidelines for the Ultra Wideband Monopole-Dielectric Resonator Antenna, IEEE Anten. Wireless Propagat. Lett., Vol. 5, pp. 373-376 , 2006

- [68] M. Haneishi and H. Takazawa, Broadband Circularly Polarized Planar Array Composed of a Pair of Dielectric Resonator Antennas, *Electron. Lett.*, Vol. 21, pp. 437-438, May 1985
- [69] R. K. Mongia, A. Ittipiboon, M. Cuhaci and D. Roscoe, Circularly Polarized Dielectric Resonator Antenna, *Electron. Lett.*, Vol. 30, pp. 1361-1362, August 1994
- [70] G. Drossos, Z. Wu and L. E. Davis, Circular Polarized Cylindrical Dielectric Resonator Antenna, *Electron. Lett.*, Vol. 32, pp. 281-283, February 1996
- [71] K. P. Esselle, Circularly Polarized Higher-order Rectangular Dielectric-Resonator Antenna, *Electron. Lett.*, Vol. 32, pp. 150-151, February 1996
- [72] Chih-Yu Huang, Jian-Yi Wu and Kin-Lu Wong, Cross-slot Coupled Microstrip Antenna and Dielectric Resonator Antenna for Circular Polarization, *IEEE Trans. on Antennas Propagat.*, Vol. 47, pp. 605-609, April 1999
- [73] K. W. Leung, W. C. Wong, K. M. Luk and E. K. N. Yung, Circularly Polarized Dielectric Resonator Antenna excited by Dual Conformal Strips, *Electron. Lett.*, Vol. 36, pp. 484-486, March 2000
- [74] K. W. Leung and S. K. Mok, Circularly Polarized Dielectric Resonator Antenna Excited by Perturbed Annular Slot with Backing Cavity, *Electron. Lett.*, Vol. 37, pp. 934-936, July 2001
- [75] R. T. Long, R. J. Dorris, S. A. Long, M. A. Khayat and J. T. Williams, Use of Parasitic Strip to Produce Circular Polarization and Increased Bandwidth for Cylindrical Dielectric Resonator Antenna, *Electron. Lett.*, Vol. 37, pp. 406-408, March 2001

- [76] A. Laisne, R. Gillard and G. Piton, Circularly Polarized Dielectric Resonator Antenna with Metallic Strip, *Electron. Lett*, Vol. 38, pp.106-107, January 2002
- [77] K. W. Leung and H. K. Ng, The Slot-Coupled Hemispherical Dielectric Resonator Antenna with a Parasitic Patch: Applications to the Circularly Polarized Antenna and Wide-Band Antenna, *IEEE Trans. on Antennas Propagat.*, Vol. 53, pp. 1762-1769, May 2005
- [78] R. Chair, S. L. S. Yang, A. A. Kishk, K. F. Lee, and K. M. Luk, Aperture Fed Wideband Circularly Polarized Rectangular Stair Shaped Dielectric Resonator Antenna, *IEEE Trans. on Antennas Propagat.*, Vol. 54, pp. 1350-1352, April 2006
- [79] G. Almpanis, C. Fumeaux, and R. Vahldieck, Offset Cross-Slot-Coupled Dielectric Resonator Antenna for Circular Polarization, *IEEE Microwave Wireless Comp. Lett*, Vol. 16, pp. 461-463, August 2006
- [80] L. C. Y. Chu, D. Guha and Y. M. M. Antar, Comb-shaped Circularly Polarized Dielectric Resonator Antenna, *Electron. Lett*. Vol. 42, pp. 785- 787, July 2006
- [81] R. D. Murch and M. T. K. Tam, Chapter 7 -Compact Circular Sector And Annular Sector Dielectric Resonator Antennas for Wireless Communication Handsets in *Dielectric Resonator Antennas*, Edited by K.M. Luk, K. W. Leung, Research Studies Press Ltd., 2003
- [82] R. K. Mongia, Half Split Dielectric Resonator Placed on a Metallic Plane for Antenna Applications, *Electron. Lett*, Vol. 25, pp. 463-464, March1989

- [83] R. K. Mongia, A. Ittipiboon, Y. M. M. Antar, P. Bhartia and M. Cuhaci, A Half-Split Cylindrical Dielectric Resonator Antenna Using Slot Coupling, *IEEE Microwave Guid. wave Lett.*, Vol. 3, pp. 38-39, 1993
- [84] G. P. Junker, A. A. Kishk and A. W. Glisson, Numerical Analysis Of Dielectric Resonator Antennas Excited in Quasi-TE Modes, *Electron. Lett.*, Vol. 29, pp. 1810-1811, October 1993
- [85] M. T. K. Tam and R. D. Murch, Half Volume Dielectric Resonator Antenna Designs, *Electron. Lett.*, Vol. 33, pp. 1914-1916, November 1997
- [86] S. G. O' Keefe, Simon P. Kingsley and S. Saario, "FDTD Simulation of Radiation Characteristics of Half-Volume HEM and TE-mode Dielectric Resonator Antennas", *IEEE Trans. on Antennas Propagat.*, Vol. 50, pp. 175-179, February 2002
- [87] M. T. K. Tam and R. D. Murch, Compact Circular Sector and Annular Sector Dielectric Resonator Antennas, *IEEE Trans. on Antennas Propagat.*, Vol. 47, pp. 837-842, May 1999
- [88] M. T. K. Tam and Ross D. Murch, "Circularly Polarized Circular Sector Dielectric Resonator Antenna, *IEEE Trans. on Antennas Propagat.*, Vol. 48, pp. 126-128, January 2000
- [89] A. A. Kishk, A. W. Glisson and G. P. Junker, Bandwidth Enhancement for Split Cylindrical Dielectric Resonator Antenna, *Progress In Electromagnetics Research, PIER* 33, pp. 97-118, 2001
- [90] D. Cormos, A. Laisne, R. Gillard, F. Le Bolzer and C. Nicolas, Compact Dielectric Resonator Antenna for WLAN applications, *Electron. Lett.*, Vol. 39, pp. 588-590, April 2003

- [91] A. Buerkle and K. Sarabandi, A wide-Band, Circularly Polarized, Magnetodielectric Resonator Antenna, *IEEE Trans. on Antennas Propagat.*, Vol. 53, pp. 3436- 3442, November 2005
- [92] H. H. B. Rocha F. N. A. Freire, R. C. S. Costa, R. S. T. M. Sohn, G. Orjubin, C. Junqueira , T. Cordaro , A. S. B. Sombra, Dielectric resonator Antenna: Operation of the magnetodielectric composites $\text{Cr}_{0.75}\text{Fe}_{1.25}\text{O}_3$ (CRFO)/ $\text{Fe}_{0.5}\text{Cu}_{0.75}\text{Ti}_{0.75}\text{O}_3$ (FCTO), *Microwave and Opt. Tech. Letters.*, Vol. 49, pp. 409 - 413, December 2007
- [93] A. Navarro, M. J. Nunez and E. Martin, Study of TE_0 and TM_0 Modes In Dielectric Resonators by a Finite Difference Time Domain Coupled with the Discrete Fourier Transform, *IEEE Trans. Microwave Theory Tech.*, Vol. 39, pp. 14–17, January 1991
- [94] N. Kaneda, B. Houshm, and T. Itoh, FDTD Analysis of Dielectric Resonators with Curved Surfaces, *IEEE Trans. Microwave Theory Tech.*, vol. 45, pp. 1645–1649, September 1997
- [95] S. Dey and Raj Mittra, A Conformal Finite-Difference Time-Domain Technique for Modeling Cylindrical Dielectric Resonators, *IEEE Trans. Microwave Theory Tech.*, Vol. 47, pp. 1737-1739, September 1999
- [96] W. Yu, and Raj Mittra, A Conformal Finite Difference Time Domain Technique for Modeling Curved Dielectric Surfaces, *IEEE Microwave Wireless Comp. Lett*, Vol. 11, pp. 25-27, January 2001
- [97] S. Shi, L. Yang, and D. W. Prather, Numerical Study of Axisymmetric Dielectric Resonators, *IEEE Trans. Microwave Theory Tech.*, Vol. 49, pp. 1614-1619, September 2001

- [98] S. M. Shum and K. M. Luk, Characteristics of Dielectric Ring Resonator Antenna with an Air Gap, *Electro. Lett.*, Vol.30, pp. 277-278, February 1994
- [99] S. M. Shum and K. M. Luk, Analysis of Aperture Coupled Rectangular Dielectric Resonator Antenna, *Electro. Lett.*, Vol.30, pp. 1726-1727, October 1994
- [100] K. P. Esselle, A Low-Profile Rectangular Dielectric Resonator Antenna, *IEEE Trans. on Antennas Propagat.*, Vol.44, pp. 1296-1297, September 1996
- [101] S. M. Shum and K. M. Luk, FDTD Analysis of a Probe Fed Cylindrical Dielectric Resonator Antenna Operating in the Fundamental Broadside Mode, *Electro. Lett.*, Vol.31, pp. 1210-1212, July 1995
- [102] S. M. Shum and K. M. Luk, FDTD Analysis of Probe-fed Cylindrical Dielectric Resonator Antenna, *IEEE Trans. on Antennas Propagat.*, Vol.46, pp. 325-333, March 1998
- [103] Y. X. Guo , K.M. Luk and K.W Leung, Characteristics of Aperture Coupled Cylindrical Dielectric Resonator Antennas on a thick Ground Plane, *Proc. IEE Microwave Ant. Propagat.*, Vol. 146, December 1999, pp. 439-442
- [104] N. Farahat, W. Yu, R. Mittra and T. Koleck, Cross-Shaped Dielectric Resonator Antenna Analysis using Conformal Finite Difference Time Domain Method, *Electro. Lett.*, Vol.37, pp. 1105-1106, August 2001
- [105] E. Semouchkina, G. Semouchkin, R. Mittra and W. Cao, Finite-Difference Time-Domain Simulation of Resonant Modes of Rectangular Dielectric Resonators, *Microwave and Opt. Tech. Letters.*, Vol. 36, pp.160-164, February 2003

- [106] K. Lan, S. K. Chaudhury and S. Safavi-Naeini, Design and Analysis of A Combination Antenna with Rectangular Dielectric Resonator and inverted L-Plate, IEEE Trans. on Antennas Propag, Vol. 53, pp. 495-501, January 2005

This chapter highlights the general characteristics, fabrication methodology and characterisation of dielectric resonators to be useful as dielectric resonator antennas. First part of the chapter is dedicated to various aspects of the DR and the DR antenna design. Basic measurement facilities used and the measurement details of the important antenna characteristics – return loss, impedance, radiation pattern, gain and radiation efficiency are explained in the second part.

3.1 INTRODUCTION

Dielectric resonators (DRs) emerged as a substitute to resonant metallic cavities and waveguides in microwave devices like filters, oscillators, and phase shifters. As for metallic cavities, the resonant frequency of a DR is determined by its dimensions and also exhibits high Q-factors. But the main difference between the two is that the wavelength in dielectric materials (non-magnetic) is reduced by a factor of one over square root of the dielectric constant, ϵ_r which is much higher than unity for most materials. Hence the resonator can be made smaller by choosing a high dielectric constant material. However, the reactive power stored in a DR during resonance is not strictly confined inside the resonator. The leakage fields from the resonator can be used for energy coupling, frequency tuning or radiation purpose. To be useful in practical applications, a DR basically requires a high dielectric constant ($\epsilon_r > 20$) for promising size reduction, high Q-factor ($Q_d >$

5000), hence a low dielectric loss factor ($\tan \delta \sim (Q_d)^{-1}$) for a stable resonance and a near-zero temperature coefficient of resonant frequency ($\tau_f \sim 0$ ppm/°C) for temperature stability and hence better circuit performance. The implication is nothing but a drastic reduction in the total cost of the RF system.

3.2 CHARACTERISTICS OF A DIELECTRIC RESONATOR

3.2.1 Dielectric Constant

An important property of a dielectric material is its ability to support an electric field while dissipating minimal energy in the form of heat. The lower the dielectric loss (the proportion of energy lost as heat), the more effective a dielectric material is. Another consideration is the dielectric constant, the extent to which a substance concentrates the lines of electric flux within.

The net flux density D can be expressed as

$$D = \epsilon_o E + P \quad (3.1)$$

where E is the electric field intensity and P is the net polarization given by

$$P = \epsilon_o \chi E \quad (3.2)$$

where χ is the electric susceptibility. Now Eq. (3.1) becomes

$$\begin{aligned} D &= \epsilon_o (1 + \chi) E \\ &= \epsilon_o \epsilon_r E \end{aligned} \quad (3.3)$$

Now we define the relative permittivity as,

$$\epsilon_r = 1 + \chi \quad (3.4)$$

in the complex form,

$$\varepsilon_r = \varepsilon_r' - j\varepsilon_r'' \quad (3.5)$$

In Eq. (3.5), the real part is called the dielectric constant and the ratio $\frac{\varepsilon_r''}{\varepsilon_r'} = \tan \delta$

is called the dissipation or loss tangent of the dielectric.

Hence it is clear that the dielectric properties of a DR are resulted from the phenomenon called dielectric polarisation that occurs when electromagnetic fields pass through them. A DR at rest contains randomly oriented permanent electric dipoles. When an external electric field is applied, the dipoles align themselves in the direction of the field and the material is said to be polarised. For most materials P vanishes as E vanishes.

3.2.2 Resonant Mode and Resonant Frequency

The modes of a cylindrical DR, placed on a large ground plane as shown in Figure 1, can be classified into three distinct types: Transverse Electric (TE), Transverse Magnetic (TM) and hybrid (HE and EH) [1]. TE with respect to the Z -axis means that electric field component in Z -direction is zero. In other words, two components of electric field perpendicular to Z -axis exist in the structure. TM mode also can be explained in a similar way. These two modes are axisymmetric, meaning that they have no azimuthal (Φ) variation. But the hybrid modes are Φ dependant, which can further be subdivided into hybrid electric (HE) and hybrid magnetic (EH) modes. In the HE mode, the E_z dominates the H_z and all other field components are expressed in terms of E_z only. Reverse is applied for the EH

mode. In general, a mode can be expressed as the mode name subscripted by three indices n , p and m which respectively represent the field variation along azimuthal, radial and the axial directions.

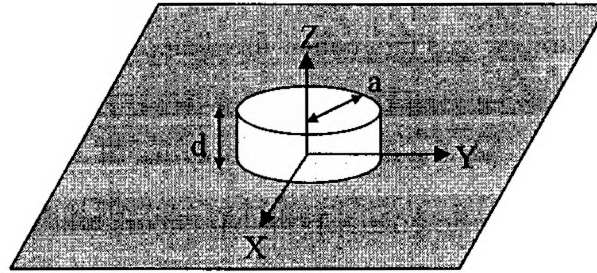


Figure 1: A cylindrical DR over a ground plane at $z = 0$

In electromagnetics, metallic waveguides and resonators are modeled using perfect electric conductor (PEC) wall or electric wall, for which the tangential component of electric field vanishes or $n \times E = 0$, n being the normal to the conductor surface. Similarly, a cylindrical dielectric resonator is modeled using the cavity model where the magnetic wall boundary is imposed on the outer surfaces of the DR, to predict its in-field distribution and the resonant frequency. According to the magnetic wall condition, $n \times H = 0$ at all the outer surfaces of the resonator with normal n , on imposing which we get the axial field components as

$$\begin{aligned}
 \text{TE: } H_z^{npm} &= J_n \left(\frac{X_{np}}{a} r \right) \left\{ \begin{array}{l} \sin(n\Phi) \\ \cos(n\Phi) \end{array} \right\} \sin \left[\frac{(2m+1)\pi}{2d} z \right] \\
 \text{TM: } E_z^{npm} &= J_n \left(\frac{X'_{np}}{a} r \right) \left\{ \begin{array}{l} \sin(n\Phi) \\ \cos(n\Phi) \end{array} \right\} \cos \left[\frac{(2m+1)\pi}{2d} z \right] \quad (3.6) \\
 n &= 1, 2, 3, \dots \quad p = 1, 2, 3, \dots \quad m = 0, 1, 2, \dots
 \end{aligned}$$

Other field components can be evaluated by substituting Eq. (3.6) in the Maxwell's equations.

The resonant frequency for the $TE_{n\text{p}m}$ / $TM_{n\text{p}m}$ mode is determined by solving the separation equation,

$$k_r^2 + k_z^2 = \epsilon_r \left(\frac{2\pi f}{c} \right)^2 \quad (3.7)$$

and is given by,

$$f_{n\text{p}m} = \frac{c}{2\pi a \sqrt{\epsilon_r}} \sqrt{\left\{ \begin{matrix} X_{np}^2 \\ X'_{np}{}^2 \end{matrix} \right\} + \left[\frac{\pi a}{2d} (2m+1) \right]^2} \quad (3.8)$$

where X_{np} is the root of the characteristic equation $J_n(X_{np}) = 0$, X'_{np} is the root of $J'_n(X'_{np}) = 0$, J_n is the n^{th} order Bessel function of the first kind and J'_n is the first derivative of J_n . Also k_r and k_z are the radial and axial wave numbers respectively. Top view of the field distributions for some modes of a cylindrical DR are shown in Figure 2 [2].

3.2.3 Quality Factor

Quality or Q-factor is a measure of the ability of the DR to store microwave energy with minimal signal loss. The inherent Q-factor of a DR solely depends on the loss factor of the dielectric material. But in practical applications, the resonator is always associated with metallic parts, in the form of shields or ground planes. In general, the loaded Q-factor of a resonant cavity can be defined as the ratio of the stored energy to the dissipated power [3].

$$Q_L = \frac{\text{Stored Energy}}{\text{Dissipated Power}} = \frac{2\omega_0 E_s}{P_{dis}} \quad (3.9)$$

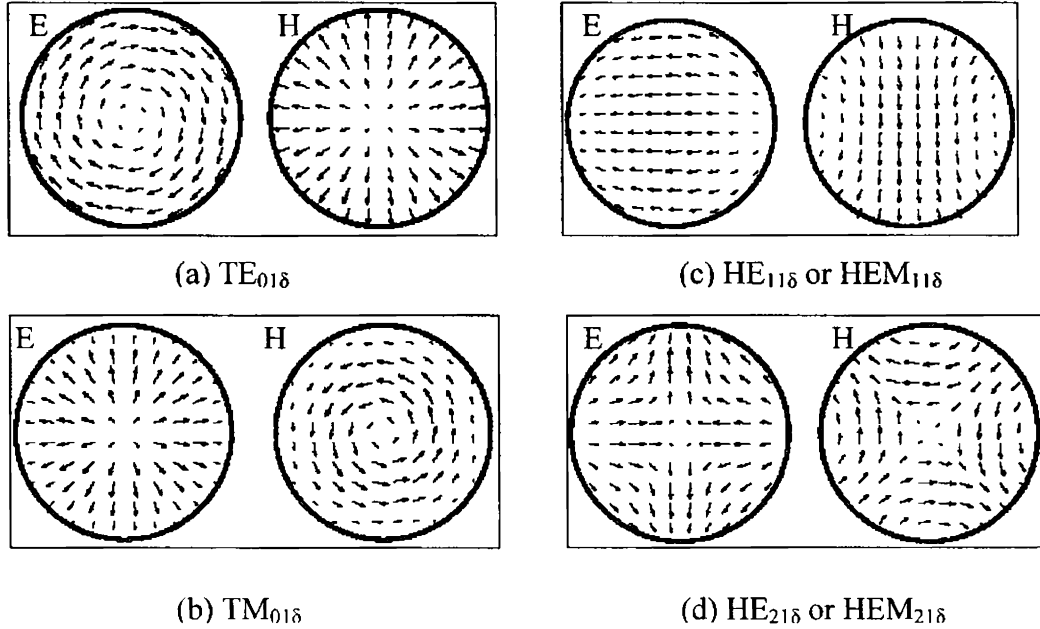


Figure 2: Field distributions inside a cylindrical DR

The denominator term, which is the total power dissipation, can occur in many ways such as conductor losses (P_c), dielectric losses (P_d), radiation losses (P_r) and/or losses in the external circuits (P_{ext}).

$$\text{i.e.;} \quad P_{dis} = P_c + P_d + P_r + P_{ext} \quad (3.10)$$

Combining equations (3.9) and (3.10), we get

$$\frac{1}{Q_L} = \frac{1}{Q_c} + \frac{1}{Q_d} + \frac{1}{Q_r} + \frac{1}{Q_{ext}} \quad (3.11)$$

where the unloaded Q is given by

$$\frac{1}{Q_u} = \frac{1}{Q_c} + \frac{1}{Q_d} + \frac{1}{Q_r} \quad (3.12)$$

Here, $1/Q_d = \tan \delta$ is the loss tangent of the dielectric. However, the material loss of the dielectric itself can be divided into intrinsic and extrinsic losses. Intrinsic losses depend on the material composition which causes the microwave energy to be converted into thermal energy. But the extrinsic losses result from the microstructural irregularities like porosity, grain boundaries, impurities etc. Theoretically, the Q-factor linearly decreases with frequency; therefore usually the product Qf in GHz is specified for DRs.

Another aspect of the Q-factor is that, if a DR of negligible losses is placed in the unshielded/open environment, then $Q_u = Q_r$, the radiation Q-factor for the lower order modes. For a given excited mode, the Q_r depends on the aspect ratio and the dielectric constant for a cylindrical DR. Then the bandwidth of the DR over which its voltage standing wave ratio ($VSWR$) conforms to a specified value S can be expressed as [1]

$$BW = \frac{S-1}{Q_u \sqrt{S}} \times 100 \% \quad (3.13)$$

3.3 FABRICATION OF THE DIELECTRIC RESONATOR

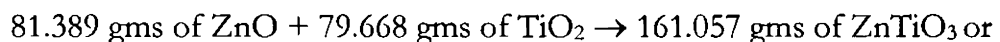
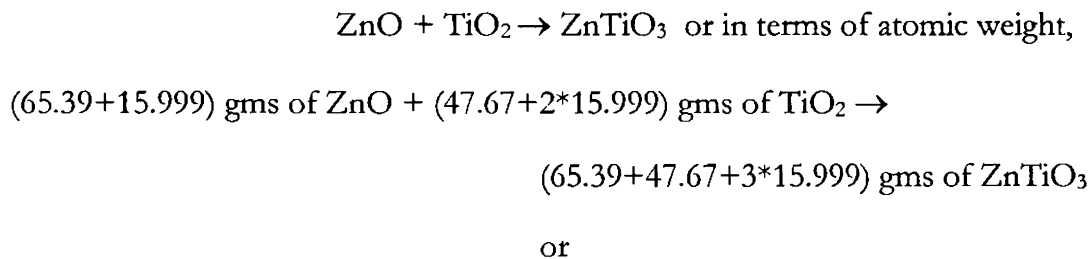
The DR is fabricated through the mixed oxide or solid state route that involves the following steps [4]:

- (i) Weighing, Mixing and Grinding
- (ii) Calcination
- (iii) Shaping
- (iv) Sintering
- (v) Finishing

3.3.1 Weighing, Mixing and Grinding

Here, the preparation of DR sample from the zinc titanate (ZnTiO_3) material is explained as an example.

We start with the chemical equation of the compound ZnTiO_3 which is



Thus 1 gm of ZnTiO_3 requires 0.5053 gm of ZnO and 0.4947 gm of TiO_2 .
Thus the stoichiometric quantities of ZnO and TiO_2 required for forming N gms

of ZnTiO_3 as the final product can be calculated easily. The next step is mixing for eliminating aggregates and/or reducing the particle size. The weighed powders of ZnO and TiO_2 are mixed well with 100–200 % of distilled water for about 12 hrs in a ball-mill, which is a motor-driven barrel that rotates on its axis. The barrel is filled with the ceramic beads made of alumina or silicon carbide that act as the grinding medium for the powder. The creamy mixer is then dried in an oven at 100°C .

3.3.2 Calcination

Calcination is the final step in the production of high purity ceramic powder. This process is the endothermic decomposition reaction in which, any salt such as carbonate or hydroxide decomposes, leaving an oxide as a solid product liberating a gas. This process causes the interaction of the constituents by the interdiffusion of their ions and so reduces the extent of the diffusion that must occur during sintering in order to obtain a homogeneous body. The calcinations conditions are the important factors determining the shrinkage of the pellet during the sintering. The surfaces of the container in immediate contact with the powder must not react with it in order to avoid contamination. The thermal conductivity of powdered materials is always low, so that a sufficiently uniform temperature can only be obtained through a depth of a few centimeters when the period at maximum temperature is 1 or 2 hours in most cases. If compound formation is to occur during calcinating or firing, the matter of neighboring particles must inter-diffuse and the time taken to complete the process is proportional to the square of the particle size. The process will clearly

be considerably slower if the particles consist of aggregates of crystals. In the present case, the well mixed powder is taken in an alumina crucible and calcined at a temperature of 1000°C in an electric muffle furnace, for 2 hrs.

3.3.3 Pellet Shaping

The calcined powder is crushed well in an agate mortar (bowl made of agate, a hard material) to form finer powder and mixed well with 4 % of Polyvinyl alcohol (PVA), an organic binder. Mixing with the binder provides sufficient strength to resist the disintegrating effect of small stress on the shaped pellets prior to sintering. Dry pressing is carried out in a die with movable top and bottom punches, made of hardened steel. The free-flowing powder is filled in the die-cavity, which is cylindrical in shape and the top punch is descended to compress the powder to a predetermined volume, to a set pressure (75–300 MPa). The green density of the pellet is not greatly increased by applying pressures exceeding 74–150 MPa. Highly polished die and punch surfaces ensure reduced wall friction. Shapes with a uniform section in the pressing direction are the easiest to produce by dry pressing. The time taken on an automatic pressing machine varies from 0.2 second for pieces of diameter around 1 mm to 5 seconds for large complex shapes.

3.3.4 Sintering

Sintering converts the compacted powder in to a denser structure of crystallites jointed to one another by grain boundaries, at elevated temperatures

below the melting point of the material. The energetic basis for sintering lies in the reduction of surface energy by transferring matter from the interior of grains along the grain boundaries to adjacent pores, which are eventually filled. Usually the powder compact is heated at fixed sintering temperature, held at this temperature for the required time and finally cooled at the room temperature. This is referred to as isothermal sintering. The organic binder is burnt out at the lower sintering temperatures. In the present case, isothermal sintering of the pellets, placed on an alumina slab at 1150°C for 5 hours is carried out after which it is cooled to the room temperature.

3.3.5 Finishing

Tool wear during the pellet shaping and variations in shrinkage during sintering and drying contribute to 1–2 % variation in the dimensions of the sintered pellets. For experimental studies, especially in the case of material characterisation, the surfaces of the pellets need to be as smooth as possible. Usually it is done by grinding and lapping the dense sample with tools consisting of silicon carbide, diamond powder etc. Here we use a silicon carbide water proof paper for finishing the pellets. A photograph of the final DR samples is shown in Figure 3.

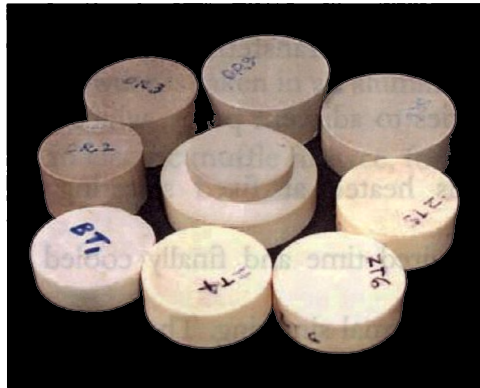


Figure 3: Photograph of the fabricated DRs

3.4 MICROWAVE CHARACTERISATION OF THE DIELECTRIC RESONATOR

Dielectric constant (ϵ_r), quality factor (Q) and temperature coefficient of resonant frequency (τ_f) of the fabricated DRs are measured using the microwave techniques as described below.

3.4.1 Hakki-Coleman Method for Measuring Dielectric Constant

There are numerous conventional methods for measuring the complex permittivity of materials at microwave frequencies. Depending on the operating principle, these methods can be classified as (1) methods that depend on the standing wave field within the dielectric (2) methods that depend on transmitted waves or waves reflected from the dielectric (3) resonance methods [5]. Cavity perturbation techniques [5, 6] are suitable for the measurement of materials available in a small volume but the measurement accuracy is limited to dielectric

constants less than 10. This is because, the sample volume required will be too small to be handled, when measuring high dielectric constant materials. For ceramic samples of higher dielectric constant, Hakki and Coleman method [7] employing a dielectric post resonator is used.

The measurement setup consists of a cylindrical DR puck sandwiched between two conducting plates (of infinite extent theoretically) to form a parallel-plate DR. This method restricts most of the stored energy to the dielectric and allows the experimental configuration to closely approximate the analytical model. If the distance between the two parallel plates is smaller than one-half wavelength, then the excited TE_{011} mode will not radiate [8] and the sides of the resonator can be left open for providing the coaxial coupling probes. The maximum dimensions of the specimen are set by the diameter of the shorting plates while the minimum dimensions by the diameter of the coupling probes. The measurement setup is shown in Figure 4.

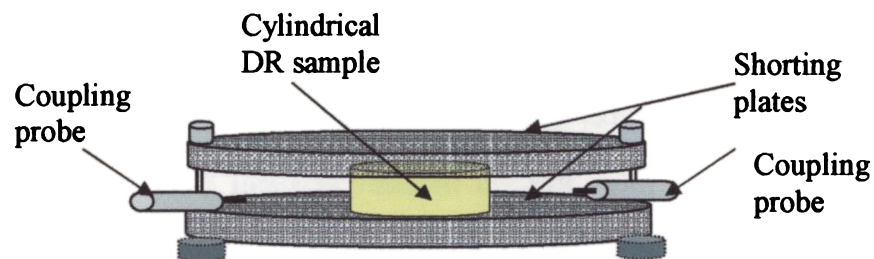


Figure 4: Hakki-Coleman setup for dielectric constant` measurement

Consider a cylindrical DR of length L and radius a placed in the above setup. Then the characteristic equation for the TE_{0pm} mode of operation is given by

$$\alpha \frac{J_0(\alpha)}{J_1(\alpha)} = -\beta \frac{K_0(\beta)}{K_1(\beta)} \quad (3.14)$$

where $J_0(\alpha)$ and $J_1(\alpha)$ are the Bessel functions of the first kind of orders zero and one respectively, while $K_0(\beta)$ and $K_1(\beta)$ are the modified Bessel functions of the second kind of orders zero and one respectively. Also

$$\alpha_p = \frac{2\pi a}{\lambda_0} \sqrt{\varepsilon_r - \left(\frac{m\lambda_0}{2L}\right)^2} \quad (3.15)$$

$$\beta_m = \frac{2\pi a}{\lambda_0} \sqrt{\left(\frac{m\lambda_0}{2L}\right)^2 - 1}, \quad (3.16)$$

where m is the axial wave number. Thus the dielectric constant can be obtained from (3.15) and (3.16) as

$$\varepsilon_r = 1.0 + \left(\frac{c}{2\pi af_0}\right)^2 (\alpha_1^2 + \beta_1^2) \quad (3.17)$$

where $c = 3 \times 10^8$ m/s, α_1 and β_1 are the first roots of the characteristics equation with $p = m = 1$ corresponding to the TE_{011} mode.

3.4.2 Khanna-Garault Method for Measuring the Quality factor

Q-measurement methods are mainly of two types – time domain and frequency domain. Time domain methods mainly depend on measuring the decay time constant τ of the stored energy in the cavity at frequency f_0 , and by using the following relation [9].

$$Q_L = 2\pi f_0 \tau \quad (3.18)$$

Three useful frequency domain techniques are the reflection method, the reactance method and the transmission method. Transmission method is the simplest and requires a transmission type cavity as shown in Figure 5.

As shown in the figure, a microstrip transmission line is fabricated on a dielectric substrate. The DR is coupled magnetically to the transmission line by placing it nearby it on the substrate. The lateral distance d between the strip and the centre of the DR determines the coupling coefficient between them. By properly adjusting d , the TE_{018} mode can be excited in the DR. In order to suppress the radiation losses, the entire structure is covered with a metallic cavity of dimensions at least 3 times the size of the DR, with a top plate that can be moved up and down using a tuning screw. The shielding conditions affect the resonant frequency and the Q of the DR.

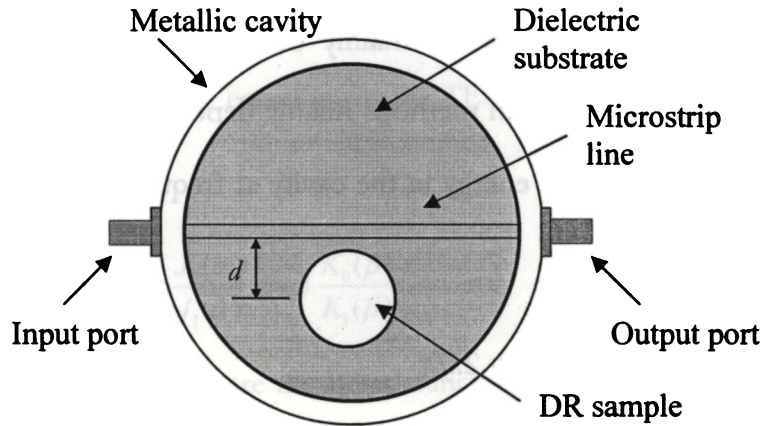


Figure 5: Top view of the Khanna-Garault cavity setup for Q-factor measurement

The degree of coupling is adjusted such that the transmission loss is of the order > -30 dB. By bringing the top metal plate close to the DR, the TE_{018} resonant frequency can be observed increasing, indicating that the stored energy in the cavity is predominantly magnetic. If the stored energy is electric, then a decrease in the resonant peak is expected. From the transmission coefficient ($|S_{21}|$) plot around the resonant frequency, the loaded and unloaded Q-factors- Q_L and Q_u respectively can be calculated as illustrated in Figure 6 [10].

In the figure, the parameter x is given by

$$x=3-10.\log\left(1+10^{-0.1|S_{21}|_{dB}}\right) \quad (3.19)$$

Now the Q-factor is given by the well-known equation, $Q = \frac{f_0}{\Delta f}$

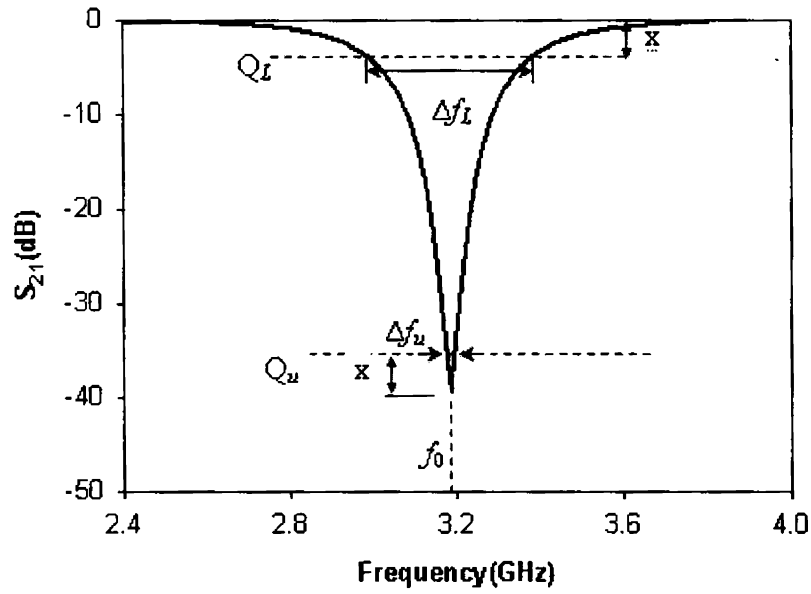


Figure 6: Measurement of Q-factor from the S_{21} curve

For the measurement of the temperature coefficient of resonant frequency (τ_f) for a particular mode of the DR, any of the above two cavity arrangements (Fig. 4 and 5) can be used. In the present study, the Khanna-Garault transmission cavity, exciting the TE_{018} mode of the DR is employed. The arrangement is mounted in a temperature stable furnace with outlets for signal coupling. The temperature is varied from 29°C to 70°C in steps, and the corresponding resonant frequencies are noted. Now τ_f can be calculated as given by Eq. (3.20).

$$\tau_f = \frac{1}{f_0} \cdot \frac{\Delta f_0}{\Delta T} \quad 10^{-6}/^\circ\text{C} \text{ or parts per million or ppm}/^\circ\text{C} \quad (3.20)$$

Here ' f_0 ' is the TE_{018} frequency at room temperature (29°C) and ' Δf_0 ' is the frequency shift for a temperature gradient of ' ΔT '. The value of τ_f can either be

positive or negative depending on whether the frequency is increasing or decreasing respectively with the rise in temperature.

3.5 EVOLUTION OF DIELECTRIC RESONATOR AS A RADIATOR

Dielectric resonators were initially used in filters, oscillators and phase shifters, by virtue of their high Q-factor, where the energy lost is negligible compared to the energy stored. When used as an antenna, the DR is designed for a low Q-factor, so that the energy lost through radiation is much higher than the energy stored. This is achieved by the proper selection of dielectric constant, geometry and feeding method for the DR placed in an open or unshielded environment. The first antenna using a cylindrical DR was successfully devised by S.A. Long *et al.* in 1983 [11], exciting the low-Q TM_{110} mode of the DR using a coaxial probe. The antenna was then named as a dielectric cavity antenna which was later transformed into the most popular name *dielectric resonator antenna* (DRA). Since the DR is fully dielectric, no threat of ohmic loss and this results in higher radiation efficiency when used as antenna. Since they are 3-D devices, when the frequency of operation is halved, the antenna becomes eight times bulkier. This puts a limit to the application of bare-DRs at frequencies below L-band, where DR loaded patch antennas are being used as a compromise.

Merits of DRAs [26]

- A wide variety of geometries can be used allowing design flexibility
- High radiation efficiency

- Compatibility with numerous existing feeding mechanisms
- Good control over size and impedance bandwidth is achievable by using wide range of dielectric constants (10–100)
- A given geometry can support different radiation patterns based on the excitation
- Resistance to tolerance errors and proximity detuning

3.6 DIELECTRIC RESONATOR GEOMETRIES

To be useful in practical antenna designs, the geometry selection of the DR is very important. Cylindrical and hemispherical DRAs are well-known for their mechanical simplicity and easy analysis. Hemispherical geometry also offers the advantage of simple interface between the dielectric and the air, compared to other geometries [13]. Also there is only one design parameter (the diameter) for the aforesaid geometry. But they exhibit mode degeneracy which can increase the cross-polarisation levels of an antenna. This problem can be avoided in a rectangular DR by properly choosing its three dimensions. Also any of the two aspect ratios can be chosen independently for a given frequency of operation [12] of a rectangular DR. Several other geometries such as ring, triangular, split-cylinder, cross, conical, elliptical, hexagonal etc. have also been evolved. For a cylindrical-ring DR, the radiation Q-factor is lower than that of corresponding cylindrical DR for certain modes, facilitating more bandwidth [1, 25]. Triangular DR [14] has an advantage over the circular and rectangular ones in that it is smallest in size when the DRs have the same dielectric constant, thickness, and

operating frequency [15]. Reduced volume DR designs in the shape of split cylinder are also available [16, 17] which considerably allows low-profile, low-volume antenna applications.

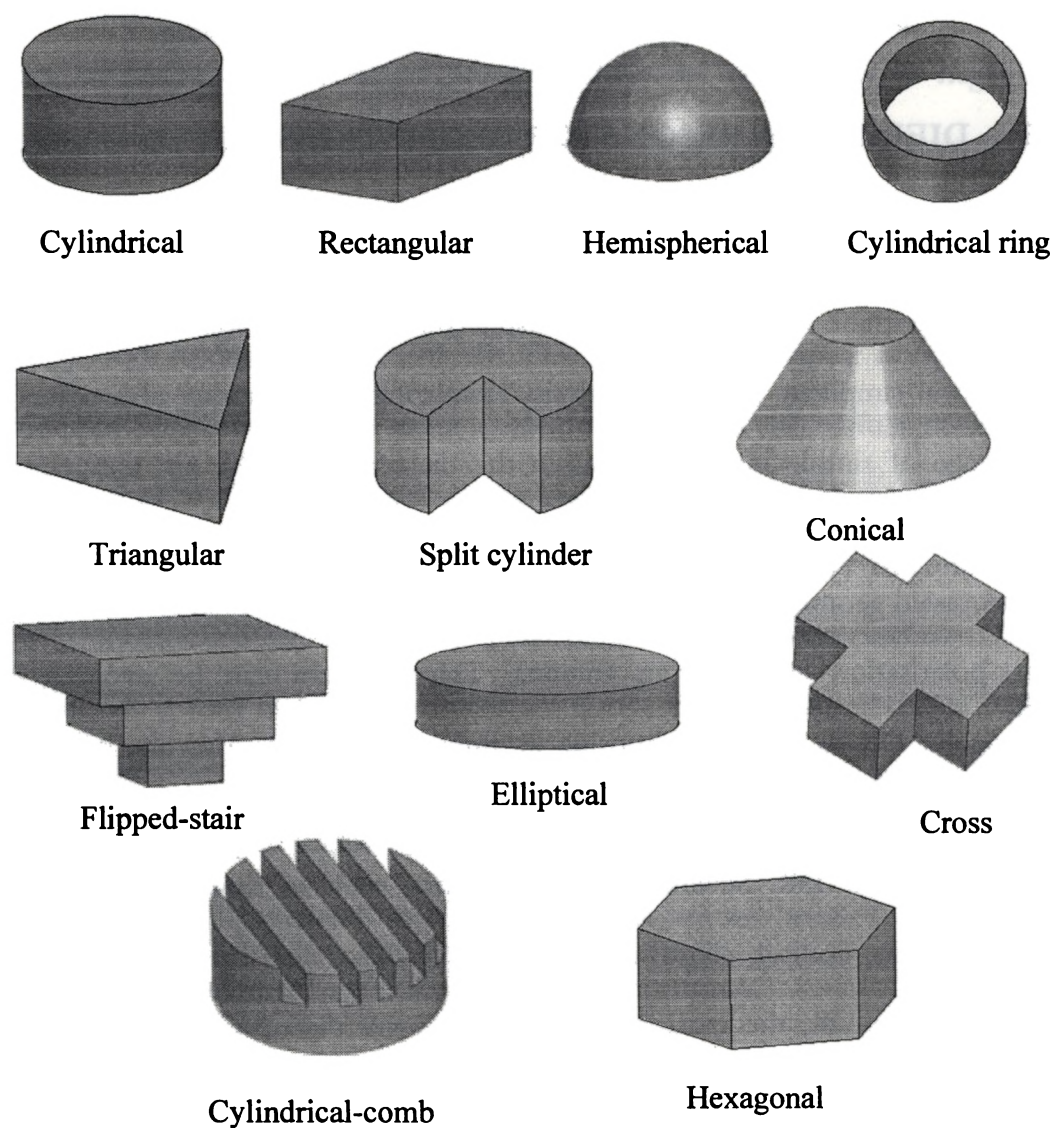


Figure 7: DR geometries used as antennas

Geometries like conical [18], stair [19], stacked triangular [20] etc. emerged for dual-band or wideband applications while those like cross [25], elliptical [21], hexagonal [22], cylindrical-comb [23] etc. came out for circular polarisation applications. Figure 7 shows the DR geometries explained so far.

3.7 MICROWAVE POWER COUPLING TECHNIQUES

Microwave power is coupled to the DR through the feed. The feed geometry and its relative position determine the type and strength of the mode excited in the DR, on which the radiation pattern relies. Numerous feeding techniques are available in the literature [26–37]. Some of the commonly used techniques are discussed below

3.7.1 Coaxial Probe

This is the simplest means for coupling energy to a DR. As shown in Figure 8(a), the DR is placed on a conducting ground plane and the central conductor of a coaxial connector extends from the bottom to the top plane to make contact with the DR. The outer conductor of the connector makes contact with the ground plane. The probe can be placed either touching the periphery of the DR or inside a hole drilled on the bottom face of the DR [26]. Amount of coupling can be controlled by varying the probe position and/or length with respect to the DR.

When the probe is at or near the periphery of the cylinder, the broadside HEM_{118} mode is excited while when the probe is inserted at the centre, the

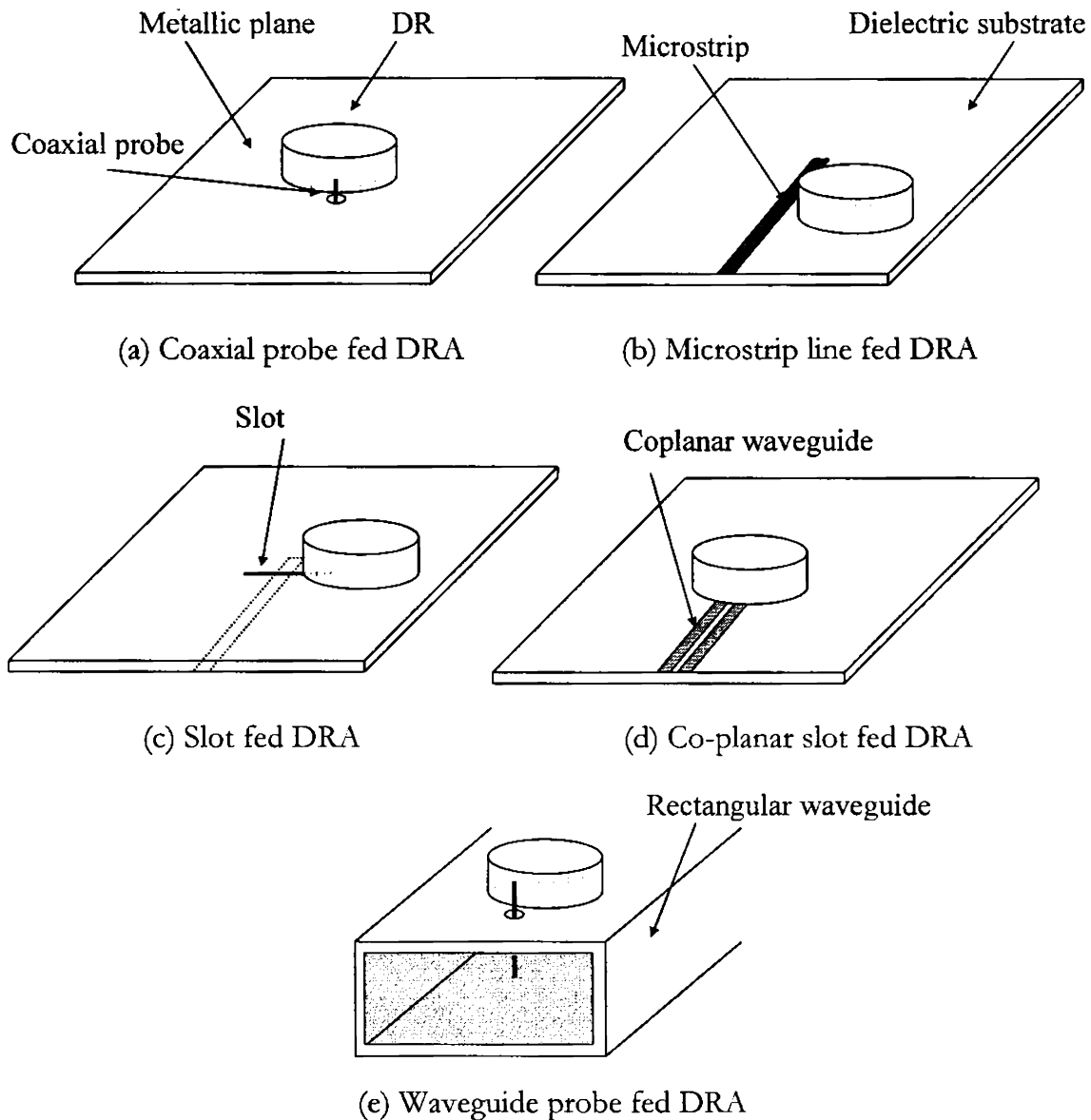


Figure 8: Microwave power coupling techniques

monopole -mode TM_{018} is excited. However this kind of coupling requires drilling a hole through the DR especially when its dielectric constant is low, which is very difficult in practice. Any direct radiation from the probe can increase the cross-polarisation in the H -plane of the DRA [12]. Also the probe introduces ohmic

loss and self-reactance at higher frequencies [13]. In addition, the air gap between the probe and the DR can prominently affect the DRA performance [24].

3.7.2 Microstrip Transmission Line

This kind of feed, which is compatible with microwave integrated circuits (MICs) couples energy magnetically to the DR. A metallic strip of definite width is etched on one side of a low loss dielectric substrate of known permittivity and thickness, the other side of which is metalised. Advantages of microstrip feed include easier fabrication, matching and analysis. Also these lines allow simple transition to/from coaxial circuits. The feed is shown in Figure 8(b).

Energy coupling and hence and the input impedance of the DRA is set by the relative position between the DR and the strip [27, 28]. Such a feed is shown to be more convenient with DRA arrays [29]. One disadvantage of the microstrip feed is that at higher frequencies, surface wave modes are also excited in the substrate which adversely affect the radiation pattern and efficiency of the DRA [1].

3.7.3 Slot or Aperture Feed

In slot-fed DRA, shown in Figure 8(c), a narrow slot is formed on the ground plane of the previous structure (Figure 8(b)), through which energy is coupled to the DR. The slot acts as a magnetic current element perpendicular to the microstrip. The magnetic coupling through the slot avoids the drawbacks of the probe coupling [13]. This also has the advantage of isolating the radiator from

the feed as well as blocking the spurious radiations from the strip [30]. Also slot coupling provides low cross-polarisation level since both the slot and the DR radiate like horizontal magnetic dipoles [12].

Length of the microstrip stub that extends beyond the slot can be used to cancel the reactance of the slot, thus allowing good impedance matching. Also this feed is well-suited in monolithic microwave integrated circuits (MMICs). But at lower frequencies, the size of the slot becomes large so that such coupling is advised at higher frequencies [31].

3.7.4 Co-planar Feed

Here, both the feed and the ground plane are etched on the same side of a substrate [32, 33]. Figure 8(d) shows the details of a co-planar slot fed DRA. This kind of feed has been found the most suitable for MMICs, arrays, circularly polarised antennas, dual-frequency structures, wide-band structures, and active antennas [33]. Impedance matching is set by the geometry and the dimensions of the slot.

3.7.5 Waveguide Feed

The primary advantage of a waveguide is that it is extremely less lossy in the millimeter wave and higher frequencies. Since the wave is completely guided within the metallic structure, there is no threat of radiation loss when used as a feed line. As both the waveguide and DR are very low-loss, they form an excellent

combination for low-loss millimeter wave communication systems [34, 35]. Coupling to the DR can be achieved through a probe [36] or a slot [37]. A waveguide probe fed DRA is shown in Figure 8(e).

3.8 APPLICATIONS OF DRs

Based on the above discussions, the key features of DRs which make them essential components in various microwave and millimeter wave systems [38] like satellite antenna, multi-channel microwave communications systems, radar systems, mobile phone systems, measuring equipments etc. are:

- High-purity, high-density ceramics minimise loss
- High dielectric constant makes possible the miniaturisation of components
- Temperature-compensated dielectric constant enables stable resonance
- A variety of shapes and coupling schemes are available for custom application requirements

These features enable DRs to be used as part of MIC/MMIC structures, forming high performance and highly stable oscillators, filters, duplexers, frequency discriminators etc. [39–42]. Recently, the application of DR as a loading element to the patch antennas and/or as a pure radiator [43] has received much attention. In addition, hollow DRs are used in active antenna applications simultaneously as the radiator and as the packaging cover, hence serving a dual-

function [44], and when also used as an oscillator load, it serves a tri-function [45]. Simultaneous use of a single cylindrical DR as an antenna as well as a filter has been recently reported [46]. Apart from antenna application, DR arrays are used as part of spatial millimeter wave power combining system [47]. DRs are also being used for material characterisation, by coating the DR with the material in the form of thin film [48], nanotubes or nanowires [49].

3.9 MEASUREMENT SETUP

Measurements of the characteristics of the DR and the radiation properties of the DRAs are carried out in the *Center for Research in Electromagnetics and Antennas* (CREMA), Department of Electronics, Cochin University of Science And Technology.

The basic measurement setup comprises of

- Network Analyser Unit
- Automated Antenna Positioner
- Standard Antenna
- Device-Under-Test (DUT)

When measuring DUTs like cavities, only the network analyser unit is used, but for antenna measurement, all the above four units are used.

3.9.1 Network Analyser Unit

Network analyser is a sophisticated instrument, generally used to measure the reflection and transmission of signals associated with an electrical network, especially at higher frequencies. The HP 8510C, a fully integrated vector network analyser (VNA) system, is used in the present study. It measures the magnitude and phase characteristics of electronic networks and components such as filters, amplifiers, attenuators and antennas. The instrument has four inputs, two independent measurement channels, and an internal microcomputer to automate measurements, conduct data processing, display results, and manage data input-output operations. The dedicated system bus provides fast digital communication between individual system instruments, allowing the network analyser to fully use the source and test set capabilities.

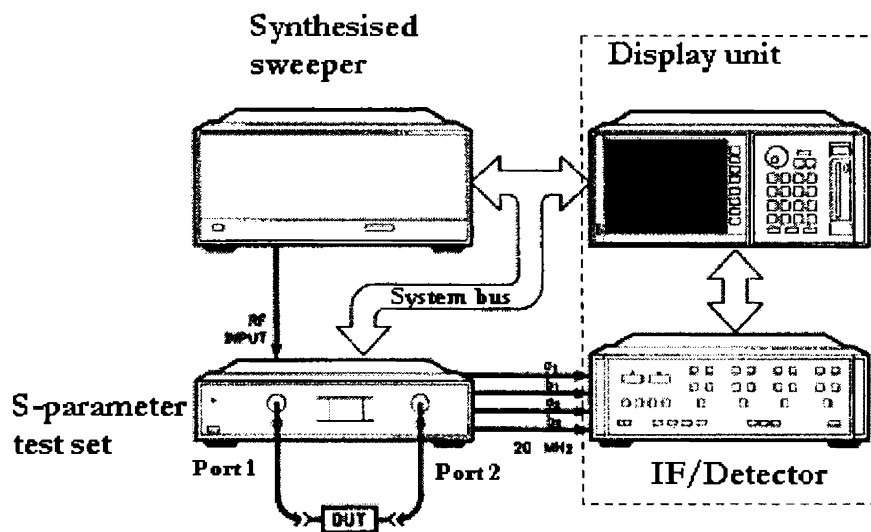


Figure 9: HP 8510C network analyser system

The minimum configuration [50] consists of a source, a test set, and the network analyser. Figure 9 shows the basic system with three major instruments.

The source uses an HP 83651B synthesised sweep oscillator to provide the RF signal. It combines the high performance and accuracy of a synthesised source with the speed and versatility of a sweep oscillator. The sweep oscillator uses an open-loop YIG (Yttrium Iron Garnet) - tuned source. It provides broadband frequency coverage (10 MHz to 50 GHz) with a precise frequency resolution of 1 Hz.

The test set HP 8517 B separates the signal produced by the source into an incident signal, sent to the DUT, and a reference signal against which the transmitted and reflected signals are later compared. The test set also routes the transmitted and reflected signals from the DUT to the receiver (IF/detector). It operates over the 45 MHz to 20 GHz range. Also two 90 dB step attenuators, which allow control of the port 1 and port 2 signal levels, are also built in the analyser.

The network analyser includes the HP 85101 display/processor and the 85102 IF/detector. The detector, together with the display/processor, processes the signals. Using its integral microprocessor, it performs accuracy enhancement and displays the results in a variety of formats.

The analyser uses a 32-bit Motorola 68000 microprocessor equipped with 1 MB of RAM, and 512 KB of EEPROM. A firmware operating system is stored

permanently in the ROM and then loaded into RAM each time power is applied. Peripheral devices such as a controller PC, printer, plotter, and disc drive can be interfaced with the analyser via GPIB ports.

In a typical measurement [51], the signal source is swept from the lower measurement frequency to the higher measurement frequency using a linear ramp controlled by the 8510. Ramp sweep offers the fastest update of the measurement display. In step-sweep mode, the source is phase-locked at each discrete measurement frequency controlled by the 8510. At the first frequency conversion stage, signal separation components in the test set apply a portion of the incident signal and the responses from the DUT to the first stage. Digital communication between the receiver and the test set pre-tunes the 65 MHz to 300 MHz voltage-tuned local oscillator (VTO) so that one of its harmonics mixes with the stimulus to produce a 1st IF frequency close to 20 MHz. Fine tuning is accomplished by comparing the IF frequency with the internal 20 MHz crystal reference and sweeping the local oscillator to track the stimulus frequency. When the local oscillator reaches its upper frequency limit, the sweep is stopped, the local oscillator is tuned again, phase lock is reestablished, and the sweep is continued. Since the first local oscillator frequency is selected algorithmically from a known stimulus frequency, the measurement is free of harmonic skip.

The second frequency conversion produces an IF frequency of 100 KHz for application to the detection and data processing elements of the receiver. Because the frequency conversions are phase-coherent and the IF signal paths are carefully matched, magnitude and phase relationships between the input signals

are maintained throughout the frequency conversion and detection stages. Automatic, fully calibrated, auto-ranging IF gain steps maintain the IF signal at optimum levels for detection over a wide dynamic range.

3.9.2 Automated Antenna Positioner

This assembly is used for the far-field measurement of the antenna-under-test (AUT). It consists of a stepper motor with gear system for rotating a circular platform over 360° on which the AUT is attached. The height of the platform can be adjusted vertically for aligning the axis of the AUT with that of the standard antenna. The platform can be rotated to any desired angle by using the controller S310C, built by the *Sophisticated Test and Instrumentation Center*, Cochin University of Science And Technology. The angular position can be precisely controlled either manually or by a MATLAB[®] program stored in the PC, interfaced with both the analyser and the controller.

3.9.3 Standard Antenna

The DRH-0118 broadband double-ridged horn antenna is used as the standard (STD) antenna that is shown in Figure 10. It is linearly polarised and operates over a frequency range of 1 to 18 GHz. These antennas have high gain, bandwidth, and power handling characteristics. They have low dispersion when used with short-pulse signals. The coaxial input to the antenna is easily adaptable to many modern network analysers. The antenna is fabricated from aluminium alloys and RT/duroid and all supporting hardwares are non-corroding for reliable

operation and long term durability in both indoor and outdoor applications. A universal mounting bracket is supplied which allows the antenna to be positioned axially in 22.5 degree increments for polarisation-sensitive measurements. The mounting bracket also has provisions for tripod attachment with a standard 1/4–20 UNC threaded fitting.

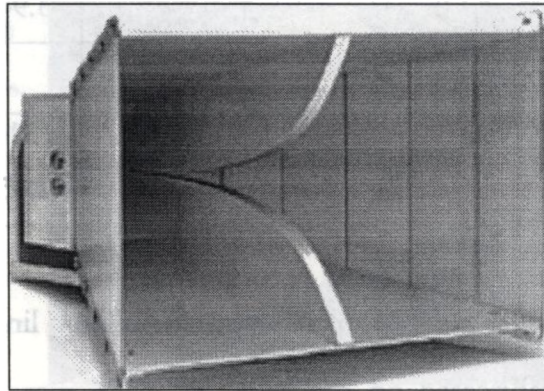


Figure 10: Photograph of the double ridged horn antenna

3.9.4 Antenna under Test

The AUT is the antenna designed using the fabricated DR. The fabrication process has been explained in section (3.3). A few DR samples are fabricated and characterised. For the antenna study, three different DRs of dielectric constant ϵ_r , diameter $2a$ and height d are used. Two of them are made of zinc titanate (ZnTiO_3) and the third is of titanium dioxide (TiO_2). The DR specifications are given in Table 1. Measured results show that titanium based compounds are having poor τ_f . But, when the easy availability and low cost of the titanates are taken into account, these are utilised in the present work.

Table 1: DRs used for AUT

DR	Diameter 2a, mm	height d, mm	Density (mass/volume), g/cm ³	Dielectric constant, ϵ_r	Q-factor	Temp. coeff. of res. freq τ_f , ppm/°C
DR-1	24	7.3	4.69	20.8	6558 at 3.94 GHz	-47.9
DR-2	27.3	8.4	4.56	”	”	”
DR-3	24	7.8	3.84	88.68	3100 at 2.45 GHz	+455.4

The DRA is fed by a 50 Ω microstrip transmission line of width (w) 3 mm and length 50 mm fabricated on one side of a 1.6 mm thick (h) microwave substrate of dielectric constant $\epsilon_r = 4$, size 115 mm x 115 mm and having a copper cladding on the opposite side. The design equations for the feed are given as Eq. (3.21) and (3.22) where an effective dielectric constant (ϵ_{eff}) is used instead of the absolute value in the equation for the characteristic impedance ($Z_o = 50 \Omega$). The merits of using microstrip feed are well-known, where fine adjustment of impedance matching between the feed and the DR can be easily achieved by adjusting the DR position relative to the feed.

$$\epsilon_{eff} = \frac{\epsilon_r+1}{2} + \frac{\epsilon_r-1}{2} \left[\frac{1}{\sqrt{1+\frac{12h}{w}}} + 0.04 \left(1 - \frac{w}{h}\right)^2 \right], \text{ if } \frac{w}{h} < 1$$

$$= \frac{\epsilon_r+1}{2} + \frac{\epsilon_r-1}{2} \left[\frac{1}{\sqrt{1+\frac{12h}{w}}} \right], \text{ otherwise} \quad (3.21)$$

$$Z_o = \frac{60}{\sqrt{\epsilon_{\text{eff}}}} \ln\left(\frac{8h}{w} + \frac{w}{4h}\right), \quad \text{if } \frac{w}{h} < 1$$

$$= \frac{120\pi}{\sqrt{\epsilon_{\text{eff}}}} \frac{1}{\left(\frac{w}{h} + 1.393 + 0.677 \ln\left[\frac{w}{h} + 1.444\right]\right)}, \quad \text{otherwise} \quad (3.22)$$

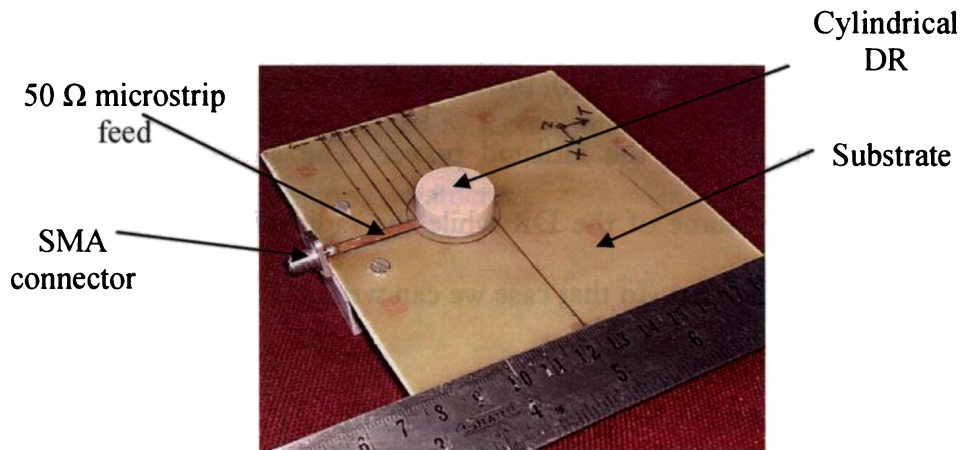


Figure 11: Narrow band-broadside mode DRA

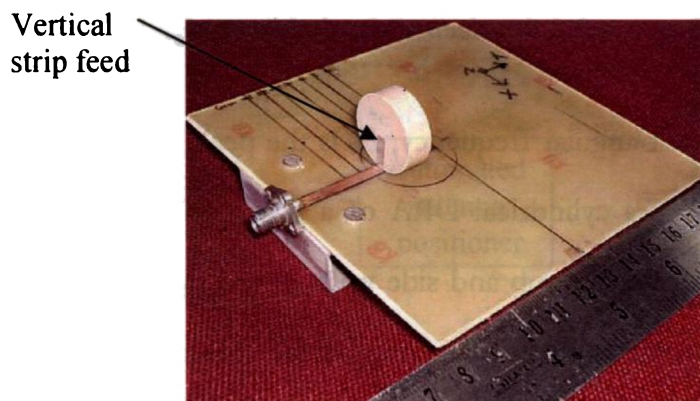


Figure 12: Wideband-conical mode DRA

Photographs of the DRAs under test are shown in Figures 11 and 12. Figure 11 shows the fundamental DRA geometry that yields a narrow bandwidth and broadside radiation pattern. The above geometry is modified into that shown

in Figure 12 for a wide bandwidth and conical radiation pattern. Further details of the design are presented in Chapter 4.

As explained in section (3.2.3), the impedance bandwidth of a DRA is inversely proportional to its unloaded Q-factor (Q_u) which in turn is directly related to the radiation Q-factor (Q_r), provided the conductor and dielectric losses are negligible compared to the radiated power. The stored energy is directly proportional to the volume of the DR while the radiated power depends on its surface area in a similar way. In that case we can write [1],

$$Q_r = \frac{2\omega_o E_s}{P_r} \propto (\epsilon_r)^p \cdot \left(\frac{DR \text{ Volume}}{DR \text{ Surface Area}} \right) \quad (3.23)$$

*where $p = 1.5$ for magnetic dipole like modes
 $= 2.5$ for electric dipole like modes*

where ω_o is the resonant angular frequency, E_s is the peak stored energy and P_r is the radiated power. For a cylindrical DRA of a given volume, the arrangement shown in Figure 11 allows the top and side walls of the cylinder to radiate freely but the radiation from the bottom wall, lying on the substrate is restricted by the ground plane. If the bottom wall of the cylinder is also allowed to radiate as shown in Figure 12, the Q_r can be considerably reduced as per Eq. (3.23) to accomplish a wideband operation.

3.10 MEASUREMENT PROCEDURE

Measurement setup is similar to that in Figure 9, except for the DUT, which is substituted by a transmission cavity for DR characterisation or by the AUT connected at one port and the standard antenna at the other port for antenna characterisation. The arrangement for antenna measurement is shown in Figure 13. The analyser is interfaced to a computer that runs a MATLAB® based software to measure the antenna parameters.

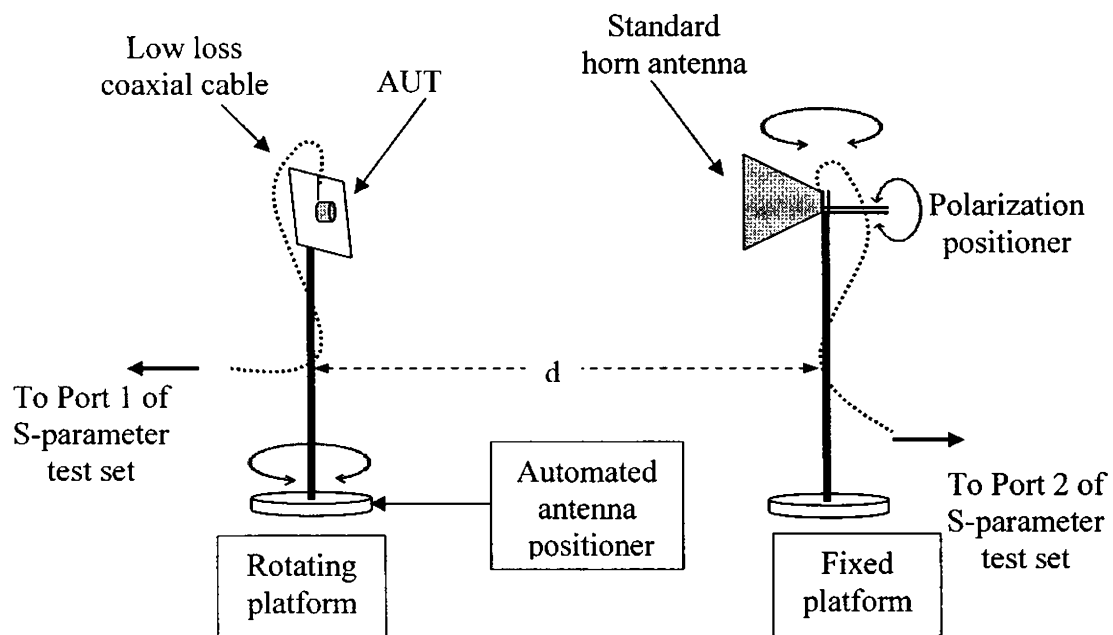


Figure 13: Arrangement for antenna measurement

3.10.1 Impedance and VSWR

These are the most important parameters as far as an antenna is concerned. Impedance of the antenna is a measure of the efficiency with which it acts as a

transducer between the source and the propagating medium. The impedance is a complex quantity with a real part, called the antenna resistance and the imaginary part, called the antenna reactance. When there is an impedance mismatch between the antenna and the source line, a part of the incident energy is reflected back to the source. The ratio of the reflected voltage (or current) to the incident voltage (or current) is termed as the input reflection coefficient (Γ). The magnitude $|\Gamma|$, when expressed in dB, it is called the return loss ($|S_{11}|$) of the antenna.

$$|S_{11}| = 20 \cdot \log_{10} (|\Gamma|) \quad (3.24)$$

The level of mismatch is also defined in terms of the voltage standing wave ratio ($VSWR$) defined as the ratio of the voltage maximum to minimum of the standing wave existing on the antenna input terminal.

$$VSWR = \frac{|V_{\max}|}{|V_{\min}|} = \frac{(1+|\Gamma|)}{(1-|\Gamma|)} \quad (3.25)$$

Once the AUT is connected to port 1, the frequency range is selected from the *stimulus* menu on the front panel of the analyser. The reflection mode is selected from the *parameter* menu. The display then gives the return loss of the AUT as a function of the frequency. By using markers, the resonant frequency, bandwidth etc. can be calculated. Usually the bandwidth is measured between the 2:1 $VSWR$ or -10 dB $|S_{11}|$ points of the plot. From the *format* menu, phase of S_{11} , $VSWR$, real and imaginary parts of the input impedance etc. can also be plotted.

3.10.2 Radiation Pattern

Radiation pattern of an antenna is the graphical representation of its radiation properties as a function of the space co-ordinates, which implies a three dimensional pattern. Because of the limits set by a practical measurement setup for measuring the 3-D pattern, usually two principal plane patterns are specified for antennas radiating in the broadside and three patterns for those with omnidirectional patterns. Generally, far-field patterns are specified for an antenna where the pattern is measured at a distance, $d > 2D^2/\lambda$, where D is the largest dimension of the antenna and λ is the operating wavelength.

As shown in Figure 13, the AUT is connected to port 1 and the STD antenna is connected to port 2 of the analyser. The height and polarisation of both antennas are then aligned for maximum transmission ($|S_{21}|$) between them. The frequency range over which $|S_{11}| < -10$ dB is selected using the *parameter* menu. Now *thru* calibration of the analyser is selected from the *calibrate* menu. This calibrates the $|S_{21}|$ data to 0 dB for every frequency point in the band. In order to suppress the spurious reflections from the nearby objects, the *time domain gating* facility of the analyser is used. The *gate span* is selected according to the largest dimension of the radiator.

The positioner is now set to *home*, which automatically sets the current angular position of the antenna as 0° . The computer software now invokes the radiation pattern routine and reads the normalised $|S_{21}|$ data for the specified frequency band, as a function of the angular position of the AUT.

3.10.3 Antenna Gain

Gain is the logarithm of the ratio of the intensity of an antenna's radiation pattern in the direction of strongest radiation to that of a reference antenna, when both antennas are fed with the same input power. If the reference antenna is isotropic, the gain is often expressed in units of dBi. The gain of an antenna is a passive phenomenon – power is not added by the antenna, but simply redistributed to provide more radiated power in a certain direction than would be transmitted by an isotropic antenna. In this thesis, the gain transfer method is used to calculate the absolute gain of the AUT. The experimental setup for gain measurement is the same as that for radiation pattern measurement. Here, an antenna of known gain G_{ref} (dBi) is used as the reference antenna. Initially, the AUT for the pattern measurement setup is replaced by the reference antenna. It is then positioned for maximum radiation in the direction of the STD antenna and the transmission coefficient or $|S_{21}|_{ref}$ (dB) is displayed on the analyser. A *thru* calibration is performed and the data is stored in the *cal set*. This is the reference gain for the AUT. Now the reference antenna is replaced with the AUT and the transmission coefficient or $|S_{21}|_{AUT}$ (dB) is recorded, which gives the relative gain. The absolute gain can then be calculated as

$$G \text{ (dBi)} = G_{ref} \text{ (dBi)} + |S_{21}|_{AUT} \quad (3.26)$$

3.10.4 Radiation Efficiency

Radiation efficiency of an antenna quantifies the resistive loss of the antenna in terms of the proportion of power radiated versus the power fed to the antenna.

$$\text{Radiation Efficiency, } \eta = \frac{P_{rad}}{P_{in}} = \frac{P_{rad}}{P_{rad} + P_{loss}} = \frac{R_{rad}}{R_{rad} + R_{loss}} \quad (3.27)$$

Where P_{rad} = power radiated (W)

P_{in} = power fed to antenna (W)

P_{loss} = power lost by the antenna (W)

R_{rad} = radiation resistance of the antenna (Ω)

R_{loss} = loss resistance of the antenna (Ω)

For physically small antennas, the Wheeler cap method [52] is highly preferred for measuring the radiation efficiency. According to this method, if a radiation shield is placed around the antenna so as to enclose its near fields as illustrated in Figure 14, the radiation resistance of the antenna is reduced to zero while the loss resistance and the stored energy remain the same as for the unshielded antenna [53]. When covering the antenna with a metal cap, the radiation is suppressed and the input power (proportional to the input resistance) is equal to the power loss (proportional to the loss resistance). Without the cap, the input power is equal to the radiated power plus the power loss (input

resistance + loss resistance). The radiation efficiency of the antenna can be obtained from these two parameters as in Eq. (3.27).

Another approach to the Wheeler cap measurement is by measuring the Q-factor of the antenna using the formula given below.

$$\eta = \frac{P_{rad}}{P_{rad} + P_{loss}} = 1 - \frac{Q_o}{Q_{loss}} \quad (3.28)$$

where Q_o = total Q-factor

Q_{loss} = dissipation Q-factor

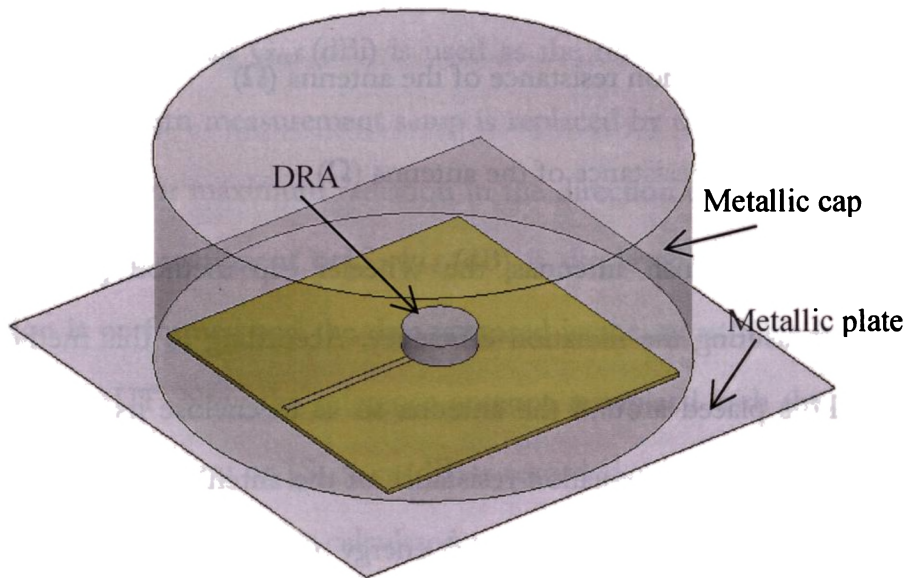


Figure 14: Wheeler cap method for measuring radiation efficiency

The Q-factor can be related to the -10 dB bandwidth as,

$$Q = \frac{S-1}{BW\sqrt{S}} \times 100\% \quad (3.29)$$

The bandwidth, BW is expressed as the ratio of the frequency bandwidth over which $VSWR$ is below a specific value S (usually 2), to the centre frequency. Thus, without the cap, the measured bandwidth corresponds to the Q_o . When the cap is placed, the radiation is suppressed and the measured bandwidth represents Q_{loss} . The size and shape of the cap is not critical in the above method. But the centering of the cap with respect to the radiator and good electrical contact between the cap and the antenna ground plane are very important [51].

CONCLUSION

The fabrication process of dielectric resonators, their general characteristics and microwave characterisation were discussed in this chapter. A detailed account of the measurement facilities used, the proposed antenna design and the measurement procedure of important antenna properties were also described.

REFERENCES

- [1] R. K Mongia and P. Bhartia, Dielectric Resonator Antennas-A Review and General Design Relations for Resonant Frequency and Bandwidth, Inter. Journal of Microwave and Millimeter-Wave Computer- aided Engineering, Vol.4, pp. 230-247 , July 1994
- [2] D. Kajfez, A. W. Glisson and J. James, Computed Modal Field Distributions for Isolated Dielectric Resonators, IEEE Trans. Microwave Theory Tech., Vol.32 ,pp. 1609-1616, December 1984
- [3] D. Kajfez, Chapter 7- Material Properties in *Dielectric resonators*, Edited by D. Kajfez and P. Guillon, Artech House, 1986
- [4] A. J. Moulson and J. M. Herbert, Chapter 3 – Processing of Ceramics in *Electroceramics: Materials, Properties, Applications*, 2nd edition, Wiley
- [5] W. E. Courtney, Analysis and Evaluation of a Method of Measuring the Complex Permittivity and Permeability of Microwave Insulators, IEEE Trans. Microwave Theory Tech., Vol.18 ,pp. 476-485, August1970
- [6] K. T. Mathew, Perturbation Theory, Encyclopedia of RF and Microwave Engineering, Wiley-VCH Publications, Vol.4, pp. 3725-3735, 2005
- [7] B. W. Hakki and P. D. Coleman, A Dielectric Resonator Method of Measuring Inductive Capacities in the Millimeter Range, IRE Tran. Microwave Theory Tech., Vol. 8, pp. 402-410, July 1960
- [8] H. A. Auda and D. Kajfez, Chapter 3- Dielectric Rod Waveguides in *Dielectric resonators*, Edited by D. Kajfez and Pierre Guillon, Artech House, 1986

- [9] D. F. Hanson, Chapter 2- Microwave resonators in *Dielectric resonators*, Edited by D. Kajfez and Pierre Guillon, Artech House, 1986
- [10] A. P. S. Khanna, Chapter 2-Oscillators in *Dielectric resonators*, Edited by D. Kajfez and Pierre Guillon, Artech House, 1986
- [11] S. A. Long, M. McAllister and L. C. Shen, The Resonant Cylindrical Dielectric Cavity Antenna, *IEEE Trans. on Antennas Propagat.*, Vol.31, pp. 406-412, May 1983
- [12] R. K. Mongia and A. Ittipiboon, Theoretical and Experimental Investigations on Rectangular Dielectric Resonator Antennas, *IEEE Trans. on Antenn. Propagat.*, Vol. 45, pp.1348-1356, September 1997
- [13] K. W. Leung, K. Y. A. Lai, K. M. Luk and D. Lin, Input Impedance of Aperture Coupled Hemispherical Dielectric Resonator Antenna, *Electron. Lett.*, Vol. 29, pp. 1165-1167, June 1993
- [14] A. Ittipiboon, R. K. Mongia, Y .M. M. Antar, P. Bhartia and M. Cuhaci, Aperture Fed Rectangular and Triangular Dipole Antennas Dielectric Resonators for Use as Magnetic Dipole Antennas, *Electron. Lett.* Vol. 29, pp. 2001-2002, November 1993
- [15] H. Y. Lo, K. W. Leung, K. M. Luk, and E. K. N. Yung, Low profile Equilateral-triangular Dielectric Resonator Antenna of Very High Permittivity, *Electron. Lett.*, Vol. 35, pp. 2164-2166, December 1999
- [16] M. T. K. Tam and R. D. Murch, Compact Circular Sector and Annular Sector Dielectric Resonator Antennas, *IEEE Trans. on Antenn. Propagat.*, Vol. 48, pp. 126-128, May 2000

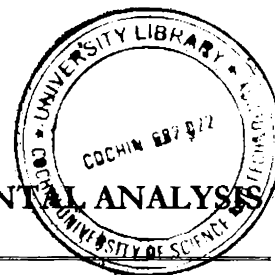
- [17] R. K. Mongia, Half Split Dielectric Resonator Placed on a Metallic Plane for Antenna Applications, *Electron. Lett.*, Vol. 25, pp. 463-464, March 1989
- [18] A. A. Kishk, Yan Yin, and A. W. Glisson, Conical Dielectric Resonator Antennas for Wide-Band Applications, *IEEE Trans. on Antenn. Propagat* Vol. 50, pp. 469-474, April 2002
- [19] R. Chair, A. A. Kishk, K. F. Lee and C. E. Smith, Wideband Flipped Staired Pyramid Dielectric Resonator Antennas, *Electron. Lett.*, Vol. 40, pp. 581- 582, May 2004
- [20] Q. Rao, T. A. Denidni, and A. R. Sebak, Broadband Compact Stacked T-Shaped DRA with Equilateral-triangle Cross Sections, *IEEE Micro. Wireless Comp. Lett.*, Vol. 16, pp. 7-9, January 2006
- [21] A. A. Kishk, An Elliptic Dielectric Resonator Antenna Designed for Circular Polarization with Single Feed, *Micro. and Opt. Tech. Letters.*, Vol. 37, pp. 454-456, June 2003
- [22] V. Hamsakutty, A.V. P. Kumar, J. Yohannan, K. T. Mathew, Coaxial Fed Hexagonal Dielectric Resonator Antenna for Circular Polarization, *Micro. and Opt. Tech. Letters.*, Vol. 48, pp. 581- 582, March 2006
- [23] L. C. Y. Chu, D. Guha and Y. M. M. Antar, Comb-shaped Circularly Polarized Dielectric Resonator Antenna, *Electron. Lett.* Vol. 42, pp. 785-787, July 2006
- [24] G. P. Junker, A. A. Kishk, A. W. Glisson, and D. Kajfez, Effect of Fabrication Imperfections from Ground-plane-backed Dielectric Resonator Antennas, *IEEE Antennas Propagat. Mag.*, vol. 37, pp. 40-47, February 1995

- [25] A. Petosa, A. Ittipiboon, Y. M. M. Antar, D. Roscoe and M. Cuhaci, Recent Advances in Dielectric Resonator Antenna Technology, *IEEE Antennas Propagat. Magazine*, Vol. 40, pp. 35-48, June 1998
- [26] A. A. Kishk, M. R. Zunoubi and D. Kajfez, A Numerical Study of a Dielectric Disk Antenna above a Grounded Dielectric Substrate, *IEEE Trans. on Antennas Propagat.*, Vol.41, pp. 813-821, June 1993
- [27] R. A. Kranenburg and S. A. Long, Microstrip Transmission Line Excitation of Dielectric Resonator Antennas, *Electro. Lett.*, Vol. 24, pp. 1156-1157, January 1988
- [28] Leung K. W., K. Y. Chow, K. M. Luk and E. K. N. Yung, Low-profile Circular Disk DR antenna of very high permittivity excited by a Microstrip line, *Electron. Lett.*, Vol. 33, pp. 1004-1005, June 1997
- [29] A. Petosa, R. K. Mongia, A. Ittipiboon, and J. S. Wight, Design of Microstrip-fed Series Array of Dielectric Resonator Antennas, *Electron. Lett.*, vol. 31, pp. 1306–1307, August 1995
- [30] A. A. Kishk, A. Ittipiboon, Y. M. M. Antar and M. Cuhaci, Slot Excitation of Dielectric Disk Radiator, *IEEE Trans. Antennas Propagat.*, Vol. 43, pp. 198-201, February 1995
- [31] A. Petosa, A. Ittipiboon, and Y. M. M. Antar, Rectangular dielectric Resonator Antennas, chapter 2 - *Dielectric Resonator Antennas*, Edited by K.M. Luk, K. W. Leung, Research Studies Press Ltd., 2003
- [32] R. A. Kranenburg, S. A. Long and J. T. Williams, Coplanar Waveguide excitation of Dielectric Resonator Antennas, *IEEE Trans. on Antennas Propagat.*, Vol. 39, pp. 119-122, January 1990

- [33] M. S. Al Salameh, Y. M. M. Antar and G. Séguin, Coplanar-Waveguide-Fed Slot-Coupled Rectangular Dielectric Resonator Antenna, *IEEE Trans. on Antennas Propagat.*, Vol.50, pp. 1415-1419, January 2002
- [34] K. W. Leung, H. Y. Lo, K. K. So, and K. M. Luk, High-permittivity Dielectric Resonator Antenna Excited by a Rectangular Waveguide, *Micro. Optical Tech. Lett.*, Vol. 34, pp. 157–158, August 2002
- [35] K. W. Leung and K. K. So, Rectangular Waveguide Excitation of Dielectric Resonator Antennas, *IEEE Trans. on Antennas Propagat.*, Vol.51, pp. 2477-2481, September 2003
- [36] I. A. Eshrah, A. A. Kishk, A. B. Yakovlev, and A. W. Glisson, Excitation of Dielectric Resonator Antennas by a Waveguide Probe: Modeling Technique and Wide-Band Design, *IEEE Trans. on Antennas Propagat.*, Vol. 53, pp. 1028-1037, March 2005
- [37] I. A. Eshrah, A. A. Kishk, A. B. Yakovlev, and A. W. Glisson, Theory and Implementation of Dielectric Resonator Antenna Excited by a Waveguide Slot, *IEEE Trans. on Antennas Propagat.*, Vol. 53, pp. 483-494, January 2005
- [38] Dielectric resonator data sheets :
1. Murata Manufacturing Co. Ltd:
<http://www1.isti.cnr.it/~salerno/Microonde/MuRataResonators.pdf>
 2. First technology innovative solutions
http://www.1firsttech.com/data_sheets_pdfs/dielectric_resonators.pdf

- [39] T. D. Iveland, Dielectric Resonator Filters for Application in Microwave Integrated Circuits, *IEEE Trans. Microwave Theory Techniques*, Vol. 19, pp. 643–652, July 1971
- [40] J. K. Plourde and C. L. Ren, Application of dielectric resonators in microwave components, *IEEE Trans. Microwave Theory Techniques*, Vol. 29, pp. 754–769, August 1981
- [41] S. J. Fiedziuszko, I. C. Hunter, T. Itoh, Y. Kobayashi, T. Nishikawa, S. N. Stitzer and K. Wakin., Dielectric Materials, Devices and Circuits, *IEEE Trans. Microwave Theory Techniques*, Vol. 50, pp. 706–720, March 2002
- [42] E. Y. Yuksel and T. T. Y. Wong, A Phase-Shifting Frequency Discriminator employing Dielectric Resonator, *Micro. and Opt. Tech. Letters.*, Vol. 36, pp. 87-89, January 2003
- [43] Y. F. Lin, C. H. Lin, H. M. Chen and P. S. Hall, A Miniature Dielectric Loaded Monopole Antenna for 2.4/5 GHz WLAN Applications, *IEEE Micro. Wireless Comp. Lett*, Vol.16, pp. 591-593, November 2006
- [44] E. H. Lim and K. W. Leung, Novel Application of the Hollow Dielectric Resonator Antenna as a Packaging Cover, *IEEE Trans. on Antennas Propagat.*, Vol. 54, pp.484-487, February 2006
- [45] E. H. Lim and K. W. Leung, Novel Utilization of the Dielectric Resonator Antenna as an Oscillator Load, *IEEE Trans. on Antennas Propagat.*, Vol. 55, pp. 2686-2691, October 2007
- [46] E. H. Lim and K. W. Leung, Use of the Dielectric Resonator Antenna as a Filter Element, *IEEE Trans. on Antennas Propagat.*, Vol. 56, pp. 5-10, January 2008

- [47] Y. Zhang, A. A. Kishk, A. B. Yakovlev and A. W. Glisson, Analysis of Wideband Dielectric Resonator Antenna Arrays for Waveguide-Based Spatial Power Combining, *IEEE Trans. Microwave Theory Tech.*, Vol. 55, pp. 1332-1340, June 2007
- [48] S. Fargeot, A. Vergonjanne, M. Aubourg and P. Guillon, Cylindrical Dielectric Resonator Antenna for Material Characterization, *Microwave and Optical Tech. Lett.*, Vol. 17, pp. 273-275, March 1998
- [49] J. B. Jarvis, M. D. Janezic and J. H. Lehman, Dielectric Resonator method for Measuring the Electrical Conductivity of Carbon Nanotubes from Microwave to Millimeter frequencies, *Journal of Nanomaterials*, Vol. 2007, Article ID 24242, pp. 1-4, 2007
- [50] Agilent Technologies 8510C Network Analyzer System Users guide
URL: <http://cp.literature.agilent.com/litweb/pdf/08510-90290.pdf>
- [51] Agilent Technologies 8510C Network Analyzer System Operating and Programming Manual
URL: <http://cp.literature.agilent.com/litweb/pdf/08510-90281.pdf>
- [52] D. M. Pozar and B. Kaufman, Comparison of Three Methods for the Measurement of Printed antenna Efficiency, *IEEE Trans. on Antennas Propagat.*, Vol. 36, pp. 136-139, January 1988
- [53] R. K. Mongia, A. Ittipiboon and M. Cuhaci, Measurement of Radiation Efficiency of Dielectric Resonator Antennas, *IEEE Microwave and Guided wave Letters*, Vol. 4, pp. 80-82, March 1994



In this chapter, design and analysis of a wideband antenna using the fabricated cylindrical dielectric resonator (DR) are discussed, with the support of simulated and measured results. Starting with the fundamental broadside operation of a cylindrical dielectric resonator antenna (DRA), a step-by-step development of the proposed wideband antenna, using a low radiation Q-factor design is presented. Computer aided high frequency structure simulator, Ansoft HFSS™ [1] is used for modeling and simulating the antenna. Antenna characteristics such as the return loss, impedance, radiation pattern, gain and radiation efficiency are measured with the help of HP 8510C vector network analyser.

4.1 BROADSIDE MODE OPERATION OF A CYLINDRICAL DRA

The antenna study is started with the cylindrical DR, DR-1 of dielectric constant, $\epsilon_{rd} = 20.8$, unloaded quality factor, $Q_u = 6558$ at 3.94 GHz, diameter, $2a = 24$ mm or $0.24 \lambda_0$ and thickness, $d = 7.3$ mm or $0.073 \lambda_0$, λ_0 being the free space wave length corresponding to the fundamental mode frequency, $f = 3.03$ GHz of the DRA.

The antenna structure used for broadside radiation operation [2, 3] of a cylindrical DR is shown in Figure 1. A 50Ω microstrip line, having a width = 3.3 mm and length = 50 mm fabricated on a 1.6 mm thick microwave substrate of dielectric constant $\epsilon_{rs} = 4$ and size 115 mm x 115 mm, feeds the DRA. This structure will operate on the fundamental broadside mode which is HEM_{118} (also

known as TM_{110} [4]) for a cylindrical DR. This mode is very attractive in terms of its lowest-Q factor compared to other modes of a cylindrical DR [5]. Impedance matching between the feed and the DR can be easily achieved by adjusting the DR position relative to the microstrip.

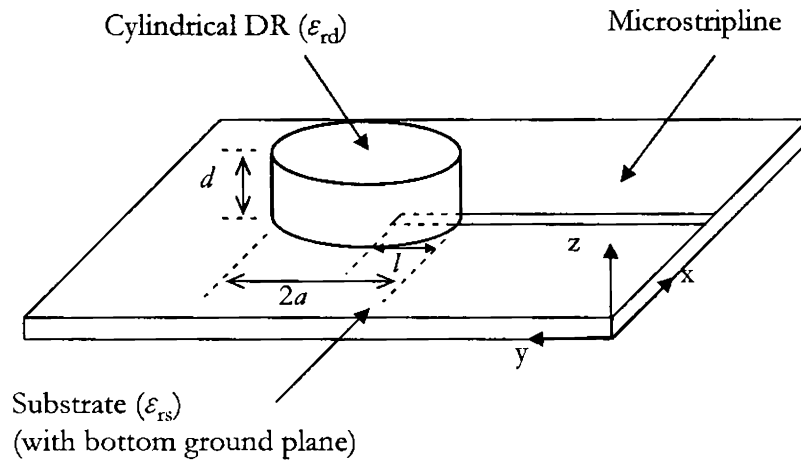


Figure 1: Broadside radiation operation of the cylindrical DR

4.2 RESULTS

Measured and simulated return loss ($|S_{11}|$) of the DRA as a function of frequency is shown in Figure 2, for an offset distance of $l = 6$ mm that corresponds to the maximum impedance matching. The DRA resonates at 3.03 GHz with a -10 dB bandwidth ranging from 2.92 to 3.144 GHz or 7.38 %. This high bandwidth is the result of the low radiation Q-factor of the excited mode. The input impedance measured is $49-j 4 \Omega$ at 3.03 GHz. Simulated resonance occurs at 3.09 GHz with a bandwidth of 4.28 %. The mismatch between the measured and simulated results is attributed to the ideal modeling of antenna

elements in HFSS™, where the dielectrics and conductors are assumed to be perfect.

In the literature [6], accurate closed form formulae for the frequencies of the resonant modes of a cylindrical DR are available. For the HEM_{116} mode, the resonant frequency is given by

$$f_r = \frac{6.324c}{2\pi a\sqrt{\epsilon_{rd} + 2}} \left[0.27 + 0.36 \frac{a}{2d} + 0.02 \left(\frac{a}{2d} \right)^2 \right] \quad (4.1)$$

where c is the velocity of light in free space. The formula yields a frequency of 3.05 GHz which is in agreement with the measured value.

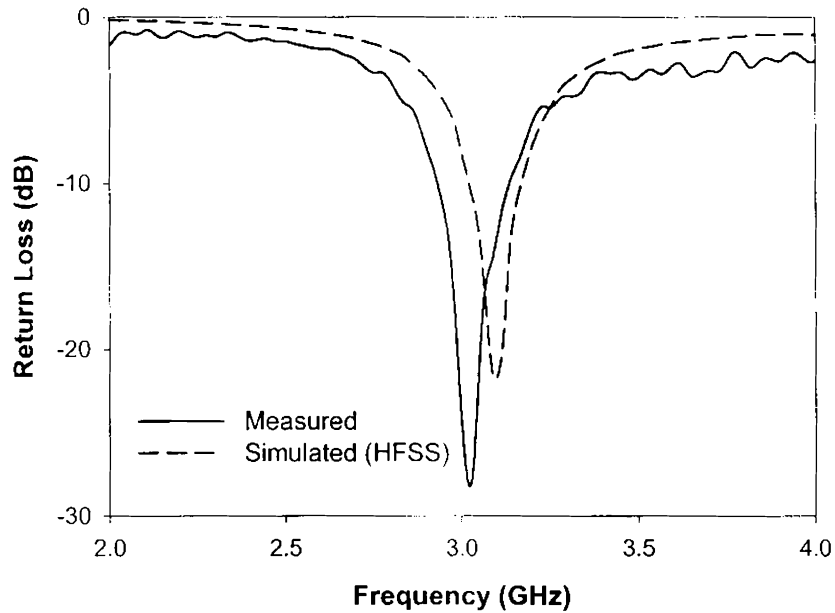


Figure 2: Measured return loss of the cylindrical DRA

Experimental Analysis

Measured far-field radiation patterns in the two principal planes, namely XZ and YZ -planes of the antenna, at 3.03 GHz are shown in Figure 3. Patterns are broadside, similar to that of a horizontal magnetic dipole, with boresight cross-polarisation levels of -22.61 dB and -16.34 dB in the XZ and YZ - planes respectively. Also the boresight front-to-back lobe ratios are -21.18 dB and -25 dB in the XZ and YZ -planes respectively and a gain of 5.71 dBi is measured at the resonant frequency of 3.03 GHz.

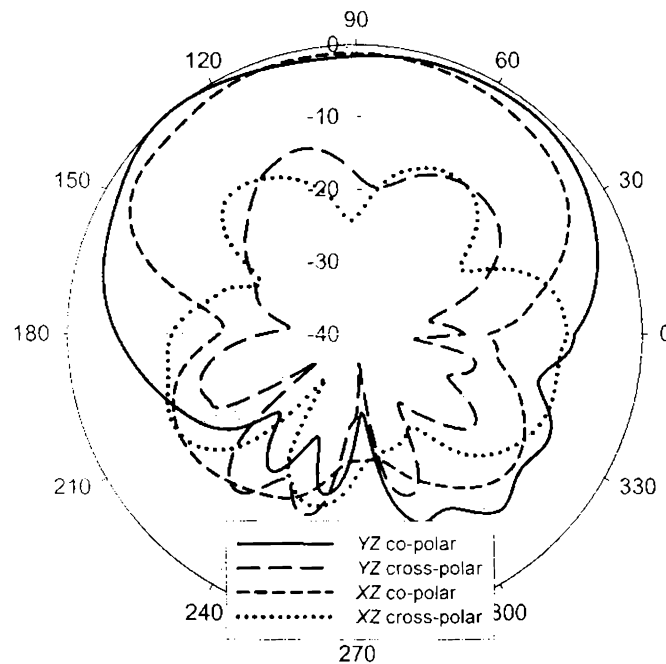


Figure 3: Measured radiation pattern of the cylindrical DRA

In the following section, the broadside design shown above is transformed into a wideband, conical beam design.

4.3 LOW Q_r / WIDE BAND DESIGN: DESIGN 1

The schematic diagram of the cylindrical DRA for achieving a low radiation Q (Q_r) is shown in Figure 4. The dimensions are as given in the previous section. The new parameter introduced here is a vertical branch of height h on which the microstrip line is terminated. The DRA is oriented with its axis along the Y -direction and a vertical branch, which is cut from a conducting tape, is attached to the DRA surface and is connected electrically to the tip of the feed line as shown in the figure.

By adjusting the parameter h , good impedance matching can be obtained in the same way as that for a broadside mode DRA. This particular design will be termed as design 1 in all the following sections.

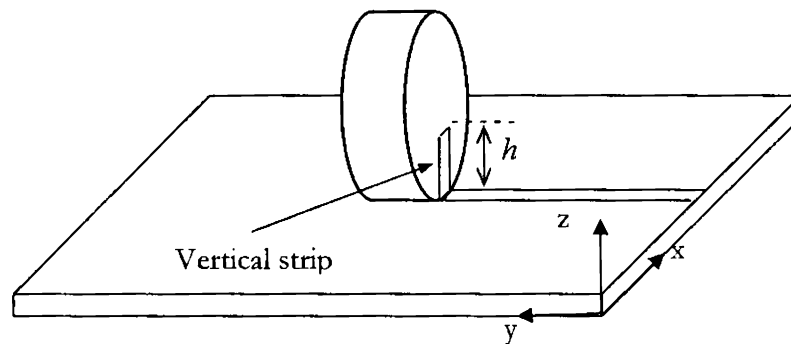


Figure 4: Wideband design of the cylindrical DRA

4.4 RESULTS

Figure 5 shows the measured return loss of the DRA design 1, for various values of h from 5 to 13 mm. It is clear that the impedance matching is very

Experimental Analysis

sensitive to the parameter h . For $h = 9$ mm, a maximum impedance bandwidth of 1120 MHz or 35.94 % from 2.556 to 3.676 GHz is observed. Bandwidth in percentage is calculated with respect to the centre frequency of the -10 dB band, which is 3.116 GHz. A minimum return loss of -42 dB is obtained at 3.2 GHz.

The wideband effect of design 1 is verified by simulation and the results are shown in Figure 6. Simulated resonant frequency is 3.23 GHz and bandwidth is 1150 MHz or 36.45 % (2.58 to 3.73 GHz) which are in good conformity with the measured values.

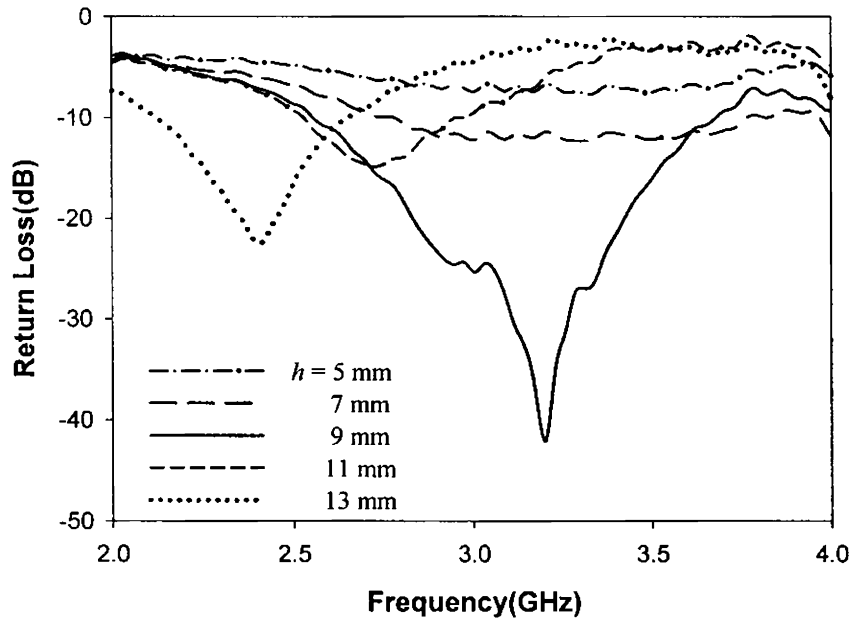


Figure 5: Measured return loss of the DRA for various strip heights (h)

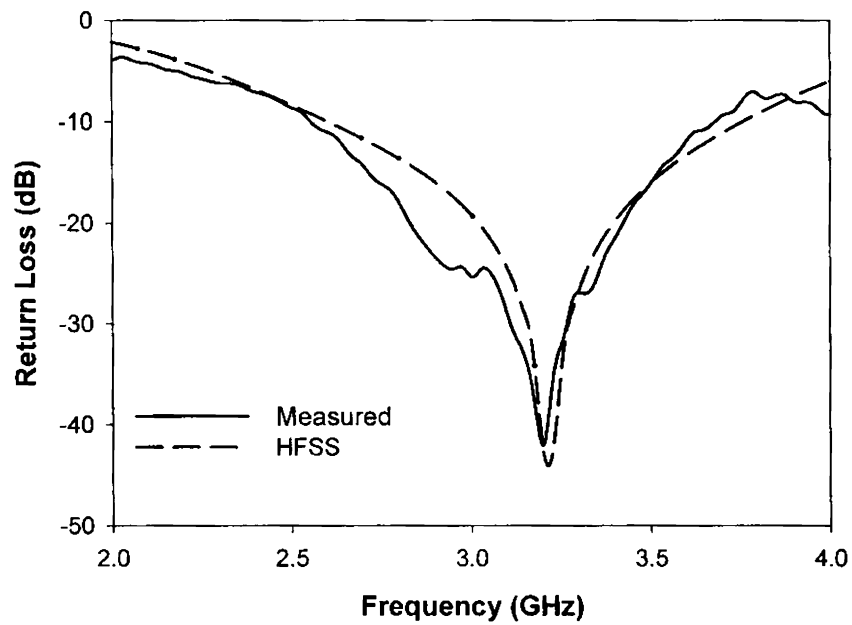


Figure 6: Measured and simulated return loss of DRA, for $h = 9$ mm

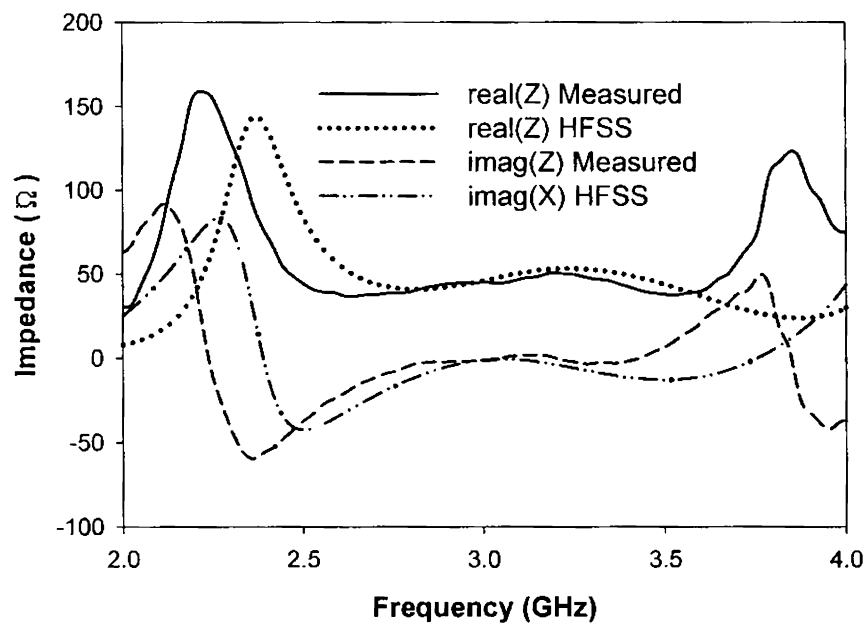


Figure 7: Measured and simulated input impedance of DRA,
for $h = 9$ mm

Measured and simulated input impedances of the DRA shown in Figure 7, justify good and steady matching over the band. The radiation patterns of the DRA are measured at 3.2 GHz and are shown in Figure 8.

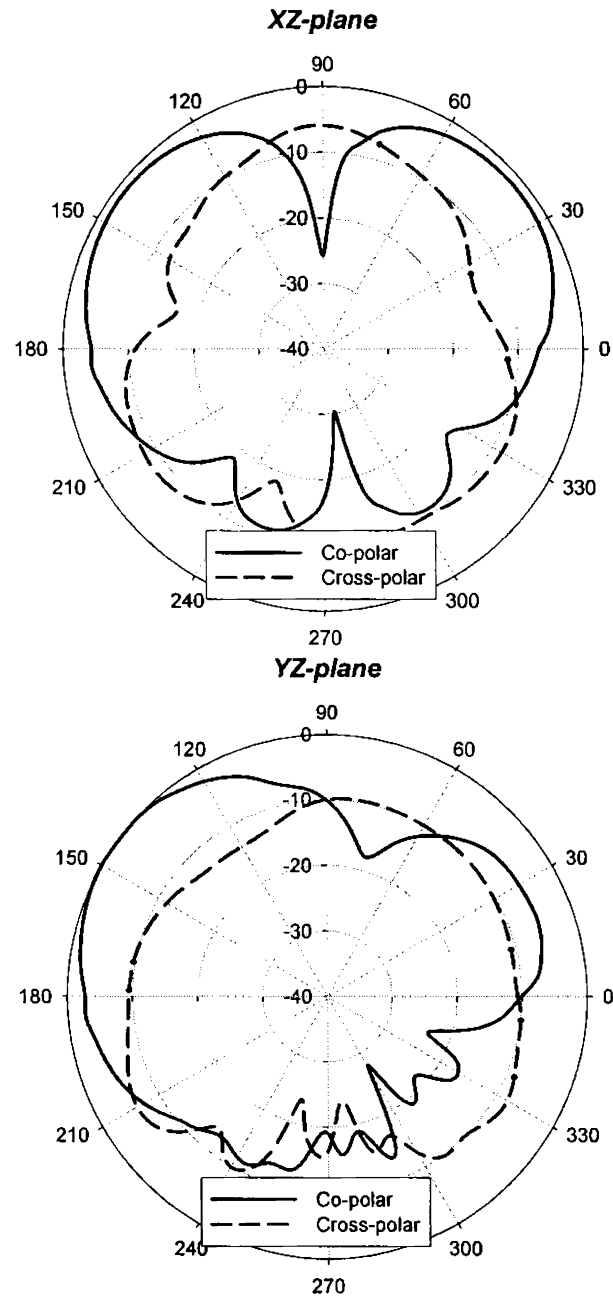


Figure 8: Measured 2-D radiation patterns of the DRA at 3.2 GHz,
for $h = 9$ mm

As evident from the patterns, the XZ -plane pattern is symmetric and conical in nature with a null of -24.71 dB occurring at the boresight or zenith ($\theta = 90^\circ$) and the maximum radiation at $\theta = 145^\circ$. The cross-polarisation is -12.42 dB in the direction of maximum radiation and -4.92 dB in the boresight. This high cross-polarisation in the boresight is due to the vertical strip, that may radiate as a monopole antenna in the similar way as for a probe coupled DRA. On the other hand, the YZ -plane pattern shows an asymmetry with a boresight null of -10.12 dB and the maximum radiation at 150° . The asymmetry is due to the effect of the coaxial cable and the connector, attached to the feed end of the DRA. The cross-polar level is around -10 dB in the boresight as well as in the peak radiation directions.

Stability of the radiation pattern over the impedance band is further studied by comparing the patterns at different frequencies in the band. The co-polar patterns for three different frequencies viz. 2.6, 3.2 and 3.6 GHz in the band are shown in Figure 9. Cross-polar patterns are simply excluded for better differentiation of the individual plots. It is clear that the symmetry and conical nature of the XZ -plane patterns are preserved in the matching band, but the pattern distortion in the YZ -plane becomes worse as moved from the lower end to the higher end of the band. This is because, the disturbance caused by the cable and the connector on the radiation increases with the frequency.

Simulated 3-D gain patterns are shown in Figure 10, which clearly show the pattern distortion or squint in the band. Measured gain is 2.98 dBi at the

Experimental Analysis

resonant frequency of 3.2 GHz, while the peak value in the band is 4.34 dBi measured at 3.48 GHz.

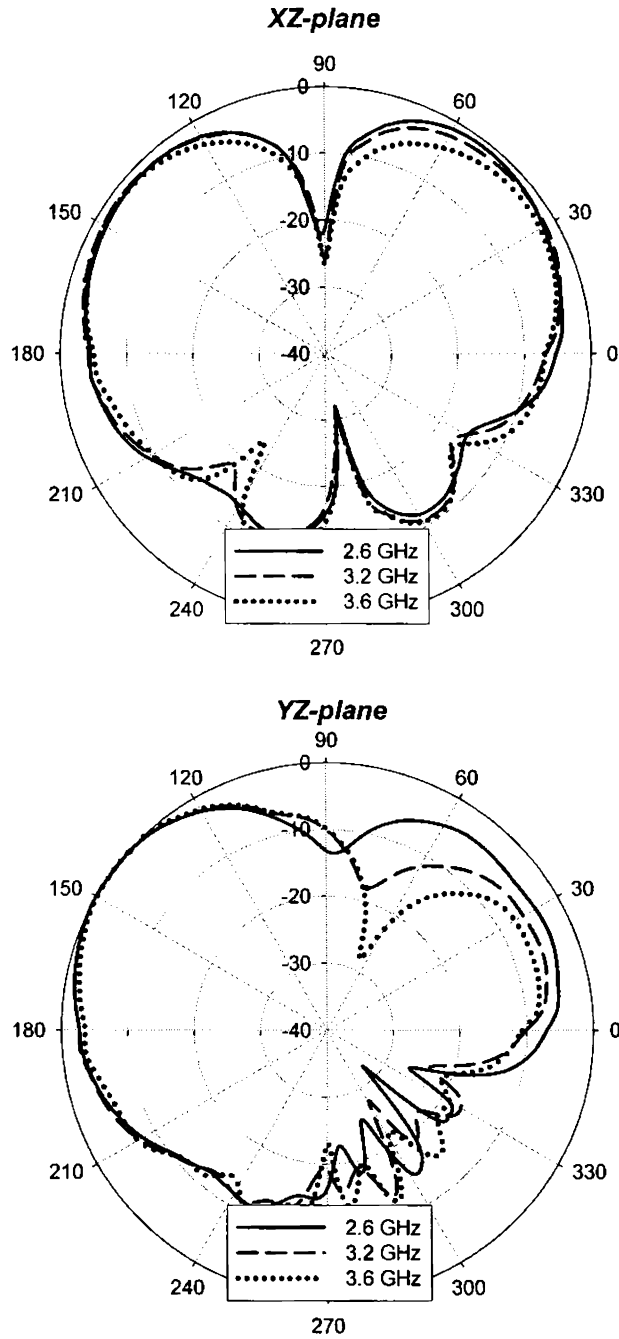


Figure 9: Measured 2-D radiation patterns of the DRA at different frequencies in the band, for $h = 9$ mm

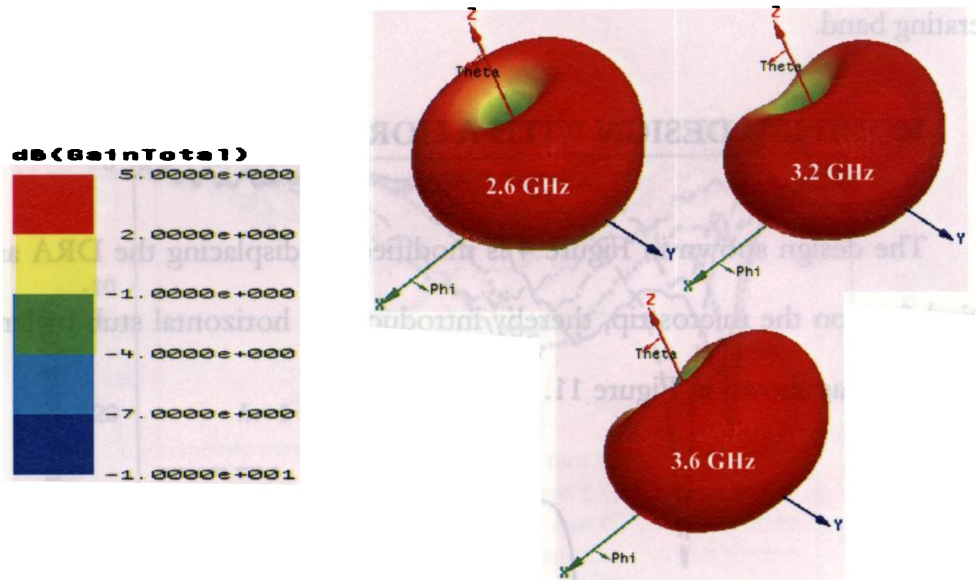


Figure 10: Simulated 3-D gain patterns of the DRA

As obvious from Figure 5, the wideband performance depends only on the parameter h . Also a change in the center frequency of the operating band requires a change in the DR properties. Thus design 1, though simple and easy to implement, lacks in some free and flexible means for tuning the operating band over a considerable range.

Incorporation of metallic sections on the feed as tuning stubs has been shown to be a potential means for tuning the impedance matching [7] of DRAs. In the present context, instead of fabricating additional metallic elements on the feed, a new approach is used to modify the design 1, wherein the vertical feed position is displaced backward from the strip end in order to add a microstrip stub of length L to the design. As will be shown, the combination of the feed height h

and stub length L effectively helps to tune the impedance matching as well as the operating band.

4.5 MODIFIED DESIGN WITH A HORIZONTAL STUB: DESIGN 2

The design shown in Figure 4 is modified by displacing the DRA and the vertical feed on the microstrip, thereby introducing a horizontal stub of length L in the design as shown in Figure 11.

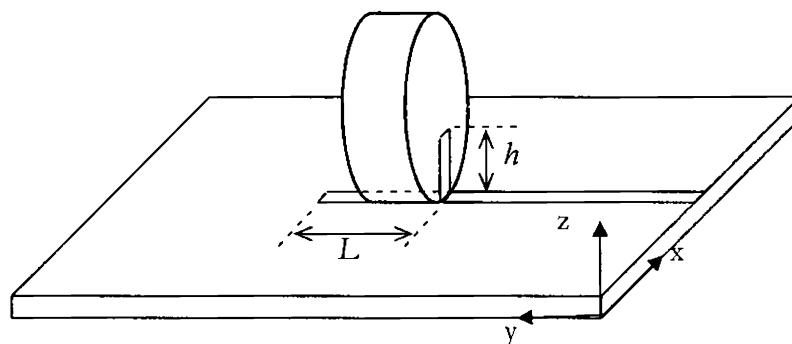
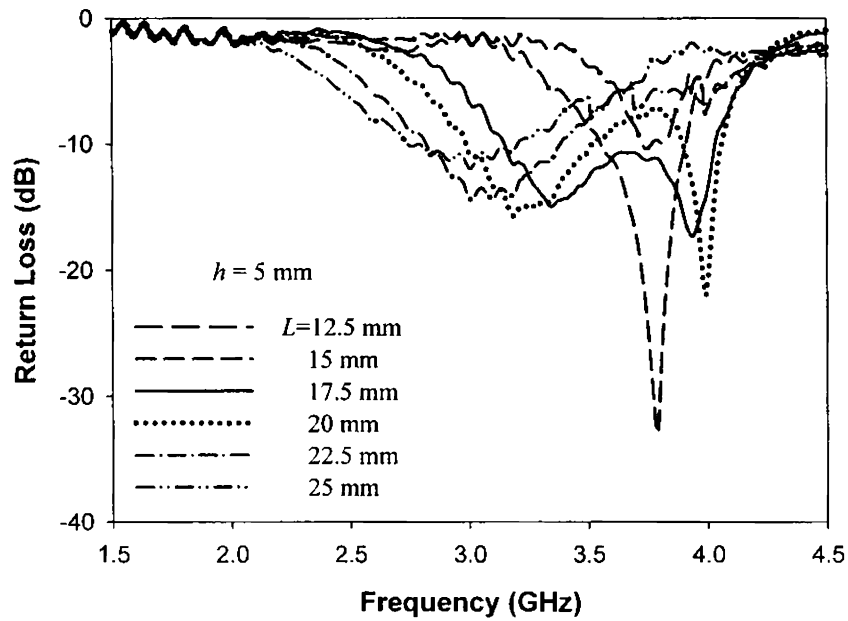


Figure 11: Modified wideband DRA design

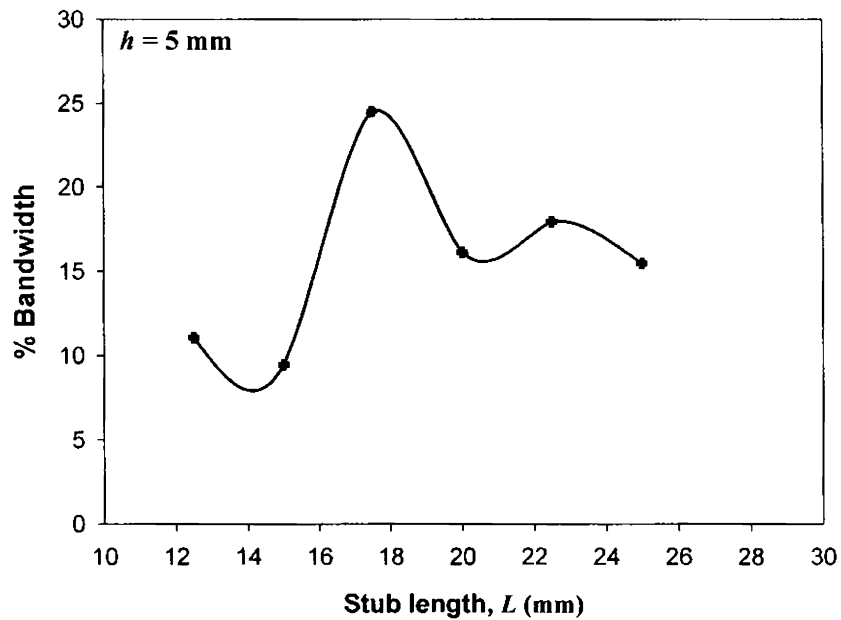
4.6 RESULTS

Plots of the measured return loss of the DRA for various strip heights (h) and stub lengths (L) for a width same as that of the microstrip are shown in Figures 12 (a), (c), (e) and (g). As the figures show, for a given h , an optimum value of L gives the maximum -10 dB bandwidth. As h is increased, the band is shifted to a lower frequency range for a given L value. The bandwidth variations with h and L are depicted in Figures 12 (b), (d), (f), and (h). The parameter L thus

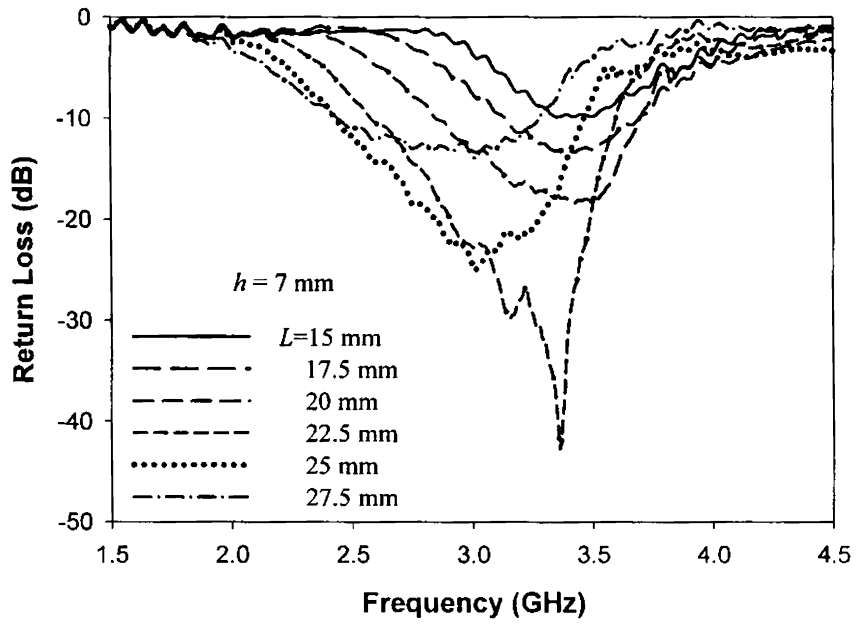
provides an additional freedom for effectively tuning the impedance and reflection characteristics of the DRA.



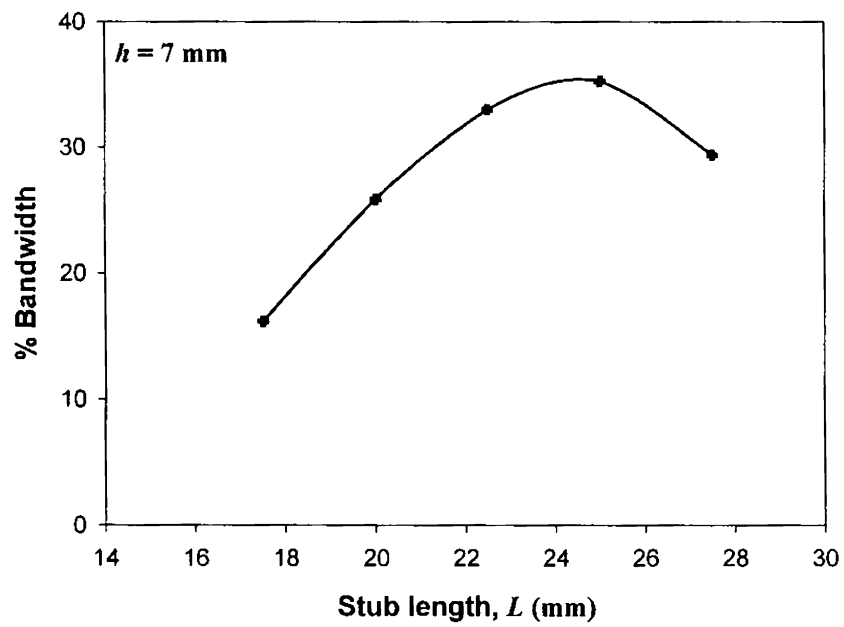
(a)



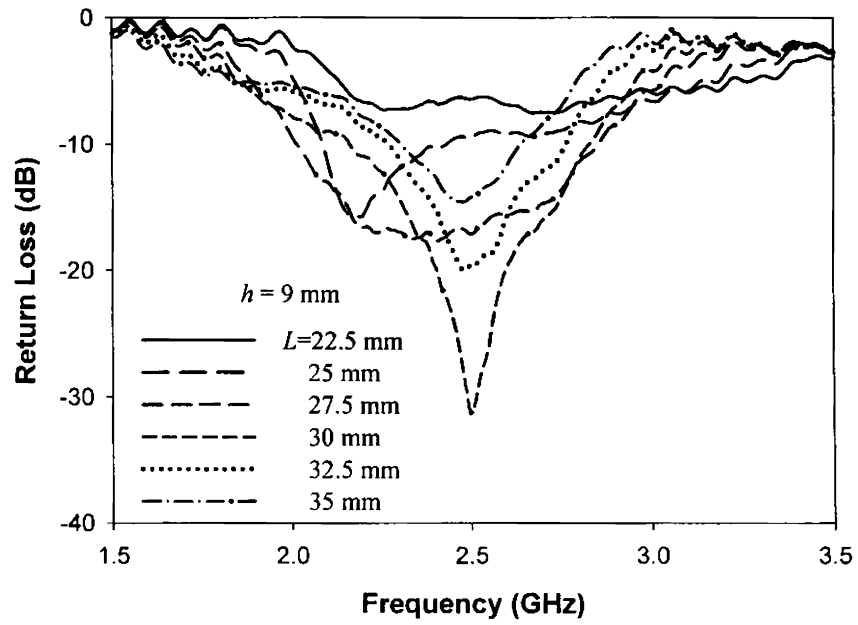
(b)



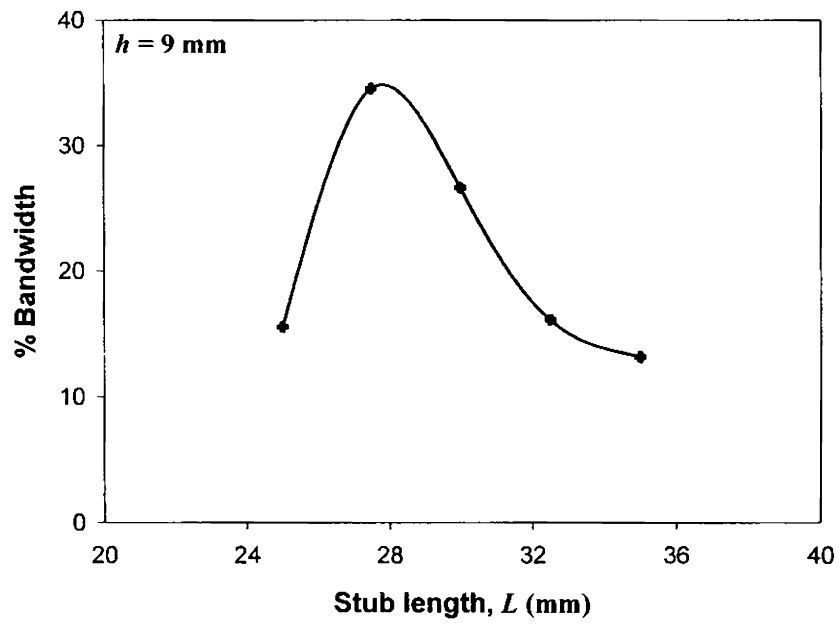
(c)



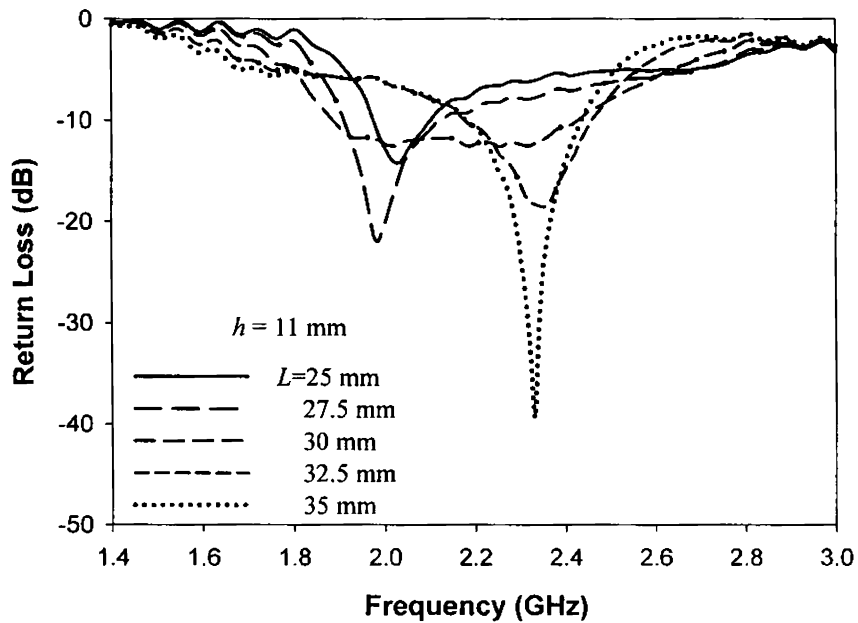
(d)



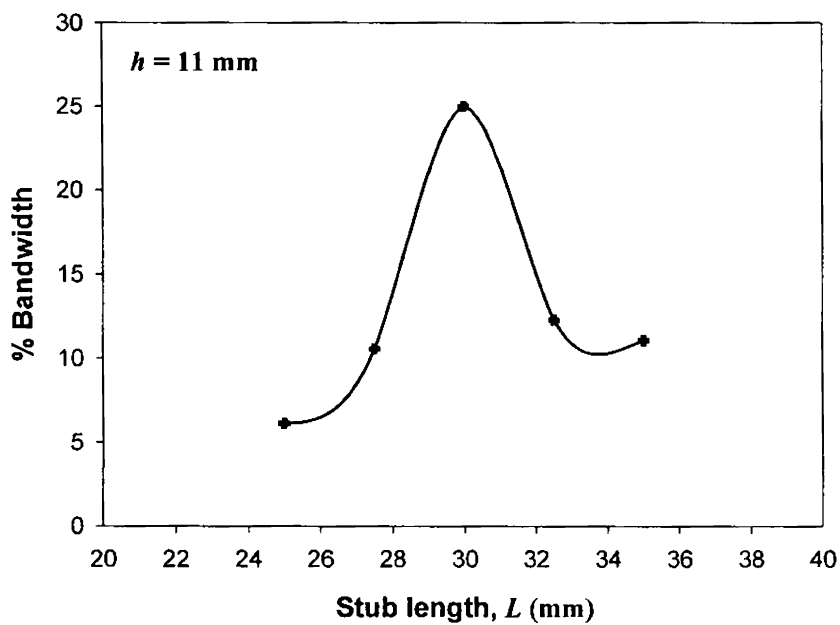
(e)



(f)



(g)



(h)

Figure 12 (a) - (h): Variation in return loss and bandwidth of the DRA with h and L

Summary of the reflection characteristics of the wideband DRA obtained from Figure 12 is given below.

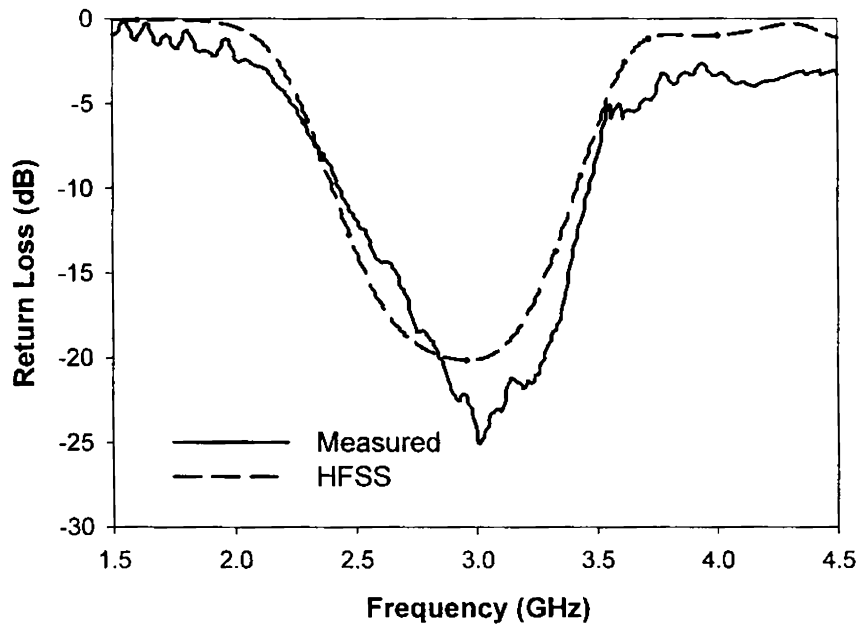
Table 1: Reflection characteristics of the DRA for optimum h and L

Strip height (h , mm)	Stub length (L , mm)	-10dB Frequency range (GHz)	Mid-band frequency (GHz)	Bandwidth (MHz)	% Bandwidth
5	17.5	3.15 – 4.03	3.59	880	24.51
7	25	2.43 – 3.47	2.95	1040	35.25
9	27.5	2.01 – 2.85	2.43	840	34.57
11	30	1.89 – 2.43	2.16	540	25

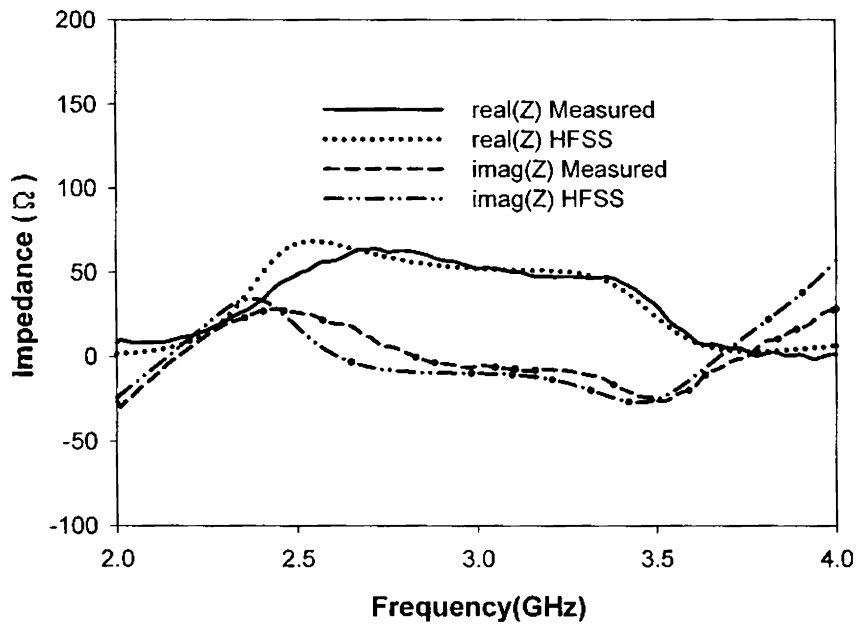
From the measured results of Table 1, optimum values of h and L can be expressed empirically as

$$h \approx \frac{\lambda_0}{3\sqrt{\epsilon_{rd}}} \quad \text{and} \quad L \approx \frac{\lambda_0}{\sqrt{\epsilon_{rd}}} \quad (4.2)$$

where λ_0 is the free space wavelength at the mid band frequency and ϵ_{rd} the dielectric constant of the DRA. Here, the designs with $h = 7$ mm, $L = 25$ (design 2a) and $h = 9$ mm, $L = 27.5$ mm (design 2b) are chosen for further analysis since these provide the broadest bandwidths in excess of 30 %. The other two designs ($h = 5$ mm, $L = 17.5$ and $h = 11$ mm, $L = 30$) will be treated later. Figure 13 compares the measured and simulated return loss and input impedance of the DRA for design 2a.



(a)



(b)

Figure 13: Measured and simulated (a) return loss (b) input impedance of the DRA, for design 2a ($h = 7$ mm and $L = 25$ mm)

Simulated -10dB bandwidth is from 2.4 to 3.41 GHz (1010 MHz) or 34.77 % at the centre frequency of 2.905 GHz, which are in good agreement with the measured results shown in Table 1 that gives a 2.43 to 3.47 GHz or 35.25 % band.

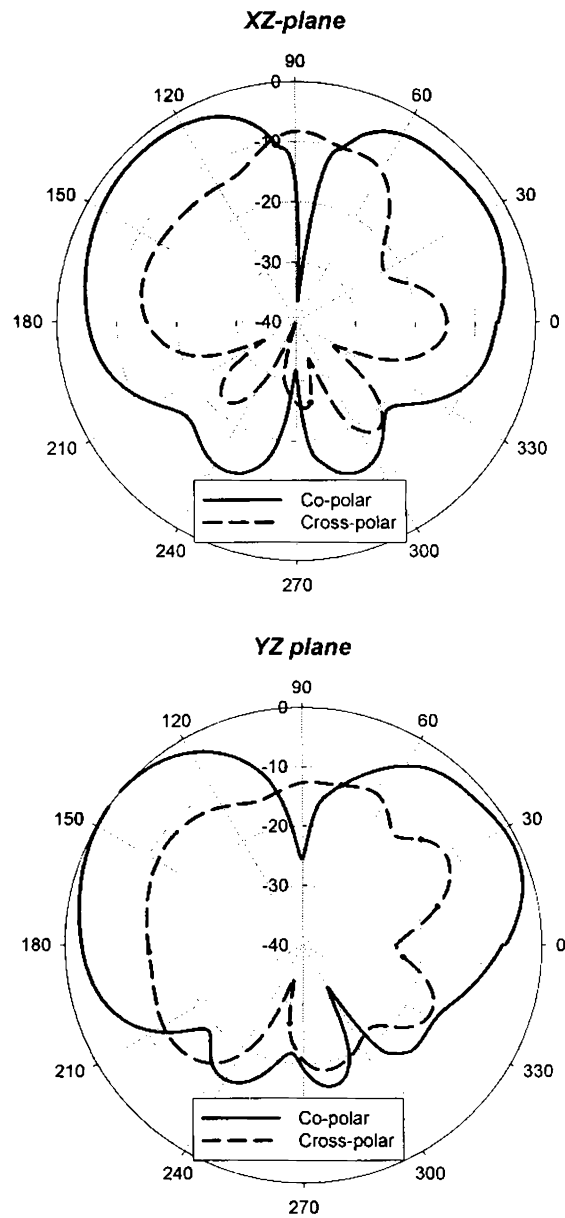


Figure 14: Measured radiation patterns at 3.01 GHz, for design 2a

Two dimensional radiation patterns measured at 3.01 GHz that corresponds to the minimum measured return loss in Figure 13 (a) are shown in Figure 14.

As observed from the radiation patterns, the conical nature is maintained in both *XZ* and *YZ*-planes than that of the design discussed in the previous section (design 1). The boresight nulls are of -36.67 dB and -24.56 dB in the *XZ* and *YZ*-planes respectively. Cross-polar levels are of -6.31 dB and -12.73 dB at the boresight respectively for the *XZ* and *YZ*-plane patterns. Peak radiation occurs at 130° and 150° respectively in the *XZ* and *YZ*-planes, with the corresponding cross-polarisations of -14.12 dB and -11.84 dB. Gain measurements yielded 4.65 dBi at the resonant frequency of 3.01 GHz and the maximum gain in the band is 5.58 dBi at 3.4 GHz.

Figure 15 shows the measured co-polar patterns at the lower, mid and upper ends of the matching band respectively at 2.5, 3.01 and 3.4 GHz. It is clear that the symmetry and conical nature of the *XZ*-plane pattern is stable in the matching band similar to the previous design. However, the *YZ*-plane pattern is less distorted with the increase in frequency unlike that in design 1. This is further confirmed by the 3-D radiation patterns of Figure 16.

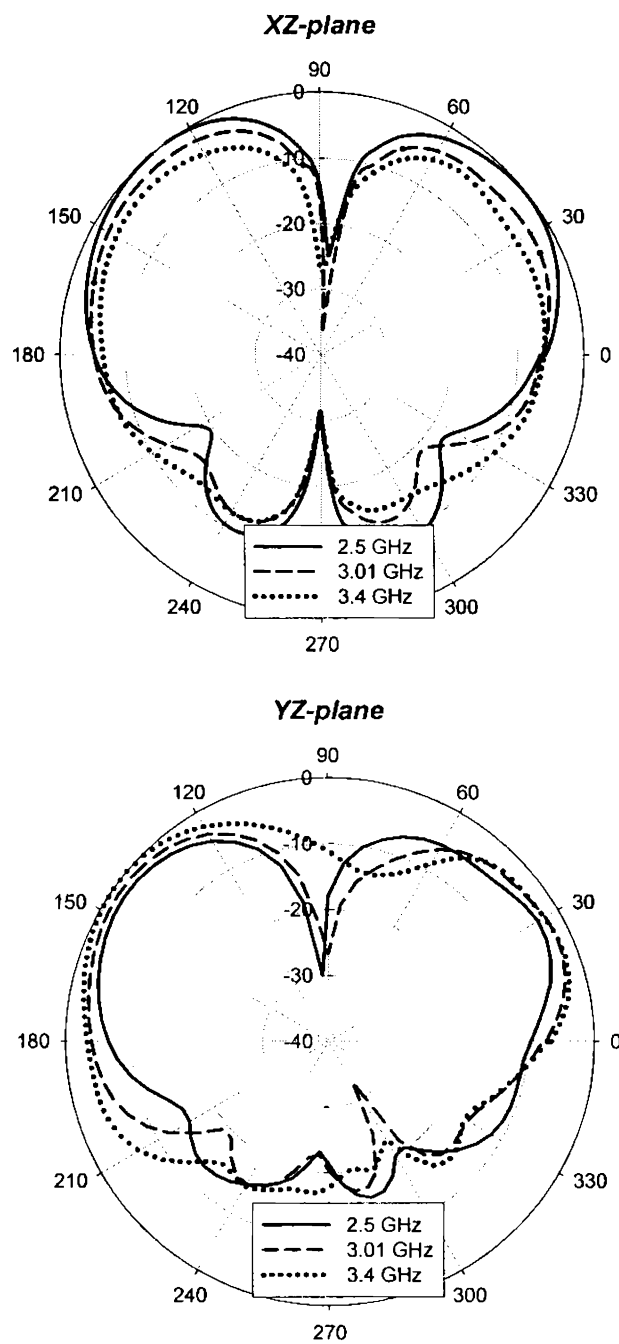


Figure 15: Measured 2-D radiation patterns of the DRA at different frequencies in the band, for design 2a

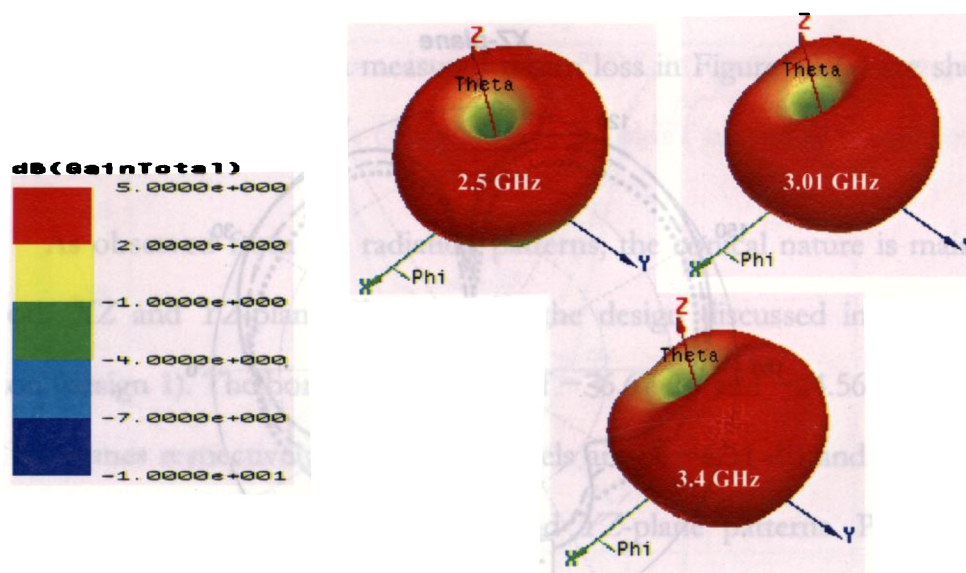
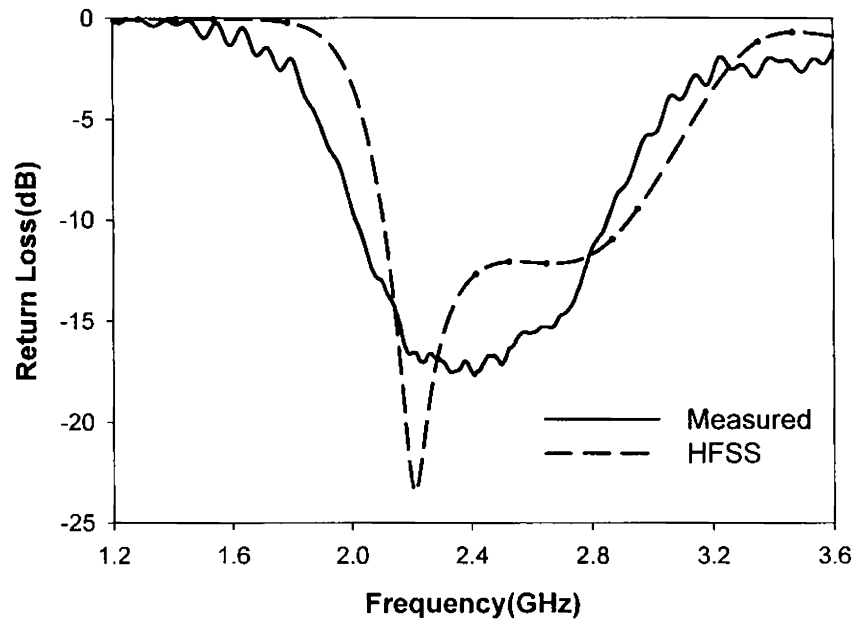
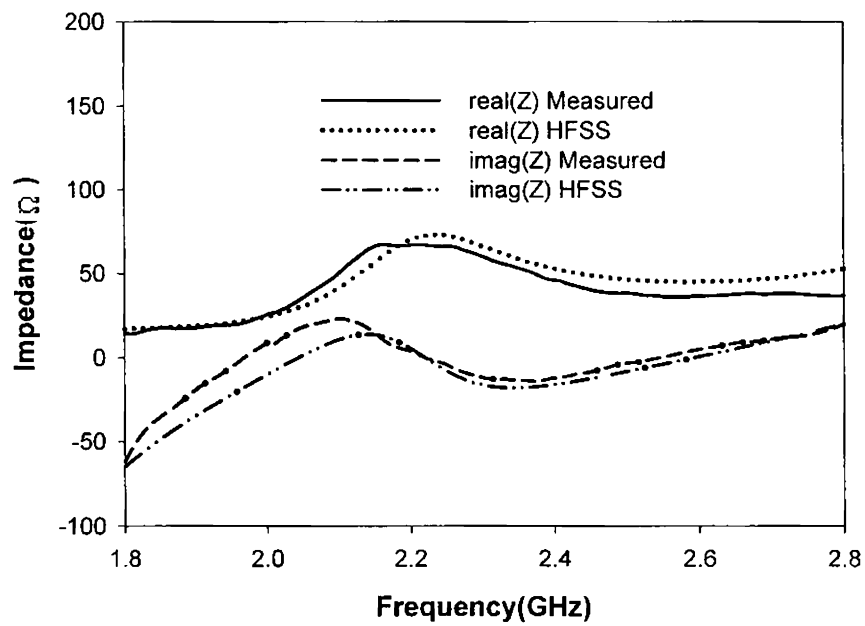


Figure 16: Simulated 3-D gain patterns of the DRA, for design 2a

For design 2b, the agreement between measured and simulated results is shown in Figure 17. Simulated bandwidth is 817 MHz or 32.42 % from 2.11 to 2.927 GHz at the mid-band frequency of 2.52 GHz, while that measured is 840 MHz or 34.57 % from 2.01 to 2.85 GHz.



(a)



(b)

Figure 17: Measured and simulated (a) return loss (b) input impedance of the DRA, for design 2b ($h = 9$ mm and $L = 27.5$ mm)

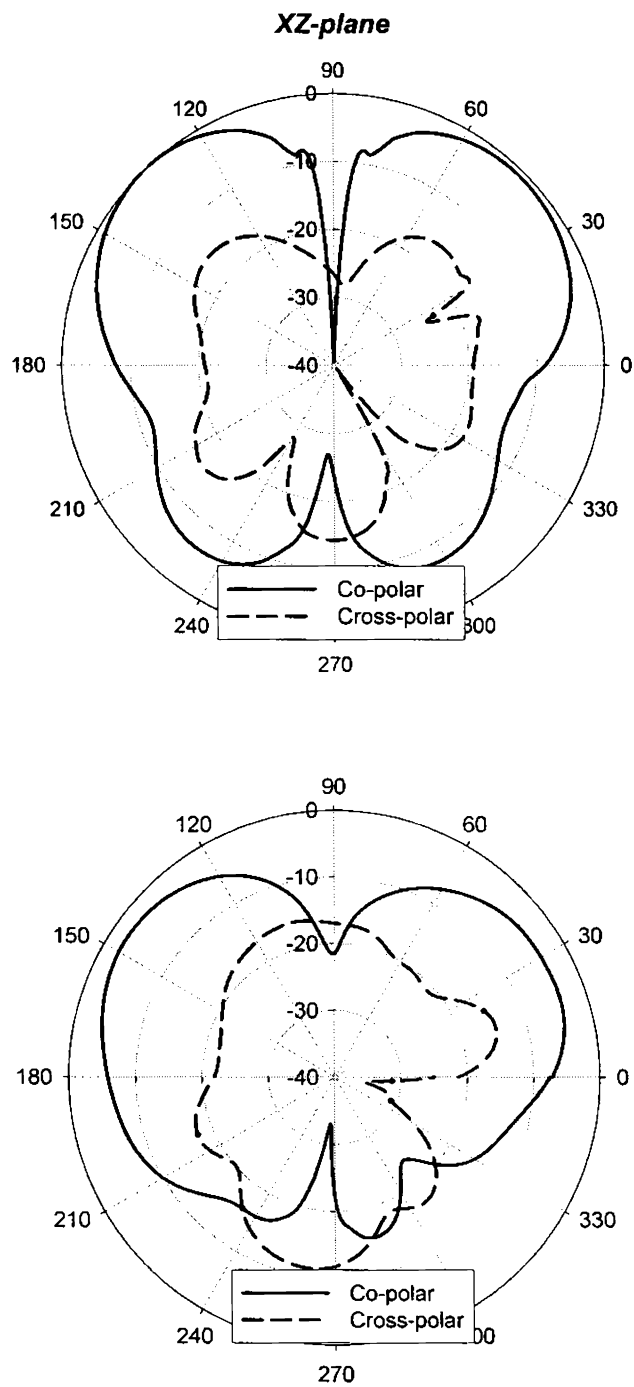


Figure 18: Measured radiation patterns at 2.43 GHz, for design 2b

Radiation patterns measured at 2.43 GHz, the centre frequency of the band are shown in Figure 18. XZ and YZ plane patterns are more symmetrical and conical shaped than those of the previous designs (design 1 and design 2a). The nulls are at -40 dB and -19.56 dB in the boresight for XZ and YZ-planes respectively. Cross-polar levels are of -26.5 dB and -14.93 dB respectively at the boresight for XZ and YZ-plane patterns. Peak radiation occurs at 130° and 150° respectively in the XZ and YZ-planes, with the respective cross-polarisations of -14.73 dB and -21.47 dB. Measured mid-band gain is 4.39 dBi and the maximum measured value in the band is 5.57 dBi at 2.36 GHz.

From the 2-D patterns measured for different frequencies, at 2.15, 2.43 and 2.8 GHz shown in Figure 19, it is clear that the design 2b produces good conical radiation patterns over the matching band. Simulated 3-D radiation patterns shown in Figure 20 also confirm the pattern stability over the band.

Measured far-field transmission coefficients ($|S_{21}|$) in the direction of maximum radiation of the DRAs so far studied are compared in Figure 21. It is clear that peak $|S_{21}|$ corresponding to design 1 is lower than that of any other designs in their respective bands, hence results in the lowest gain of all. The peak gain of the broadside DRA is comparable to that of design 2. Table 2 compares the various aspects of the wideband designs so far described.

Radiation patterns at other two combinations of h and L , i.e. $h = 5$ mm, $L = 17.5$ and $h = 11$ mm, $L = 30$, shown in Table 1, were also measured. The patterns measured at the centre frequencies of the corresponding bands i.e. 3.59

Experimental Analysis

GHz and 2.16 GHz respectively, are shown in Figure 22. As observed, the conical nature of the patterns is much deteriorated at the higher frequency (3.59 GHz). Also these designs provide maximum gains around 4 dBi.

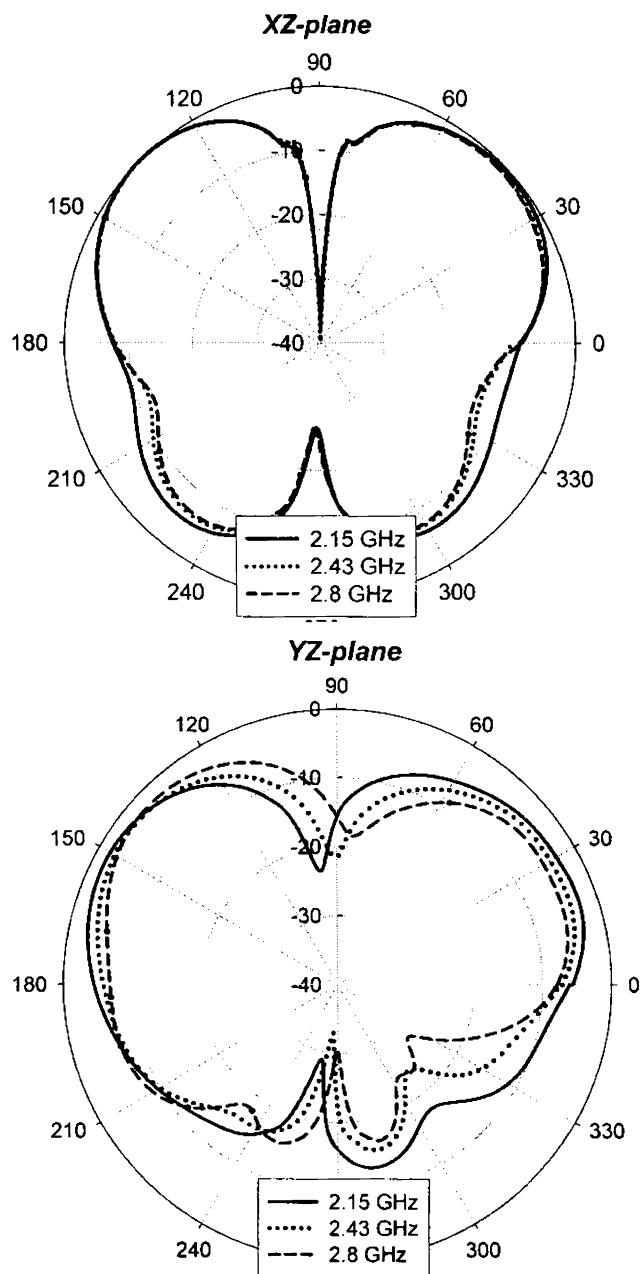


Figure 19: Measured 2-D radiation patterns of the DRA at different frequencies in the band, for design 2b

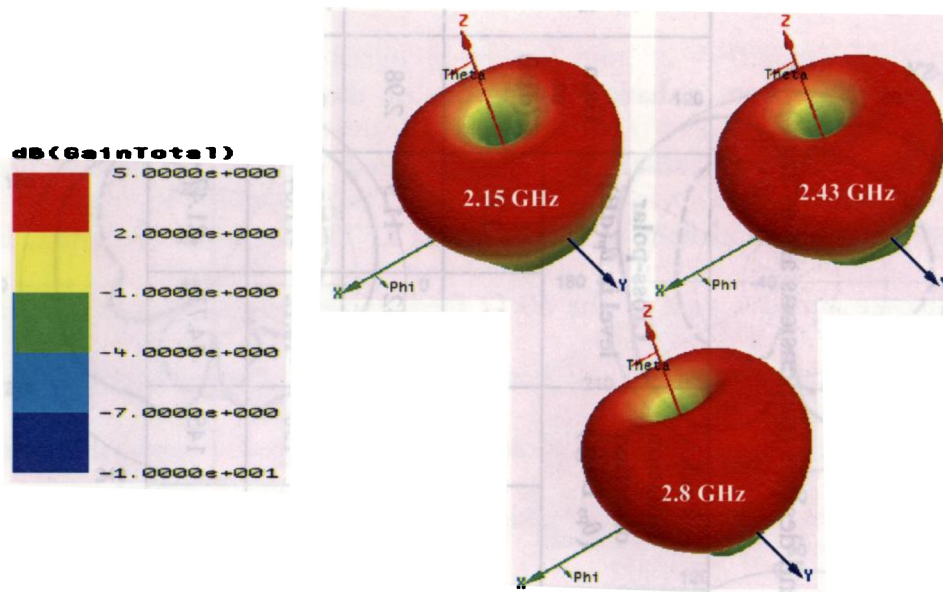


Figure 20: Simulated 3-D gain patterns of the DRA for design 2b

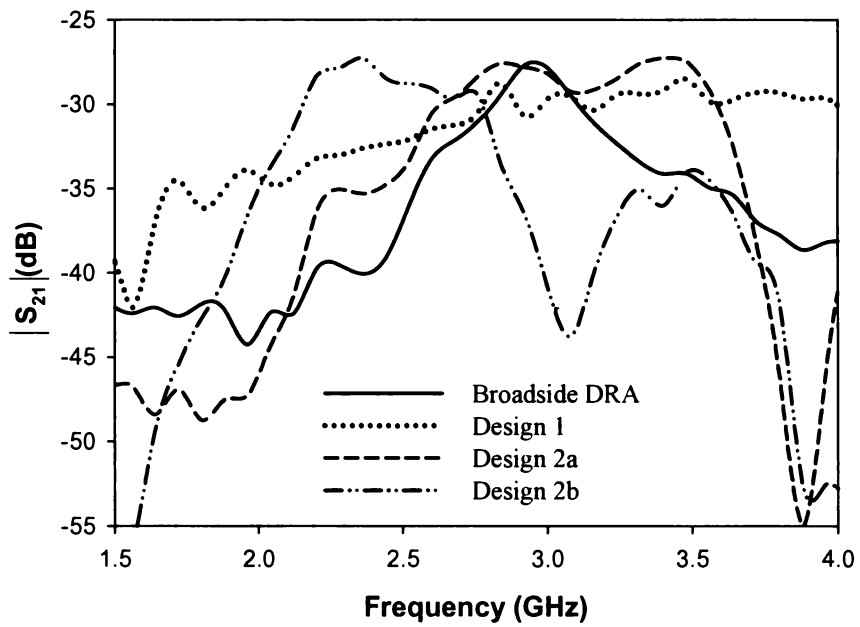


Figure 21: Comparison of the far-field $|S_{21}|$ of the DRAs

Table 2: Comparison of the results of the wideband designs (dimensions are in 'mm')

Design parameters (h, L - mm)	-10 dB band (GHz, %)	Frequency of interest (f_0 , GHz)	Boresight null level (dB)		Boresight Cross-polar level (dB)		Peak radiation direction (θ_p , Deg.)		Cross-polar level in θ_p (dB)		Gain at f_0 (dBi)	Maximum gain in the band (dBi)
			XZ- <i>plane</i>	YZ	XZ	YZ	XZ	YZ	XZ	YZ		
Design 1 (9,0)	2.556 – 3.676, 35.94	3.2	-24.71	-10.12	-4.92	-10	145	150	-12.42	-11.5	2.98	4.34 (at 3.48 GHz)
Design 2a (7,25)	2.43–3.47, 34.25	3.01	-36.67	-24.56	-6.31	-12.73	130	150	-14.12	-11.84	4.65	5.58 (at 3.4 GHz)
Design 2b (9,27.5)	2.01–2.85, 34.57	2.43	-40	-19.56	-26.5	-14.93	135	145	-14.73	-21.47	4.39	5.57 (at 2.36 GHz)

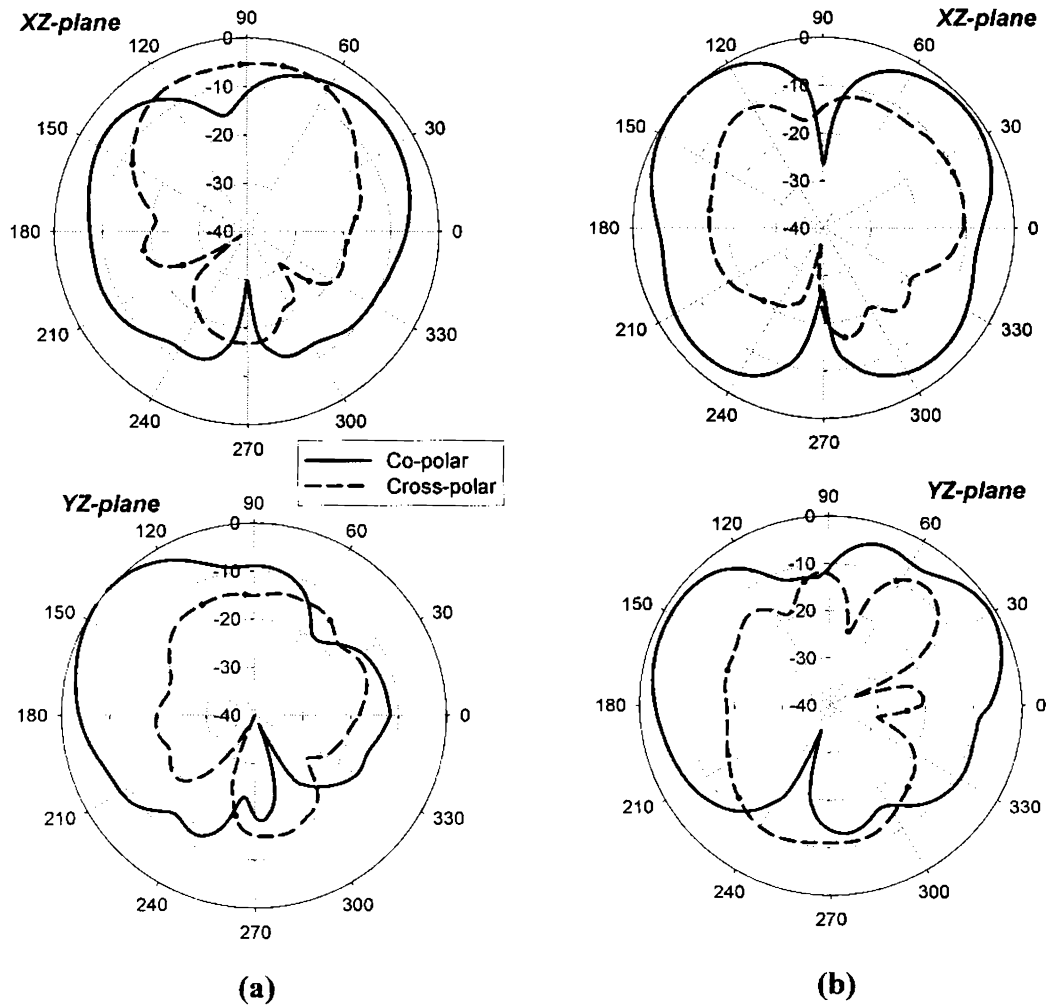


Figure 22: Measured radiation patterns for (a) $h = 5$ mm, $L = 17.5$ at 3.59 GHz

(b) $h = 11$ mm, $L = 30$ at 2.16 GHz

4.7 RADIATION FROM THE ANTENNA FEED

In this section, radiation properties of the wideband antenna feed are studied. As described earlier, the antenna feed consists of two sections of microstrip transmission lines of length h and L . The section of length L lies on the substrate and is a part of the 50Ω feed. However, the section of height h extends vertically into the air, and hence can act as a vertical monopole radiator under the influence of the large ground plane. Figure 23 shows the simulated resonance curves of the feeds with various dimensions.

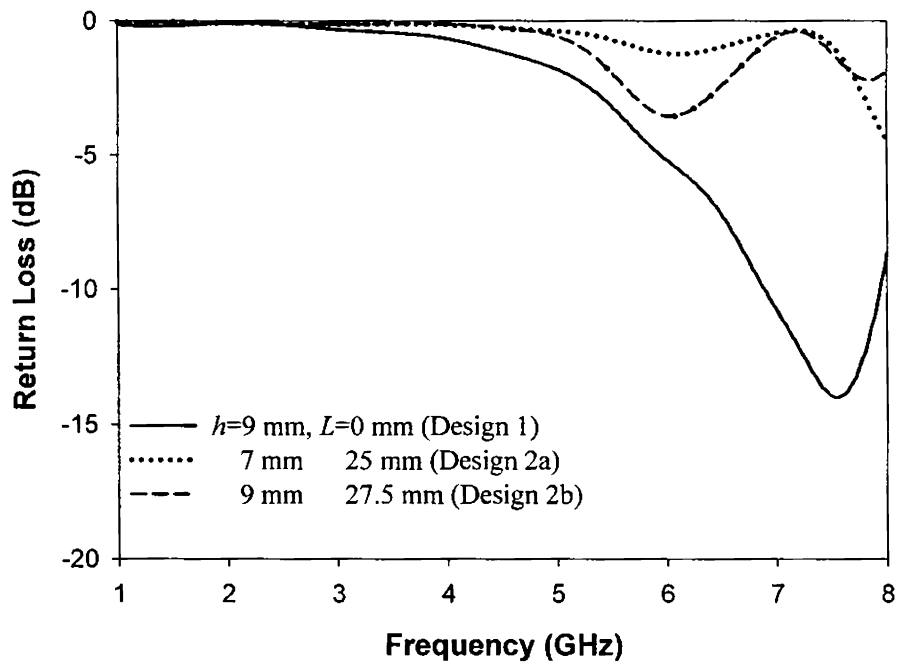


Figure 23: Simulated return loss of the feed

As can be observed from the figure, a -14 dB deep resonance exists at 7.55 GHz for the feed of design 1 ($h = 9$ mm, $L = 0$ mm). This value is approximately equal to the resonant frequency of a $\lambda/4$ monopole of length $h = 9$ mm. Simulated 3-D radiation pattern at 7.55 GHz is given in Figure 24.

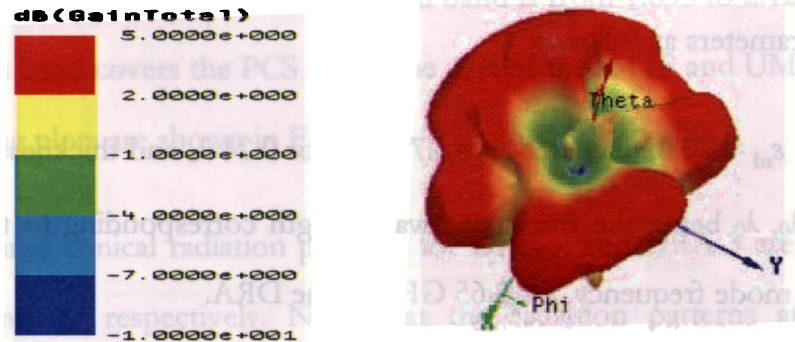


Figure 24: Simulated radiation pattern of the feed at 7.55 GHz

As observed from the above figure, the radiation pattern is not of a well defined shape, so that it can hardly be used for any application purpose. This monopole radiation can influence the radiation performance of the DRA if the operating band includes the monopole band also, which could happen when using DRs with low value of dielectric constant (ϵ_{rd}). This is because, firstly, a higher value of h will be needed for better impedance matching of a low ϵ_{rd} DR, and hence the monopole resonance will occur at a frequency lower than that in the present case ($h = 9$ mm). Secondly, the DR will operate at a higher frequency because of the low ϵ_r . Consequence is an effective resonating band, merged by the individual bands of the DR and the monopole at the lower and the higher ends

respectively, with the radiation pattern distorted towards the higher end of the band.

4.8 WIDEBAND DESIGN USING OTHER DRs – RESULTS

Validity of the wideband design (Design 2) is verified using other DRs also having parameters as follows:

(1) **DR-2:** $\epsilon_{rd} = 20.8$, diameter $2a = 27.3$ mm or $0.24 \lambda_0$ and thickness $d = 8.4$ mm or $0.074 \lambda_0$, λ_0 being the free space wave length corresponding to the measured broadside mode frequency, $f = 2.65$ GHz of the DRA.

(2) **DR-3:** $\epsilon_{rd} = 88.68$, diameter $2a = 24$ mm or $0.166 \lambda_0$ and thickness $d = 7.8$ mm or $0.054 \lambda_0$, λ_0 corresponds to the measured broadside mode frequency, $f = 2.04$ GHz of the DRA.

The antennas using the above DRs (1) and (2) will be referred respectively as DRA-1 and DRA-2 in the following discussion. HFSS™ simulation is used to optimise the design parameters to yield maximum matching bandwidth and the simulated return loss plots are presented in Figures 25 and 26 respectively for DRA-2 and DRA-3. Tuning of the impedance characteristics is appealing from Figures 25(a) and 26(a). For DRA-2, selection of $h = 10$ mm and $L = 31$ mm gives a bandwidth from 1.9 to 2.65 GHz or 33 %. Measured return loss is compared with the simulated one in Figure 25(b). A matching band from 1.849 to 2.549 GHz or 32 % is obtained for the measurement. This band covers some important wireless communication bands like PCS (1.85 to 1.99 GHz), UMTS (1.9

to 2.2 GHz), WiBro (2.3 to 2.39 GHz) and WLAN (ISM: 2.4 to 2.484 GHz) [Table 2, Chapter 1]. The above figure also shows two merged resonances, at 1.9 GHz and 2.41 GHz constituting the matching band.

For DRA-3, a maximum simulated bandwidth of 11.15 % is achieved for $h = 5$ mm and $L = 30$ mm, while the measured band is from 1.835 to 2.125 GHz or 14.65 %. This band covers the PCS and some part of the IMTS and UMTS bands. Corresponding plots are shown in Figure 26.

Measured conical radiation patterns for DRA-2 and DRA-3 are shown in Figure 27 and 28 respectively. Note that the radiation patterns at the two resonances, at 1.9 GHz and 2.41 GHz for DRA-2 are shown in Figure 27, revealing that both resonances have the same radiation characteristics. Measured gain is 3.74 dBi at 1.9 GHz and 3.95 dBi at 2.41 GHz. Also the maximum measured gain in the band is 4.71 dBi, at 2.3 GHz. For DRA-3, the radiation patterns at 1.945 GHz, which is the frequency giving minimum reflection and also is the mid-band frequency, are plotted in Figure 28. Gain measurement yielded a maximum gain of 3.88 dBi at 1.945 GHz, for DRA-3.

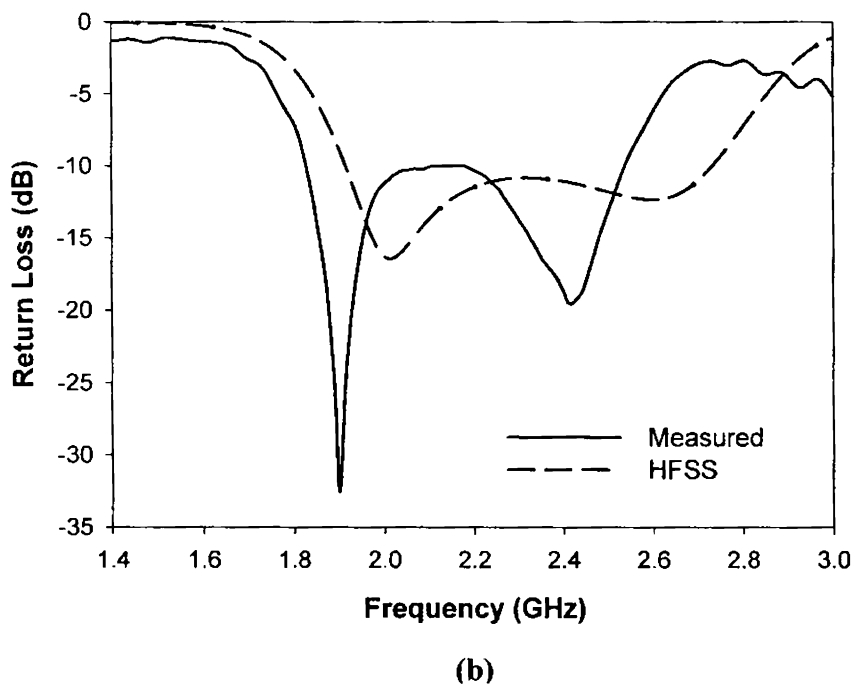
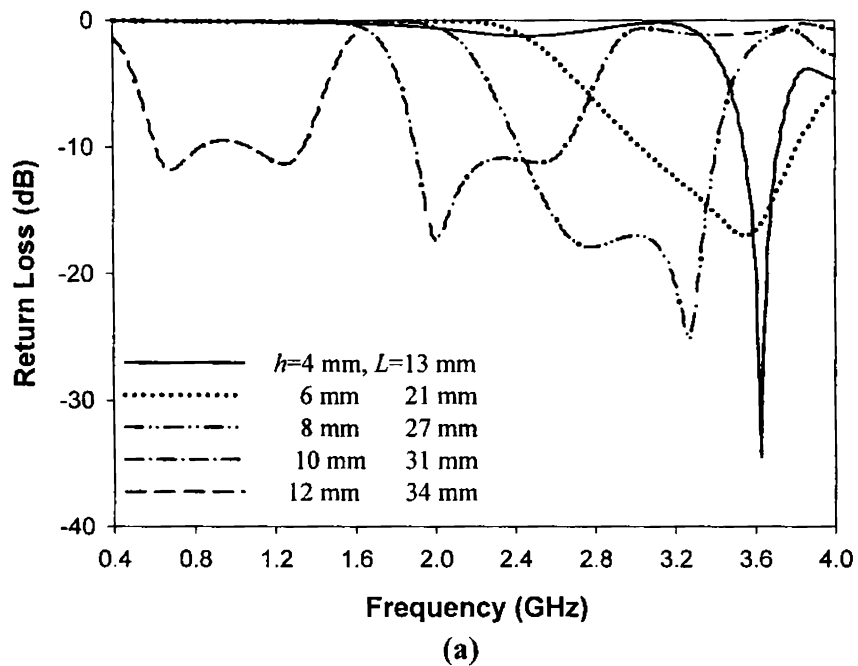
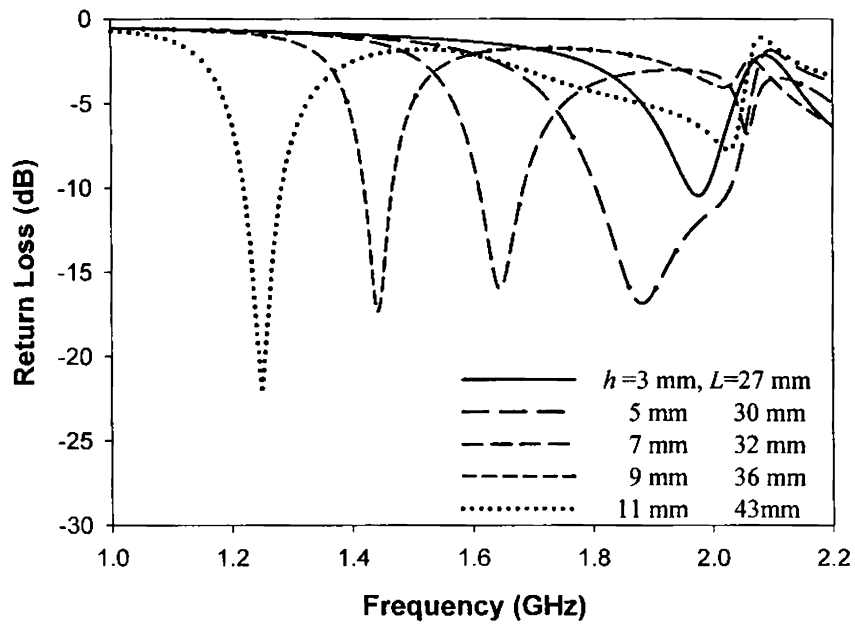
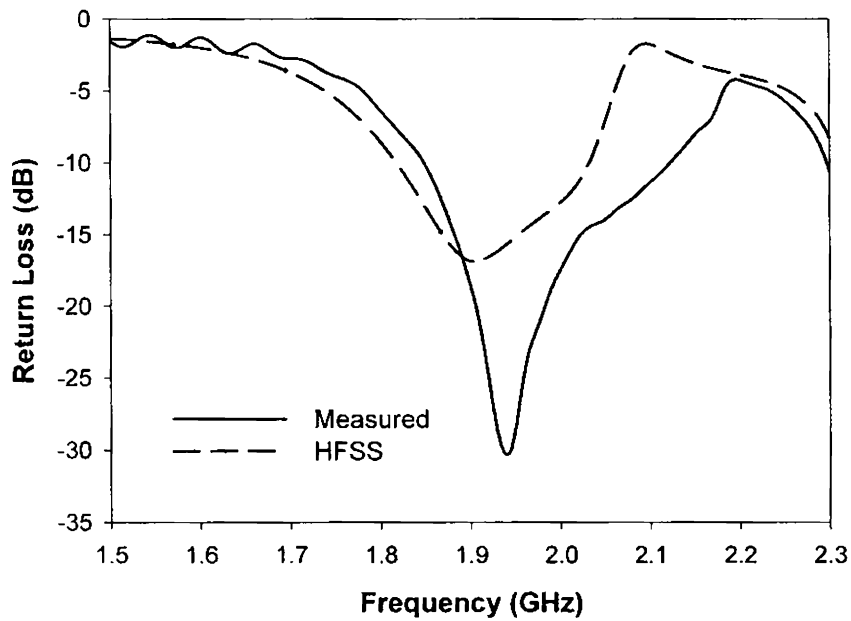


Figure 25: (a) Simulated return loss of DRA-2 for various h and L
 (b) Measured and simulated return loss for $h = 10$ mm and $L = 31$ mm



(a)



(b)

Figure 26: (a) Simulated return loss of DRA-3 for various h and L
 (b) Measured and simulated return loss for $h = 5$ mm and $L = 30$ mm

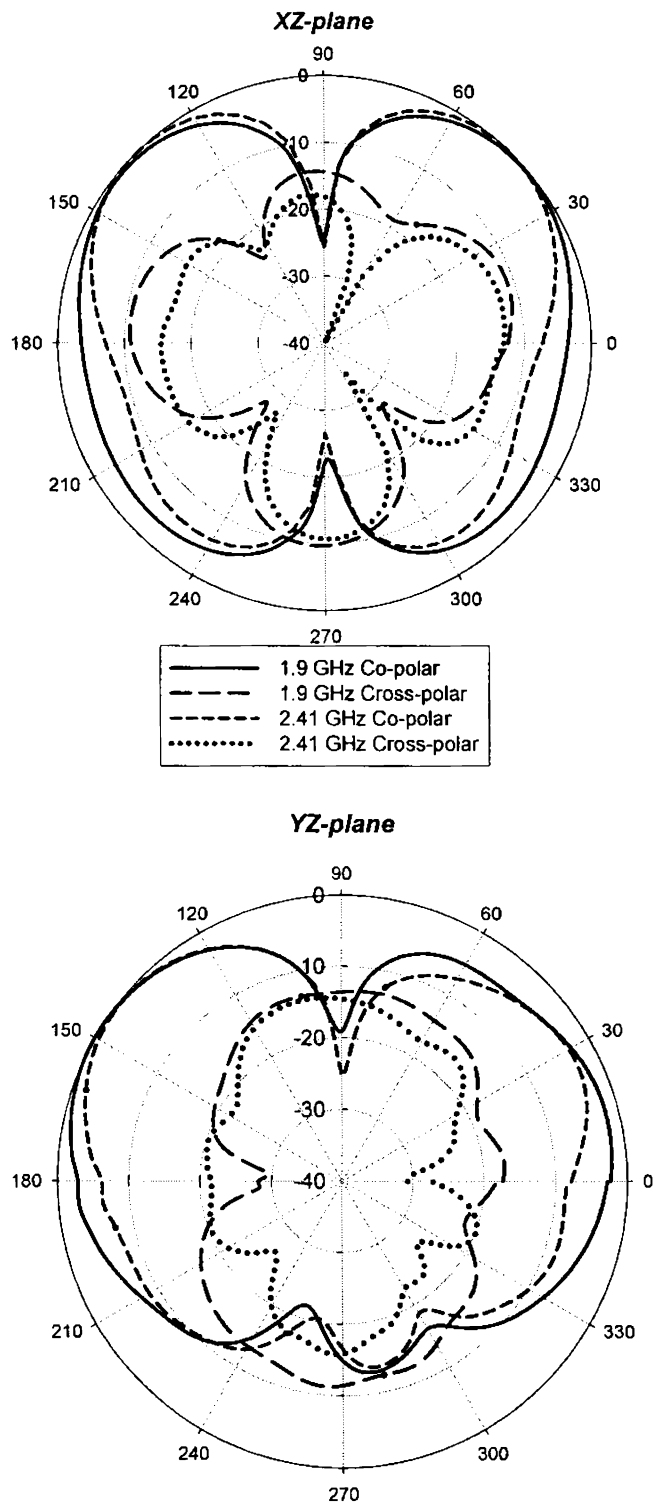


Figure 27: Measured radiation patterns for DRA-2

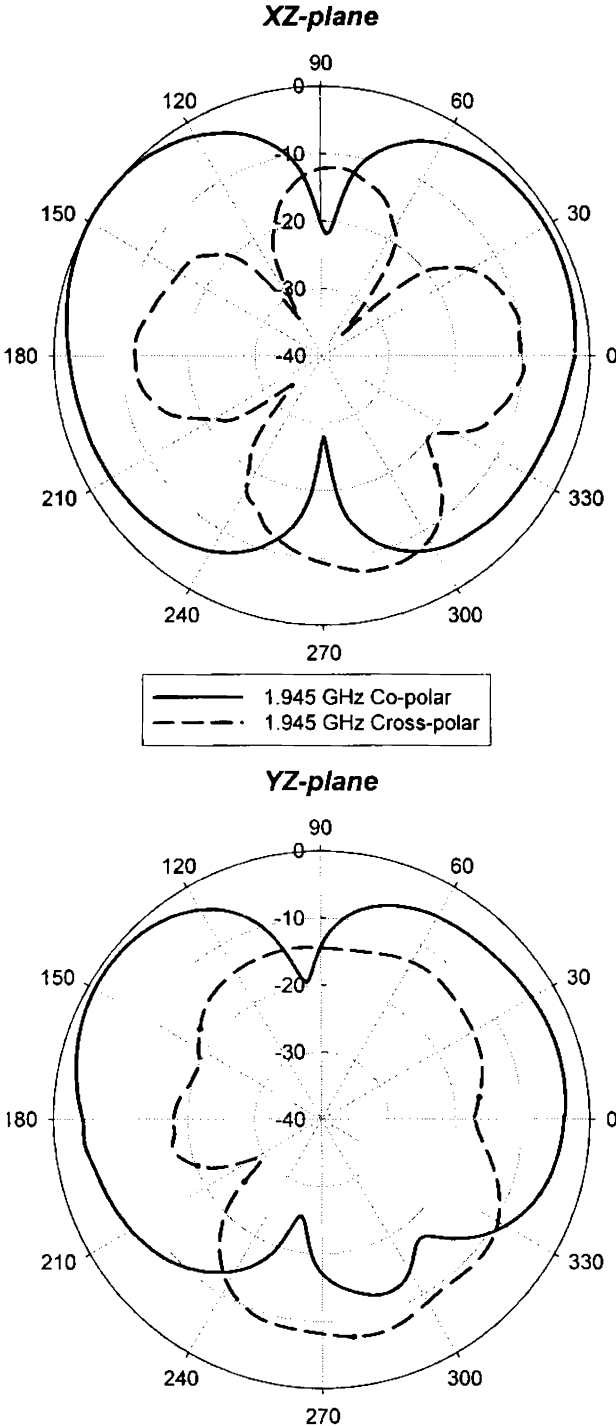


Figure 28: Measured radiation patterns for DRA-3

Table 3: Summary of the radiation properties of DRA-2 and DRA-3 (dimensions are in 'mm')

DRA with (ϵ_{rd} , $2a$, d , h , L)	-10 dB band (GHz, %)	Freq. of interest (f_0 , GHz)	Boresight null level (dB)		Boresight Cross- polar level (dB)		Peak radiation direction (θ_p , Deg.)		Cross-polar level in θ_p (dB)		Gain at f_0 (dBi)	Maximum gain in the band (dBi)
			XZ- <i>plane</i>	YZ	XZ	YZ	XZ	YZ	XZ	YZ		
DRA-2 (20.8, 27.3, 8.4, 10, 31)	1.849 – 2.549 , 32	1.9	-24.64	-19.12	-14.36	-13.6	140	150	-14	-19.3	3.74	4.71 (at 2.3 GHz)
		2.41	-24.59	-24.26	-18	-14.56	135	140	-16	-20.83	3.95	
DRA-3 (88.68, 24, 7.8, 5, 30)	1.835 – 2.125 , 14.65	1.945	-20	-15	-12.3	-14.4	145	145	-14.71	-18	3.88	3.88 (at 1.945 GHz)

4.9 RADIATION EFFICIENCY

Radiation efficiencies of the DRAs are measured using the Wheeler cap method (Section 3.10.4, Chapter 3). A cylindrical metallic cap of diameter = 17 cm and height = 7.5 cm was used as the radiation shield, for the DRA. Measured efficiencies in the respective operating bands are given in Table 4.

Table 4: Measured radiation efficiencies of the DRAs so far studied (dimensions are in 'mm')

DRA	Broadside	Design 1	Design 2a	Design 2b	DRA-2	DRA-3
$(\epsilon_{rd}, 2a, d, h, L)$	(20.8,24,7.3 -, -)	(20.8,24,7.3 9, -)	(20.8,24,7.3 7, 25)	(20.8,24,7.3 9, 27.5)	(20.8,27.3,8.4 10,31.25)	(88.68,24,7.8 5,30)
Radiation Efficiency (%)	85.3	96.24	93.07	92.85	91.65	76.08

From the above table, it can be made out that the wideband design offers higher radiation efficiency than the fundamental design of a cylindrical DR. Also it is deduced that the DR with low ϵ_r is a better radiator than that with high ϵ_r , since the energy storage is more in the case of the latter. However, promising size reduction can not be achieved with a lower ϵ_r DR, unless special design rules are followed. Thus, when the use of a DR as an antenna is concerned, the choice of ϵ_r is as per the requirement of the antenna engineer.

4.10 WIDEBAND DESIGN USING A DIFFERENT SUBSTRATE

In order to confirm the suitability of the wideband design (design 2) with different substrate for the feed, the DRA is simulated using a 50 mm x 4.93 mm microstrip line formed on a 1.6 mm thick RT/Duroid substrate of $\epsilon_r = 2.2$. The feed was designed using Eq. 3.21 and 3.22 in Chapter 3. The DR parameters are, $\epsilon_r = 20.8$, $2a = 24$ mm and $d = 7.3$ mm, the same as those of DR-1. The -10 dB impedance bands, almost the same as those obtained on the $\epsilon_r = 4$ substrate, are found here also as,

Band 1: 2.43 to 3.45 GHz, for $h = 7$ mm, $L = 31.5$ mm

Band 2: 2.1 to 2.91 GHz, for $h = 9$ mm, $L = 37$ mm as shown in Figure 29.

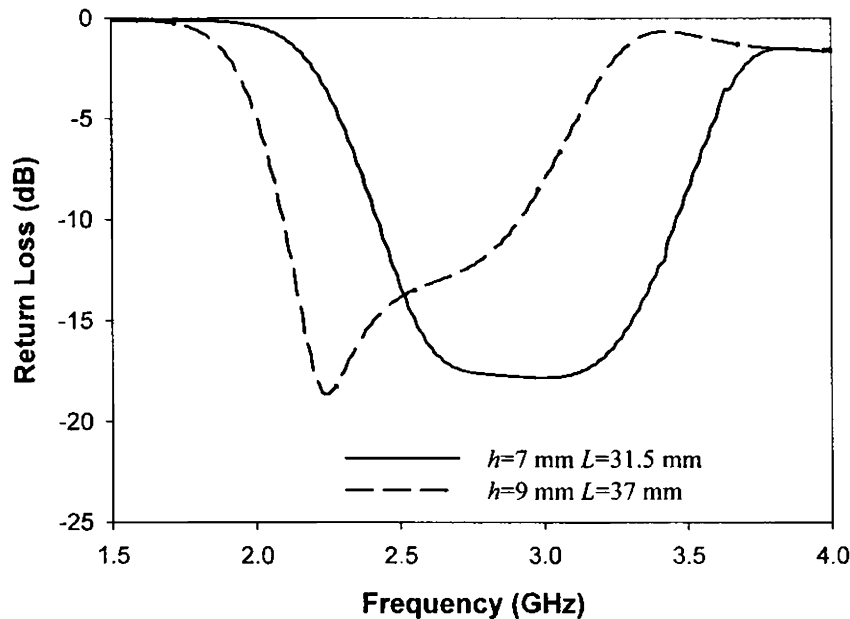


Figure 29: Simulated return loss of the wideband DRA excited by a microstrip feed on an RT/Duroid substrate

CONCLUSION

Development of a wideband cylindrical DRA was presented with the help of measurements using HP 8510C vector network analyser and simulations using Ansoft HFSS™. A bandwidth in excess of 30 % with stable conical radiation pattern and good gain was obtained for the proper design. High radiation efficiencies in excess of 90 % were obtained, due to the inherent low loss of the DR. Effect of various design parameters on the DRA performance was also studied. The mid-band frequency of the operating band can be tuned by changing the topological and/or material properties of the DRA. However, medium permittivity DRs are preferred for the design, since they provide wider bandwidths, better gains and higher radiation efficiencies than high permittivity DRs.

REFERENCES

- [1] High Frequency Structure Simulator (HFSS), Ansoft Corporation, Pittsburgh, PA
- [2] R. A. Kranenburg and S. A. Long, Microstrip Transmission Line Excitation of Dielectric Resonator Antennas, *Electro. Lett.*, Vol. 24, pp. 1156-1157, January 1988
- [3] K. W. Leung, K. Y. Chow, K. M. Luk and E. K. N. Yung, Low-profile Circular Disk DR Antenna of Very High Permittivity Excited by a Microstrip Line, *Electro. Lett.*, Vol. 33, pp. 1004-1005, June 1997
- [4] C. S. De Young and S. A. Long, Wideband Cylindrical and Rectangular Dielectric Resonator Antennas, *IEEE Anten. Wireless Propagat. Lett.*, Vol. 5, pp. 426-429, 2006
- [5] D. Kajfez, A. W. Glisson and J. James, Computed Modal Field Distributions for Isolated Dielectric Resonators, *IEEE Trans. Microwave Theory Tech.*, Vol.32 ,pp. 1609-1616, December 1984
- [6] R. K Mongia and P. Bhartia, Dielectric Resonator Antennas—A Review and General Design Relations for Resonant Frequency and Bandwidth, *Inter. Journal of Microwave and Millimeter-Wave Comp. aided Eng.*, Vol. 4, pp. 230-247, July 1994
- [7] K. Lan, S. K. Chaudhury and S. Safavi-Naeini, Design and Analysis of A Combination Antenna with Rectangular Dielectric Resonator and inverted L-Plate, *IEEE Trans. on Antennas Propagat.*, Vol. 53, pp. 495-501, January 2005

FINITE DIFFERENCE TIME DOMAIN TECHNIQUE

This chapter reviews the scope of finite difference time domain (FDTD) technique for the analysis of antenna problems. Using the FDTD approach, the broadband DRA measured in the previous chapter is modeled and analysed. MATLAB® is used for developing the FDTD codes. Finally the measured and computed results are compared.

5.1 INTRODUCTION

Among the numerical methods being employed for solving problems related to electromagnetics, finite difference methods (FDMs) developed by A. Thom in the 1920s are more frequently used and more universally applied than any other method. This technique is based on approximating differential equations by finite difference equations. That is, FDM relates the value of the dependant variable at a point in the solution region to the values at some neighbouring points. It mainly involves three steps- **(1)** dividing the solution region into a grid of nodes **(2)** approximating the given differential equation by finite difference equivalent that relates the dependant variable at a point in the solution region to its values at the neighbouring points **(3)** solving the difference equations subject to the prescribed boundary conditions and/or initial conditions.

5.2 FDTD IN ELECTROMAGNETICS

The FDTD method can be classed as a special case of the FDM. In this approach introduced by K. S. Yee [1] in the mid-1960s, the computational volume is sampled in space and the field quantities are evaluated at discrete intervals of time. The time step and the spatial increment are so chosen as to avoid aliasing error and instability of the computation. Maxwell's curl equations are solved for each cell by a knowledge of the field quantity (E or H) at the previous time step and that (H or E) at the immediately neighbouring cell. The field updating process is stopped when the field quantities over the computational volume reaches a steady state. Because of the limited computer resources, the computation volume is terminated by using an appropriate absorbing boundary condition (ABC) such as Mur's ABC, Liao's ABC, perfectly matched layer (PML), Switched boundary condition (XBC) etc. Care must be taken to minimise errors due to reflection introduced by such boundaries.

FDTD offers the following advantages

- FDTD is a very versatile and flexible modeling technique. The strength of FDTD lies in the fact that it provides an easy understanding on the temporal physical phenomena and what to be anticipated from a given model
- The central difference nature of the FDTD method makes it a relatively accurate (second-order accuracy in both time and space), compared to other first-order schemes

- ➔ FDTD is a time domain technique, and when a time-domain pulse is used as the source, a wide frequency range is solved with only one simulation
- ➔ The field values for each time step are stored in arrays and their distribution over the computational domain at any instant of time can be easily plotted using the visualisation capabilities of the digital computers
- ➔ A wide variety of linear and non-linear dielectric and magnetic materials can be easily modeled
- ➔ FDTD provides the E and H fields directly which are of prime interest in most EMI/EMC modeling applications

The total memory storage and the computational time are directly related to the number of field unknowns in the problem space, which in turn depends on the electrical size of the problem space and the space resolution. The fineness of the grid is generally determined by the dimensions of the smallest feature to be modeled and the smallest wavelength. Large objects with regions that contain small, complex geometries may require large, dense grids.

5.3 FDTD COMPUTATIONS

Formulation of the FDTD method begins by considering the differential form of Maxwell's two curl equations which govern the propagation of electric and magnetic fields in a medium. The medium is assumed to be uniform, isotropic, and homogeneous. Also the medium is assumed to be lossless i.e., absence of volume currents or finite conductivity. With these assumptions, Maxwell's curl equations may be written as

$$\begin{aligned}\mu \frac{\partial H}{\partial t} &= -\nabla \times E \\ \varepsilon \frac{\partial E}{\partial t} &= \nabla \times H\end{aligned}\tag{5.1}$$

where $\mu = \mu_0 \mu_r$ and $\varepsilon = \varepsilon_0 \varepsilon_r$, are the permeability and permittivity of the medium respectively. Subscript '0' indicates free space and 'r' indicate relative value. In order to solve these continuous partial differential equations by FDTD, a first-order finite difference scheme, based on central-difference approximation is used on both the time and space. The central difference scheme is used in the FDTD method because it is the most accurate compared with the other types of finite difference schemes.

For example, let one component of the electric or magnetic field be $F(x, y, z, t)$, and is sampled as $F(i\Delta x, j\Delta y, k\Delta z, n\Delta t)$. Then the central difference schemes for the X-direction and time 't' are expressed as

$$\begin{aligned}\frac{\partial F(x, y, z, t)}{\partial x} &\approx \frac{(F(x + \Delta x/2, y, z, t) - F(x - \Delta x/2, y, z, t))}{\Delta x} \\ &= \frac{(F^n(i + 0.5, j, k) - F^n(i - 0.5, j, k))}{\Delta x}\end{aligned}\tag{5.2}$$

$$\begin{aligned}\frac{\partial F(x, y, z, t)}{\partial t} &\approx \frac{(F(x, y, z, t + \Delta t/2) - F(x, y, z, t - \Delta t/2))}{\Delta t} \\ &= \frac{(F^{n+0.5}(i, j, k) - F^{n-0.5}(i, j, k))}{\Delta t}\end{aligned}$$

The electric or magnetic field is discretised in both space and time, as indicated by $i\Delta x, j\Delta y, k\Delta z$ and $n\Delta t$, so that the calculation space is divided into small cubes as shown in Figure 1(a). A small cube of volume $\Delta x.\Delta y.\Delta z$ is referred

to as an FDTD cell. The side is called a cell edge, and its length Δx , Δy or Δz is called a cell size.

5.4 THE YEE ALGORITHM

In the 3-dimensional case, the six field locations (x, y and z components of \vec{E} and \vec{H} fields) are considered to be interleaved in space as shown in Figure 1(b), which is considered as the FDTD unit cell as defined by Yee [1]. Here, the midpoint of each cell is selected under spatial discretisation and the component of \vec{E} is defined at the midpoint of the cell. For convenience in the calculation, the \vec{H} field is not calculated at the same point as \vec{E} , but is staggered alternately with respect to \vec{E} . Thus the calculation of \vec{H} field is performed at the spatial locations between any two adjacent \vec{E} field components. The spatial discretisation for the \vec{H} , in fact, overlaps half a cell on either side.

This natural arrangement of the field components is ideal for defining the central differences for the Maxwell's equations to yield the six field components as:

$$\begin{aligned}
 H_{x\ i+1,j+0.5,k+0.5}^{n+0.5} &= H_{x\ i+1,j+0.5,k+0.5}^{n-0.5} + \frac{\Delta t}{\mu \Delta x} \left(E_{y\ i+1,j+0.5,k+1}^n - E_{y\ i-1,j+0.5,k}^n \right) - \frac{\Delta t}{\mu \Delta y} \left(E_{z\ i-1,j+1,k+0.5}^n - E_{z\ i+1,j,k+0.5}^n \right) \\
 H_{y\ i+0.5,j+1,k+0.5}^{n+0.5} &= H_{y\ i+0.5,j+1,k+0.5}^{n-0.5} + \frac{\Delta t}{\mu \Delta x} \left(E_{z\ i+1,j+1,k+0.5}^n - E_{z\ i,j+1,k+0.5}^n \right) - \frac{\Delta t}{\mu \Delta z} \left(E_{x\ i+0.5,j+1,k+1}^n - E_{x\ i+0.5,j+1,k}^n \right) \\
 H_{z\ i+0.5,j+0.5,k+1}^{n+0.5} &= H_{z\ i+0.5,j+0.5,k+1}^{n-0.5} + \frac{\Delta t}{\mu \Delta y} \left(E_{x\ i+0.5,j+1,k+1}^n - E_{x\ i-0.5,j,k+1}^n \right) - \frac{\Delta t}{\mu \Delta x} \left(E_{y\ i+1,j+0.5,k+1}^n - E_{y\ i,j+0.5,k+1}^n \right) \\
 E_{x\ i+0.5,j,k}^{n+1} &= E_{x\ i+0.5,j,k}^n + \frac{\Delta t}{\epsilon \Delta y} \left(H_{z\ i+0.5,j+0.5,k}^{n+0.5} - H_{z\ i+0.5,j-0.5,k}^{n+0.5} \right) - \frac{\Delta t}{\epsilon \Delta z} \left(H_{y\ i+0.5,j,k+0.5}^{n+0.5} - H_{y\ i+0.5,j,k-0.5}^{n+0.5} \right) \\
 E_{y\ i,j+0.5,k}^{n+1} &= E_{y\ i,j+0.5,k}^n + \frac{\Delta t}{\epsilon \Delta x} \left(H_{z\ i,j+0.5,k+0.5}^{n+0.5} - H_{z\ i,j+0.5,k-0.5}^{n+0.5} \right) - \frac{\Delta t}{\epsilon \Delta z} \left(H_{x\ i+0.5,j+0.5,k}^{n+0.5} - H_{x\ i-0.5,j+0.5,k}^{n+0.5} \right) \\
 E_{z\ i,j,k+0.5}^{n+1} &= E_{z\ i,j,k+0.5}^n + \frac{\Delta t}{\epsilon \Delta y} \left(H_{x\ i+0.5,j,k+0.5}^{n+0.5} - H_{x\ i-0.5,j,k+0.5}^{n+0.5} \right) - \frac{\Delta t}{\epsilon \Delta x} \left(H_{y\ i,j+0.5,k+0.5}^{n+0.5} - H_{y\ i,j-0.5,k+0.5}^{n+0.5} \right)
 \end{aligned} \tag{5.3}$$

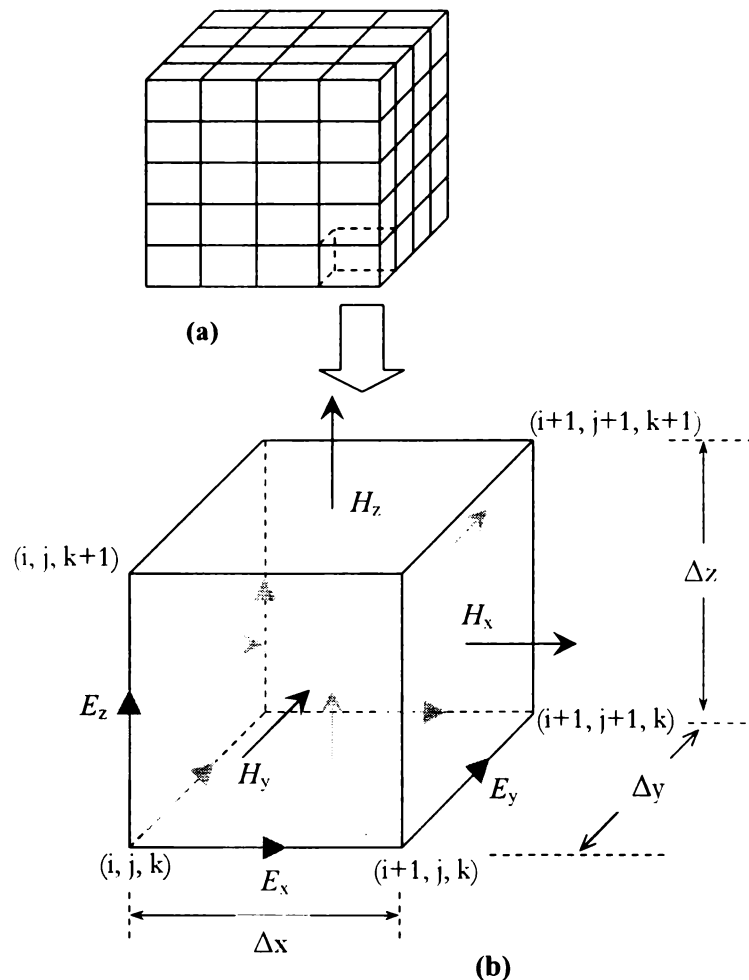


Figure 1: (a) FDTD lattice (b) unit cell

Here, not only the placement of the E and H nodes are off in space by half a space step, but the time instants when the E or H fields are calculated are also off by half a time step. That is, if the components of E are calculated at $n\Delta t$, where Δt is the discretisation unit in time and n is any non-negative integer, the components of H are calculated at $(n + 0.5)\Delta t$. For this reason, the Yee algorithm is also called the leapfrog algorithm.

5.5 CELL SIZE AND TIME STEP

FDTD method insists finer cells, since the field value is assumed to be a constant over a cell for computational accuracy. The side of each cell is often set as $\lambda/10$ or less at the highest frequency of interest because the grid dispersion error is proportional to the cell sides [2] as follows

$$E \propto \left(\sqrt{(\Delta x^2 + \Delta y^2 + \Delta z^2)} / \lambda \right)^2 \quad (5.4)$$

However, in some situations, such as accurate calculation of antenna impedances or radar cross sections, $\lambda/20$ or smaller size may be necessary. Here the wavelength in the material should be used to determine the minimum cell size if some portion of the computational space is filled with a dielectric material. For the problem involving high-permittivity dielectrics in a free space, it is better to use non-uniform cells, that is, smaller cells in the dielectrics, and larger cells outside.

Once the cell size is determined, the maximum size of the time step Δt immediately follows from the Courant–Friedrich–Lewy stability condition [3], given by Eq. (5.5), which ensures that the numerical error generated in one step of the calculation does not accumulate and grow as the time-marching progresses.

$$\Delta t \leq \frac{1}{v_{\max}} \left(\frac{1}{\Delta x^2} + \frac{1}{\Delta y^2} + \frac{1}{\Delta z^2} \right)^{-1/2} \quad (5.5)$$

where v_{\max} is the maximum phase velocity of the wave in the computational volume. The grid dispersion error is minimised by the equality in Eq. (5.5). This however, leads to instability in some cases because of a round-error in the computer. One method of avoiding this is to select 99.5 % of Δt calculated by Eq. (5.5).

In the present work for modeling the DRA, a cubical cell with $\Delta x = \Delta y = \Delta z = 0.5$ mm is chosen to meet the aforesaid criteria, and also to fit an integral number of cells in the computational space. In addition, cubical cell is recommended for minimum grid dispersion error [2]. This yields the time step as $\Delta t = 0.95744$ picoseconds.

5.6 ANTENNA ANALYSIS

An antenna, when considered as an object, comprises of structures of different geometries, dimensions and properties. A set of conductors and dielectrics surrounded by free space constitutes a basic antenna. FDTD assumes perfect conductor approximation for antenna feeds, patches, ground planes, stubs etc. and perfect dielectric approximation for substrates, dielectric resonators, radomes etc.

In the present context, the DRA studied is of parameters as explained in sections (4.3) and (4.5), in the previous chapter. The cylindrical DR is of dielectric constant $\epsilon_{rd} = 20.8$, diameter $2a = 24$ mm and thickness $d = 7.3$ mm. A 50Ω microstrip transmission line, having a width 3.3 mm and length 50 mm fabricated

on a 1.6 mm thick microwave substrate of dielectric constant $\epsilon_{rs} = 4$ and size 115 mm x 115 mm or $1.15 \lambda_0 \times 1.15 \lambda_0$, feeds the DR. The antenna geometries analysed using FDTD are shown in Figure 2.

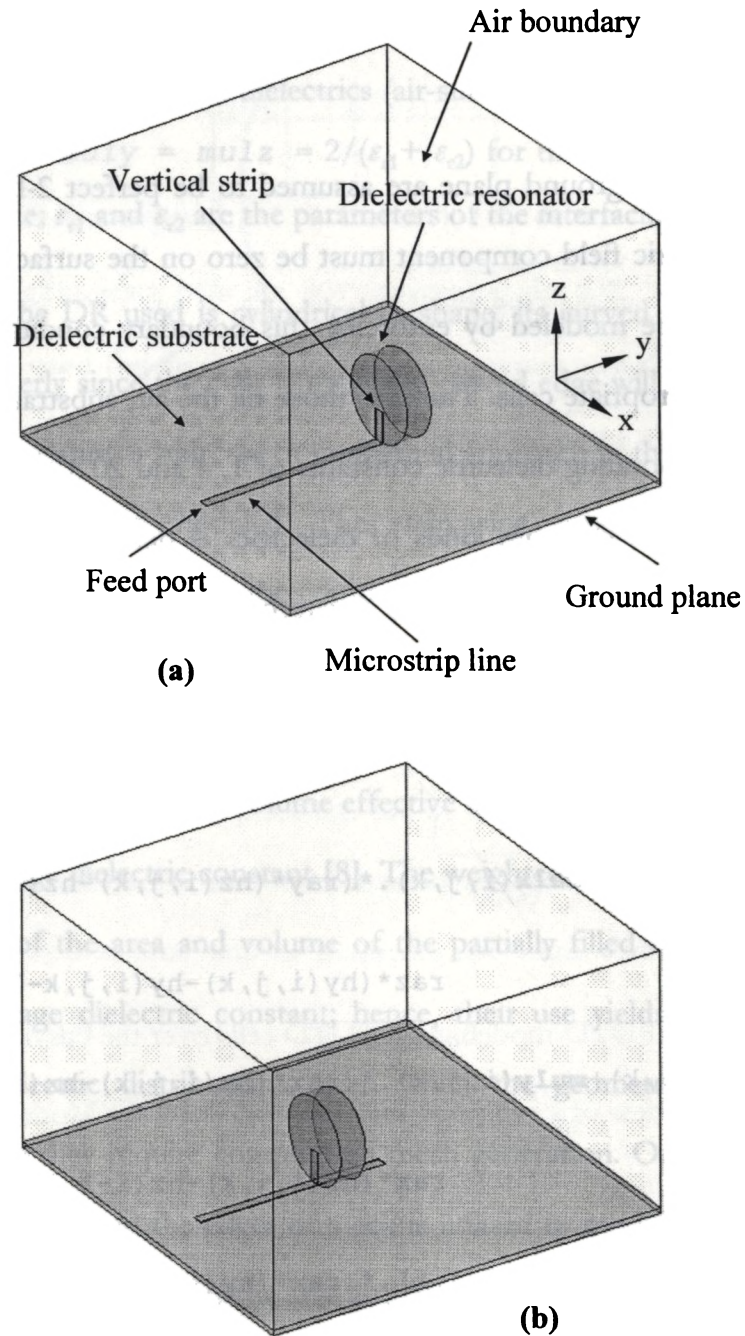


Figure 2: DRA geometries analysed using FDTD (a) Design 1 (b) Design 2

5.6.1 OBJECT MODELING

In FDTD, objects are modeled by assigning the constitutive parameters like permittivity, permeability and conductivity to the corresponding cells in the computational space.

Microstrip and ground plane are assumed to be perfect 2-D conductors. The tangential electric field component must be zero on the surface of a perfect conductor; hence are modeled by enforcing this boundary condition on to the plane (s) of the appropriate cells. The cells those fill the air, substrate and DR are assigned the corresponding dielectric constants of 1, 4 and 20.8 respectively. The interface between two or more kinds of dielectrics is defined by enforcing the average value of permittivity to the intersecting cells [4]. The above is implemented in the FDTD code by incorporating additional parameters *mulx*, *muly* and *mulz* in the *E* field components in Eqn. (5.3) as shown below.

$$\begin{aligned} ex(i, j, k) &= ex(i, j, k) + \mathbf{mulx}(i, j, k) .* (\mathbf{ray} * (hz(i, j, k) - hz(i, j-1, k))) - \\ &\quad \mathbf{raz} * (hy(i, j, k) - hy(i, j, k-1))) / \mathbf{eps0}; \\ ey(i, j, k) &= ey(i, j, k) + \mathbf{muly}(i, j, k) .* (\mathbf{raz} * (hx(i, j, k) - hx(i, j, k-1))) - \\ &\quad \mathbf{rax} * (hz(i, j, k) - hz(i-1, j, k))) / \mathbf{eps0}; \\ ez(i, j, k) &= ez(i, j, k) + \mathbf{mulz}(i, j, k) .* (\mathbf{rax} * (hy(i, j, k) - hy(i-1, j, k))) - \\ &\quad \mathbf{ray} * (hx(i, j, k) - hx(i, j-1, k))) / \mathbf{eps0}; \end{aligned}$$

where, $r_{ax}=\Delta t/\Delta x$; $r_{ay}=\Delta t/\Delta y$; $r_{az}=\Delta t/\Delta z$;

\Rightarrow For conductors, $m_{ulx} = m_{uly} = m_{ulz} = 0$

\Rightarrow For dielectrics, $m_{ulx} = m_{uly} = m_{ulz} = 1/\epsilon_r$; $\epsilon_r = 1, 4$ and 20.8 for air, substrate and DR respectively

\Rightarrow For interfaces between dielectrics (air-substrate, air-DR and DR-substrate), $m_{ulx} = m_{uly} = m_{ulz} = 2/(\epsilon_{r1} + \epsilon_{r2})$ for the cells on both sides of the interface; ϵ_{r1} and ϵ_{r2} are the parameters of the interfacing dielectrics.

Since the DR used is cylindrical in shape, its curved surface needs to be modeled properly since the cells lying at the curved edge will partially include the DR. By incorporating a staircase or conformal approach in the Yee algorithm, the curved edges can be modeled. The staircasing procedure, though simple, introduces significant errors in the computation, even with a fine cubical grid (side $\sim \lambda/25$) [5]. Several enhanced FDTD methods for modeling curved dielectric surfaces have been proposed [6–8]. These are implemented by a calculation procedure based on weighted volume effective dielectric constant [6, 7] or a linear weighted average dielectric constant [8]. The weighted volume approaches require computation of the area and volume of the partially filled cells. Also these deal with the average dielectric constant; hence, their use yields the same effective value for dielectric distributions, even when the geometry of the fillings is different. Also they require complicated mesh generation. On the other hand, in [8] the information on the edges of a cell is utilised to modify the Yee algorithm, thereby avoiding the need for the area and/or volume calculations.

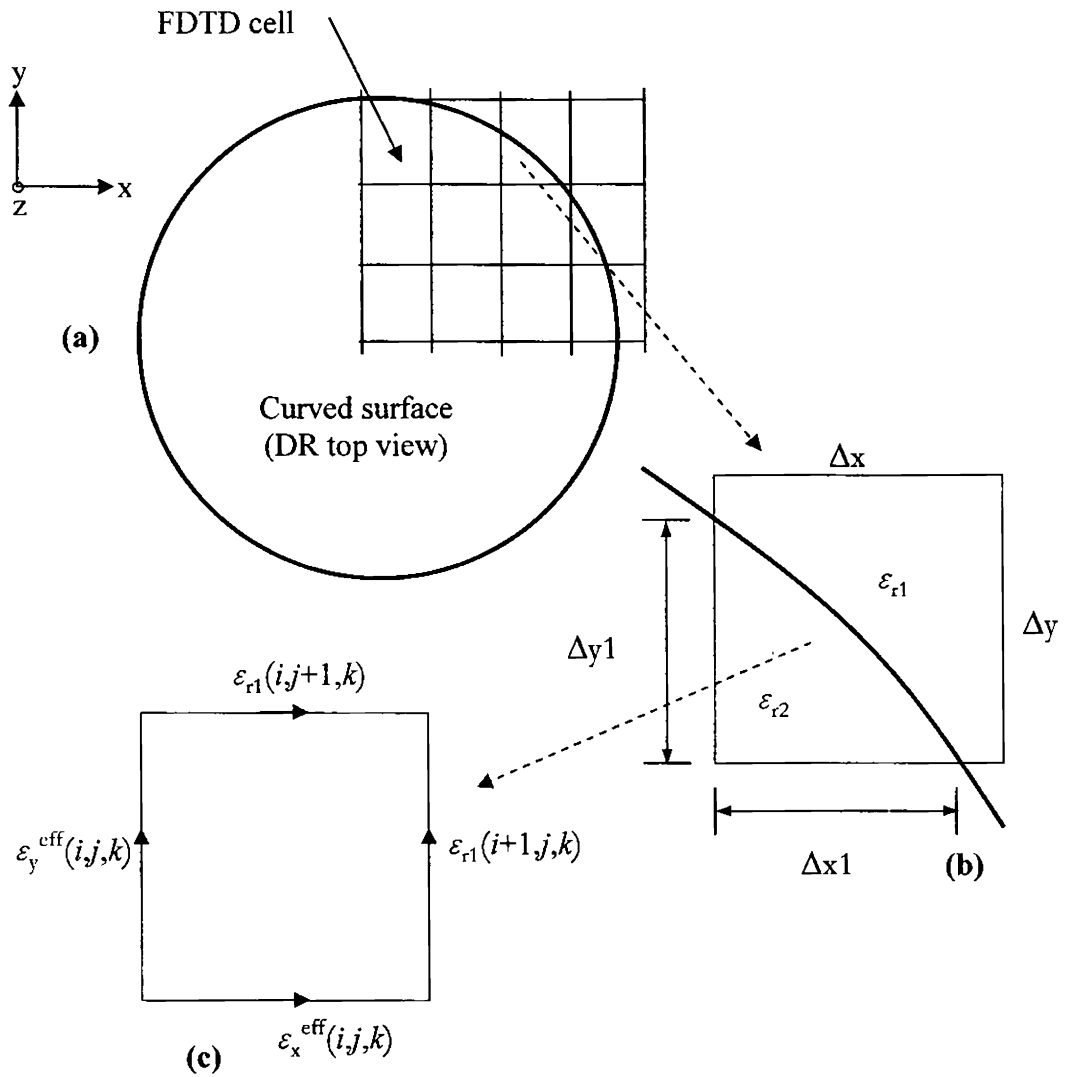


Figure 3: Conformal FDTD modeling (a) FDTD cells over the curved surface

(b) Enlarged view of a cell filled with two dielectrics (b) Modeled cell

If it is assumed that the curved surface lies in the XY -plane, in the present conformal method, a cell at the interface is modeled by a linear weighted average

dielectric constant as shown in Figure 3. Effective dielectric constants for the particular cell are defined as:

$$\varepsilon_x^{\text{eff}}(i, j, k) = [\varepsilon_{r2} \cdot \Delta x1(i, j, k) + \varepsilon_{r1} \cdot (\Delta x - \Delta x1(i, j, k))] / (\Delta x) \quad (5.6)$$

$$\varepsilon_y^{\text{eff}}(i, j, k) = [\varepsilon_{r2} \cdot \Delta y1(i, j, k) + \varepsilon_{r1} \cdot (\Delta y - \Delta y1(i, j, k))] / (\Delta y) \quad (5.7)$$

However, the edges $(i, j+1, k)$ and $(i+1, j, k)$ of the cell, which indicate the immediate neighbouring cells are not penetrating the DR, so that the dielectric constant ε_{r1} is used for those cells. Now the parameters, $mulx = 1/\varepsilon_x^{\text{eff}}(i, j, k)$, $muly = 1/\varepsilon_y^{\text{eff}}(i, j, k)$ and $mulz = 1/\varepsilon_{r2}$ are used in the FDTD computations, to model the cells of interest.

5.6.2 SOURCE SIGNAL

For exciting the structure, a wide variety of excitation waveforms such as plane wave, pulse, modulated pulse etc. can be used. However, a Gaussian pulse is the most preferred one in frequency-dependent applications since it is having a smooth waveform in time, and its frequency spectrum is also Gaussian in shape centered at zero [9].

$$\begin{aligned} \text{The Gaussian pulse is defined as, } p(t) &= e^{-\left[\frac{(t-t_0)}{T_s}\right]^2} & 0 \leq t \leq 2t_0 \\ &= 0 & \text{otherwise} \end{aligned} \quad (5.8)$$

For spread time, $T_s = 15$ ps and peak time, $t_0 = 3T_s$, the pulse is plotted in Figure 4. The frequency spectrum of the above pulse can be obtained by using the following relation.

$$\text{Amp (dB)} = 10 \cdot \log [\text{abs} \{ \text{FFT} (p(t)) \}] \quad (5.9)$$

The operator FFT is the fast Fourier transformation and the spectrum is shown in Figure 5. Though the highest frequency content of the pulse is $1/(2 \cdot \Delta t) = 522.23$ GHz, it is clear that the Fourier amplitude is within 3 dB only below 8.75 GHz, as determined by the pulse parameter T_s . This frequency range is sufficient for exciting the DRA.

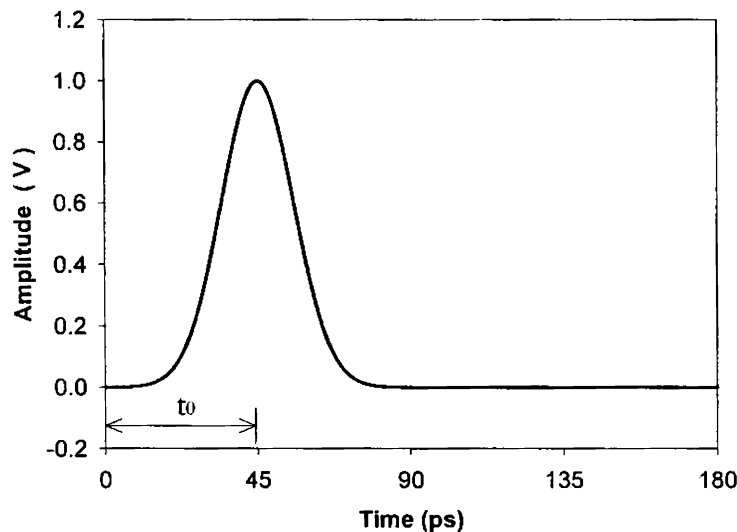


Figure 4: Gaussian pulse

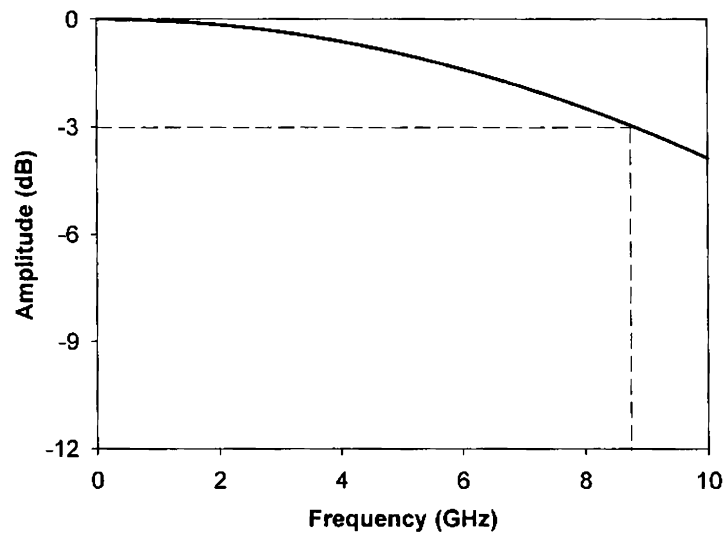


Figure 5: Spectrum of the Gaussian pulse

5.6.3 FEED MODELING

In practice, microwave energy is fed to the microstrip transmission line through an SMA connector soldered between the edges of the strip and the ground plane. This can be modeled in FDTD by assigning several electric field cells within the area along the thickness of the substrate coming under the strip.

As seen in the above section, the amplitude of the exciting pulse is above zero for only a very short fraction of the total computational time, especially for resonant geometries such as antennas. Once the pulse amplitude drops, the source voltage becomes essentially zero and the source effectively becomes a short circuit. Any reflections from the antenna which return to the source are totally reflected to the computational space and a large number of time steps are required

to stabilise the source signal. A dissipation mechanism can be added by modeling the Gaussian source V_s with a series internal resistance R_s [10] as shown in Figure 6.

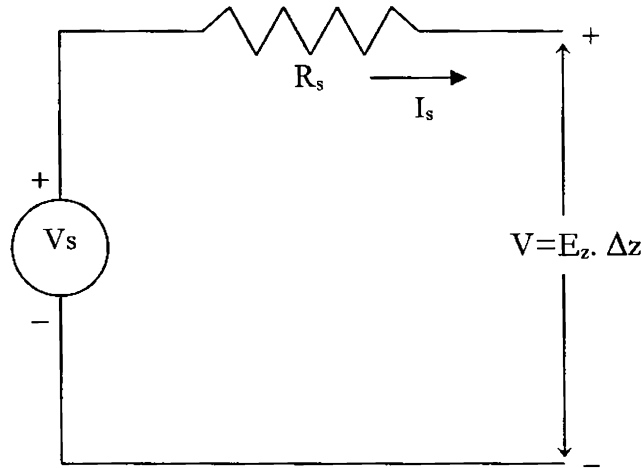


Figure 6: Source with series resistance

The value of the internal resistance does not appear to be critical. A reasonable choice for R_s is to use the value of the characteristic impedance of the transmission line i.e. $Z_0 = 50 \Omega$. Usually, a voltage source that corresponds to an electric field E in the z direction at a certain source location $(i_s \Delta x, j_s \Delta y, k_s \Delta z)$ is used. If the source resistance R_s is set zero, then the usual delta gap electric field at the source location, at the n^{th} time step is simply given by

$$E_s^n(i, j, k) = V_s(n\Delta t) / \Delta z \quad (5.10)$$

When R_s is included,

$$E_s^n(i, j, k) = (V_s(n\Delta t) + I_s^{n-1} R_s) / \Delta z \quad (5.11)$$

By applying Ampere's circuital law by taking the line integral of the magnetic field around the feed point shown in Figure 7, the source current can be obtained as,

$$I_s^{n-1/2} = (H_x^{n-0.5}(i_s, j_s-1, k_s) - H_x^{n-0.5}(i_s, j_s, k_s))\Delta x \quad (5.12)$$

$$+ (H_y^{n-0.5}(i_s, j_s, k_s) - H_y^{n-0.5}(i_s-1, j_s, k_s))\Delta y$$

Thus an electric field located at the Z-edge of the cell just above the ground plane and directly below the end of the strip line is used as the feed. A stair-stepped perfect conductor transition from the feed cell to the microstrip edge is formed to provide a relatively smooth connection from the single electric feed location to the microstrip. This is illustrated in Figure 8.

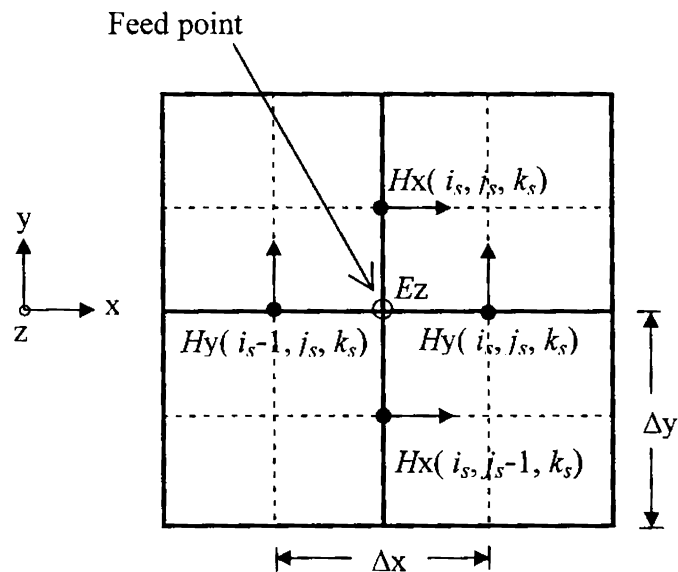


Figure 7: Magnetic field components around the feed point

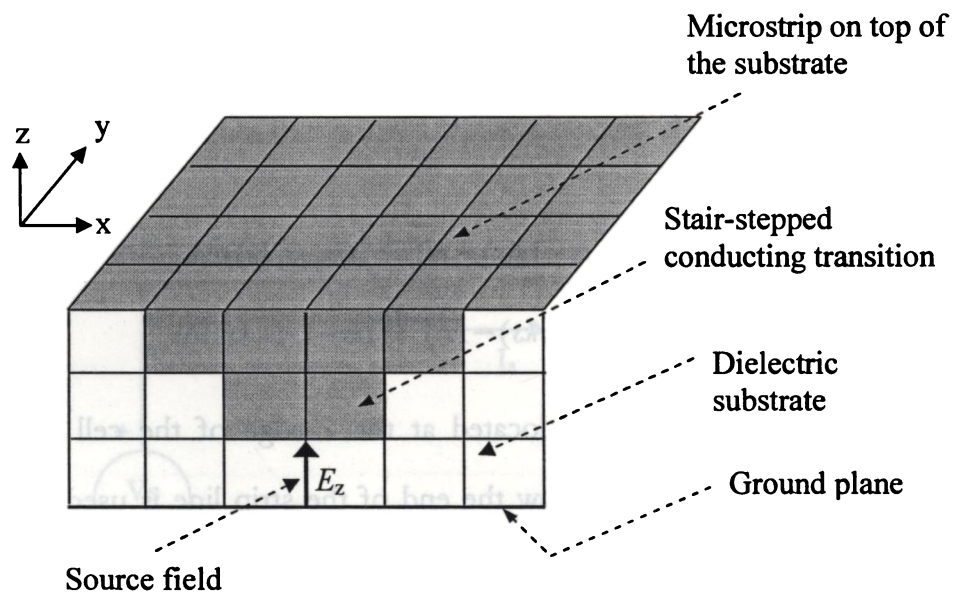


Figure 8: Source modeling in FDTD

Once the pulse is launched, the fields in the structure are computed for successive time steps until all the field intensities in the domain decay to a negligible steady-state value. At this instant, the input impedance of the antenna can be calculated as follows

$$Z_{in}(f) = \frac{V_s(f)}{I_s(f)} \quad (5.13)$$

Where $V_s(f)$ and $I_s(f)$ are the FFTs of the time domain source voltage and current respectively. The antenna return loss can be calculated from Z_{in} as follows,

$$RL_{dB}(f) = 20 \cdot \log \left(\frac{Z_{in}(f) - Z_0}{Z_{in}(f) + Z_0} \right) \quad (5.14)$$

where $Z_0 = 50 \Omega$, the characteristic impedance of the transmission line

5.6.4 ABSORBING BOUNDARY CONDITION

When analysing open problems such as electromagnetic scattering and antennas, it is necessary to truncate the FDTD computational space by a virtual boundary, because of the storage limit of computer. When the electromagnetic fields arrived at the truncation or boundary, they will reflect back into the computational space and cause erroneous computation unless the boundary absorbs the incident field perfectly. This can be made possible by forcing the incident fields to obey some conditions at the boundary which are termed as the absorbing boundary conditions (ABCs). The farther from the scatterers or the antennas the absorbing boundary is located, the better is the absorption. This is because these waves become more like plane waves as they travel farther from the radiating structure, and also because the absorbing boundary is usually effective for a plane wave at normal incidence. However, the dimensions of the absorbing boundary are limited by the available computer memory.

ABCs can be classified roughly into two – (1) those derived from an approximate differential equation that expresses a traveling plane wave at the boundary, and (2) those in which the incident wave is absorbed by a virtual electromagnetic absorber. The Mur's absorbing boundary condition [11] and Berenger's Perfectly Matched Layer (PML) [12] are examples of the former and the latter classes respectively. In terms of accuracy, PML is the best available ABC,

but its physical interpretation is very difficult to understand and the storage required for implementation is much larger than the Mur's ABC. As far as the limited computer resources are concerned, Mur's ABC is used for analysing the DRA.

A plane wave having an Z-component of electric field E_z propagating in the y direction should satisfy the following differential equation

$$\left(\frac{\partial}{\partial y} - \frac{1}{v} \frac{\partial}{\partial t} \right) E_z = 0 \quad (5.15)$$

Discretizing Eq.(5.15) using the central difference method, we get the Mur's first order ABC equation. For example, the ABC at the $y = 0$ plane, that is the FDTD layer $(i, 1, k)$, is given by

$$E_z^n(i, 1, k) = E_z^{n-0.5}(i, 2, k) + \frac{v\Delta t - \Delta z}{v\Delta t + \Delta z} \left[E_z^n(i, 2, k) - E_z^{n-0.5}(i, 1, k) \right] \quad (5.16)$$

Similar expressions can be obtained for the other 5 layers constituting the boundaries of the computational volume. However, the amount of reflection from the boundary becomes worse when the angle of incidence of the field increases. This limits the reflection coefficient of Mur's ABC to some -30 to -40 dB.

5.6.5 FDTD PARAMETERS FOR THE DRA

Based on the discussions made so far, the FDTD parameters used in the analysis of the DRA are given as:

- ⇒ Cell dimensions, $\Delta x = \Delta y = \Delta z = 0.5 \text{ mm} \ll \lambda_0/20$, λ_0 being the lowest wavelength expected to exist in the structure
- ⇒ Time step = 0.95744 ps
- ⇒ Gaussian pulse parameters, $T_s = 15 \text{ ps}$ and $t_0 = 3 T_s$
- ⇒ Side of the computational volume
 - = side of substrate = 115 mm = 230 cells
- ⇒ Width of the microstrip = width of the vertical strip = 3.3 mm ≈ 7 cells
- ⇒ Length of the microstrip = 50 mm = 100 cells
- ⇒ Thickness of the substrate = 1.6 mm ≈ 3 cells
- ⇒ Diameter of the DR = 24 mm = 48 cells
- ⇒ Height of the DR = 7.3 mm ≈ 15 cells
- ⇒ Height of the computational volume = 61 cells, i.e., 10 cells above the DR

5.6.6 THE FDTD ALGORITHM

The complete FDTD algorithm is given below.

```
%-----%
1: Define the structure to be simulated

    a) Define the dielectric and magnetic constants
       c0,eps0,mu0,eps_sub and eps_dr
    b) Calculate epseff1 = (1+eps_sub)/2
```

```
epseff2 = 1+eps_dr)/2

% substrate-DR boundary doesn't occur in the design %

c) Define the antenna dimensions

d) Define the cell size (dx, dy and dz) and the
   number of cells along x, y and z directions

e) Calculate the sampling time step dt

f) Initialise  $E_x$ ,  $E_y$ ,  $E_z$  and  $H_x$ ,  $H_y$ ,  $H_z$  arrays to zero

g) Initialise Mur's ABC arrays buffx, buffy and buffz
   to zero

h) Define the entire computational volume as air by
   setting variables  $\rightarrow mulx = muly = mulz = 1$ 

i) Call the DR modeling routine

j) Define the dielectric substrate
    $\rightarrow mulx = muly = mulz = 1/eps\_sub$ 

k) Define air-substrate boundary
    $\rightarrow mulx = muly = 1/epseff1;$ 

l) Define the microstrip and the ground plane
    $\rightarrow mulx = muly = 0;$ 

m) Define the vertical feed  $\rightarrow mulx = mulz = 0$ 

n) Define the stair step transition for the feed

2: Define Gaussian pulse parameters,  $T_s = 15ps$ ,  $t_0 = 3T_s$ 

3: Set up counter  $T = 0$  and  $Total\_step = 5000$ 

4: if  $T \geq Total\_step$ , go to step 14

else
```

5: increment time step $T = T+1$ and calculate $t = (T-1)*dt$

6: Calculate source current, s_curr from Ampere's Law around the feed point

$$s_curr = (H_x(x_s, y_s-1, z_s) - H_x(x_s, y_s, z_s)) * dx + (H_y(x_s, y_s, z_s) - H_y(x_s-1, y_s, z_s)) * dy;$$

7: Calculate Gaussian pulse value $p(t) = e^{-((t-t_0)/T_s)^2}$

8: Assign the total field value to the feed point cell,

$$E_z(x_s, y_s, z_s) = (p(T) + s_curr(T) * 50) / dz$$

9: Calculate source voltage $s_volt = E_z(x_s, y_s, z_s) * dz$

10: Evaluate and store H -field update equations

11: Evaluate and store E -field update equations

12: Apply Mur's first order boundary condition for the tangential E -fields on the external boundaries of the computational volume

13: update Mur's arrays

13: go to step 4

14: Calculate input impedance as,

$$Z_{in}(f) = \text{fft}(s_volt) / \text{fft}(s_curr)$$

15: Calculate return loss as,

$$RL(f) = (Z_{in}(f) - 50) / (Z_{in}(f) + 50)$$

16: Save the results in the computer memory

17: End

%----- **DR modeling routine** -----%

1: Define a cube of side=2a and height=h
 $\rightarrow mulx = muly = mulz = 1/eps_dr$
 2a = DR diameter, h = DR height

2: Define the cells outside the DR periphery as air
 $\rightarrow mulx = muly = mulz = 1$

3: Define the air-DR boundary

$$\rightarrow mulx = mulz = 1/epseff2$$

4: Define $mulx$ and $mulz$ for the curved periphery of the DR by conformal mapping

%------%

5.7 RESULTS

Figure 9 shows the FDTD model of the DRA on the XZ-plane, obtained by plotting the parameter $mulx$, which is the inverse of the dielectric constant. The contrast in dielectric constants among various materials in the structure is evident from the model.

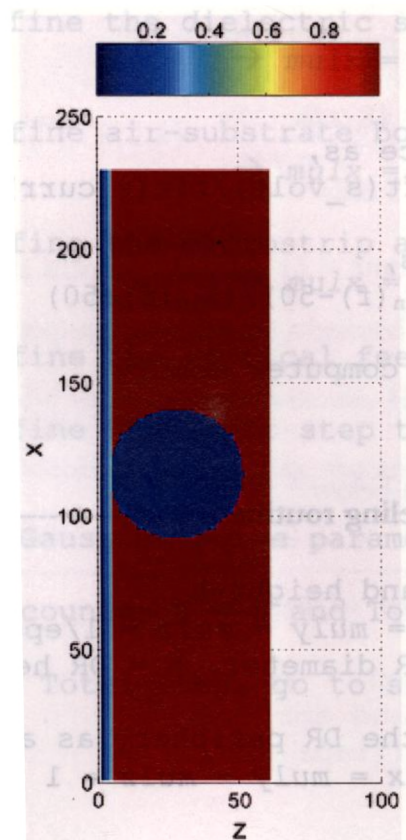


Figure 9: FDTD model of the DRA, XZ-plane

Figure 10 shows the voltage and current waveforms obtained at the source point as a function of the FDTD time steps, for design 1. It is clear that the applied Gaussian pulse propagated all over the computational space, converging to almost zero amplitude at about 5000 time steps. The input impedance and return loss of the antenna are computed from the source voltage and source current by Eq. (5.13) and (5.14) respectively.

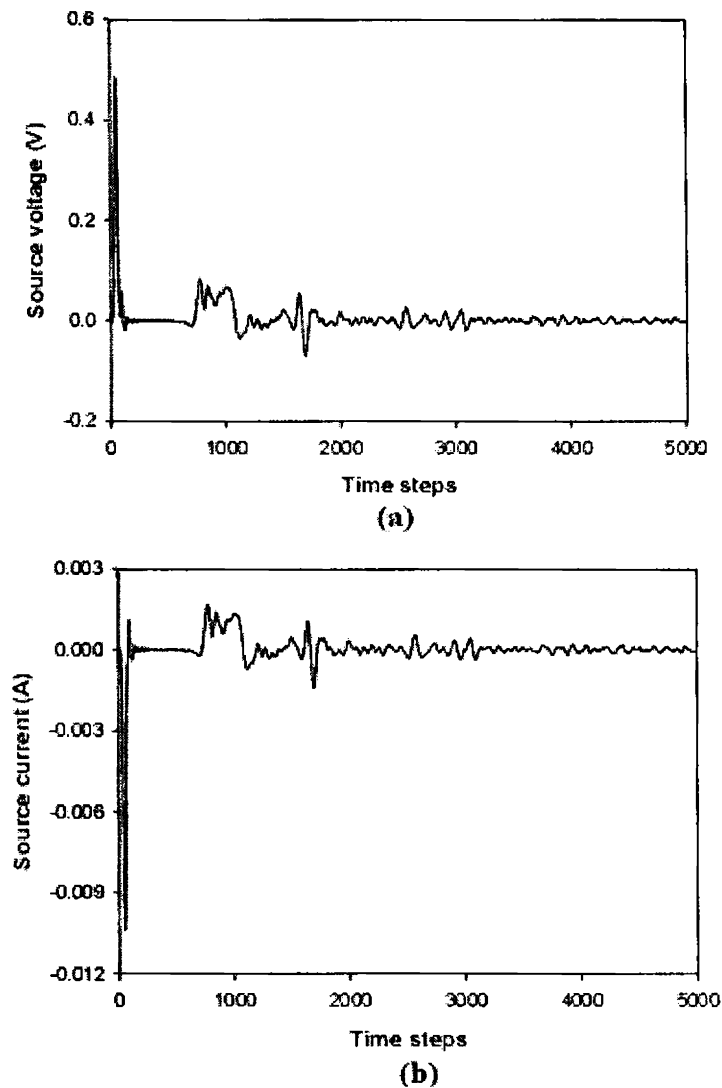


Figure 10: (a) voltage and (b) current waveforms at the source point

The near or in-field distributions in the model at a given frequency f_0 are obtained by stimulating the model with a sinusoidal voltage signal of frequency f_0 and unity amplitude, represented by $v(t)=\sin(2\pi f_0 t)$. The desired field components on the desired layer can then be visualised using the MATLAB® code. The near-field distributions are essential in determining the radiation properties of the antenna.

5.7.1 DESIGN 1

Computed impedance and return loss are shown in Figure 11 for the optimum design parameter $h = 9$ mm. Computed matching band (-10 dB) lies over a band of 2.5 to 3.7 GHz or 38.71 % at the mid-band frequency of 3.1 GHz. The return loss is minimum (-36 dB) at 3.312 GHz. The measured return loss is minimum at 3.2 GHz in a band of 2.556 to 3.676 GHz or 35.94 %. It is clear that the conformity between the computed and measured results is good showing the effectiveness of the FDTD method, except for the 3.38 % shift in the resonant frequency toward the right.

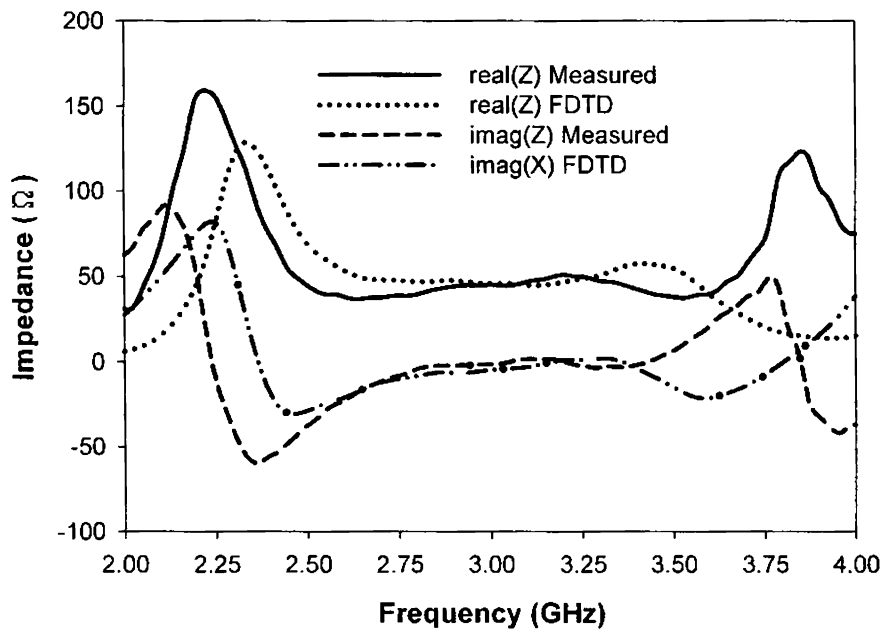
Distribution of the electric field components E_x , E_y and E_z on the XZ-plane of the structure, lying at the DR-air boundaries at 3.312 GHz (computed frequency with minimum return loss) are shown in Figures 12 (a), (b) and (c) respectively. Face 1 is the plane containing the DR with the vertical strip, and face 2 is the opposite plane. The boundary conditions applied for the metallic and dielectric bodies in the FDTD algorithm are very clear from the figure. On the vertical metallic strip on face 1, E_x and E_z which are the tangential components of

electric field vanish and only E_y , the normal component exists. The magnitudes of E ($mag E$) on the faces are calculated from the field components by using the following relation,

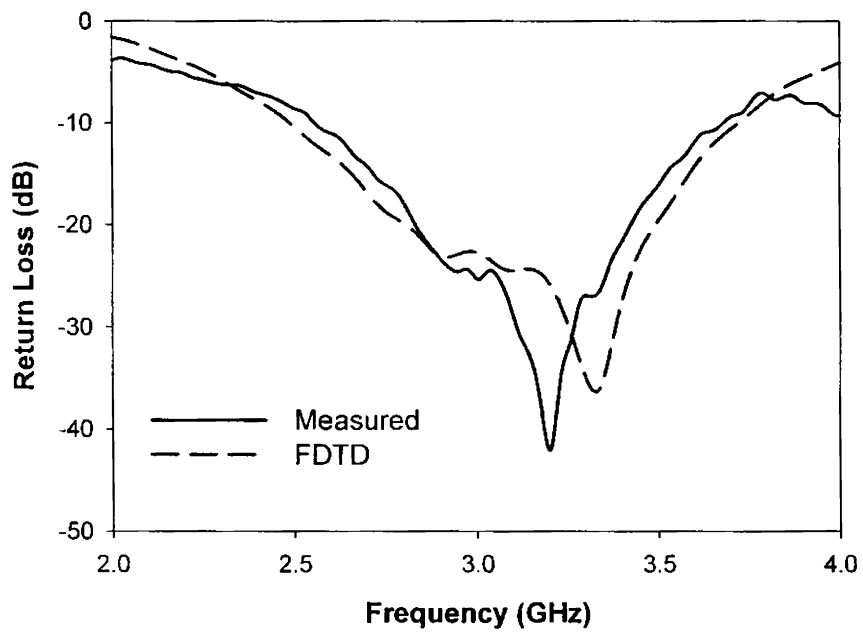
$$mag E = \sqrt{E_x^2 + E_y^2 + E_z^2} \quad (5.17)$$

The magnetic field (H) distribution can be obtained using a similar treatment and are shown in Figures 12 (d), (e) and (f).

Figure 13 illustrates the $mag E$ plots on the boundary planes of the DRA at 3.312 GHz. Additional faces on the YZ and XY -planes at the DR-air boundary are also defined in addition to the XZ -planes, to study the field distributions around the DR. Here faces 1' and 2' correspond to the YZ -plane and the top-face corresponds to the XY -plane.



(a)



(b)

Figure 11: Measured and computed (FDTD) (a) Input impedance and (b) Return Loss of the DRA for design 1

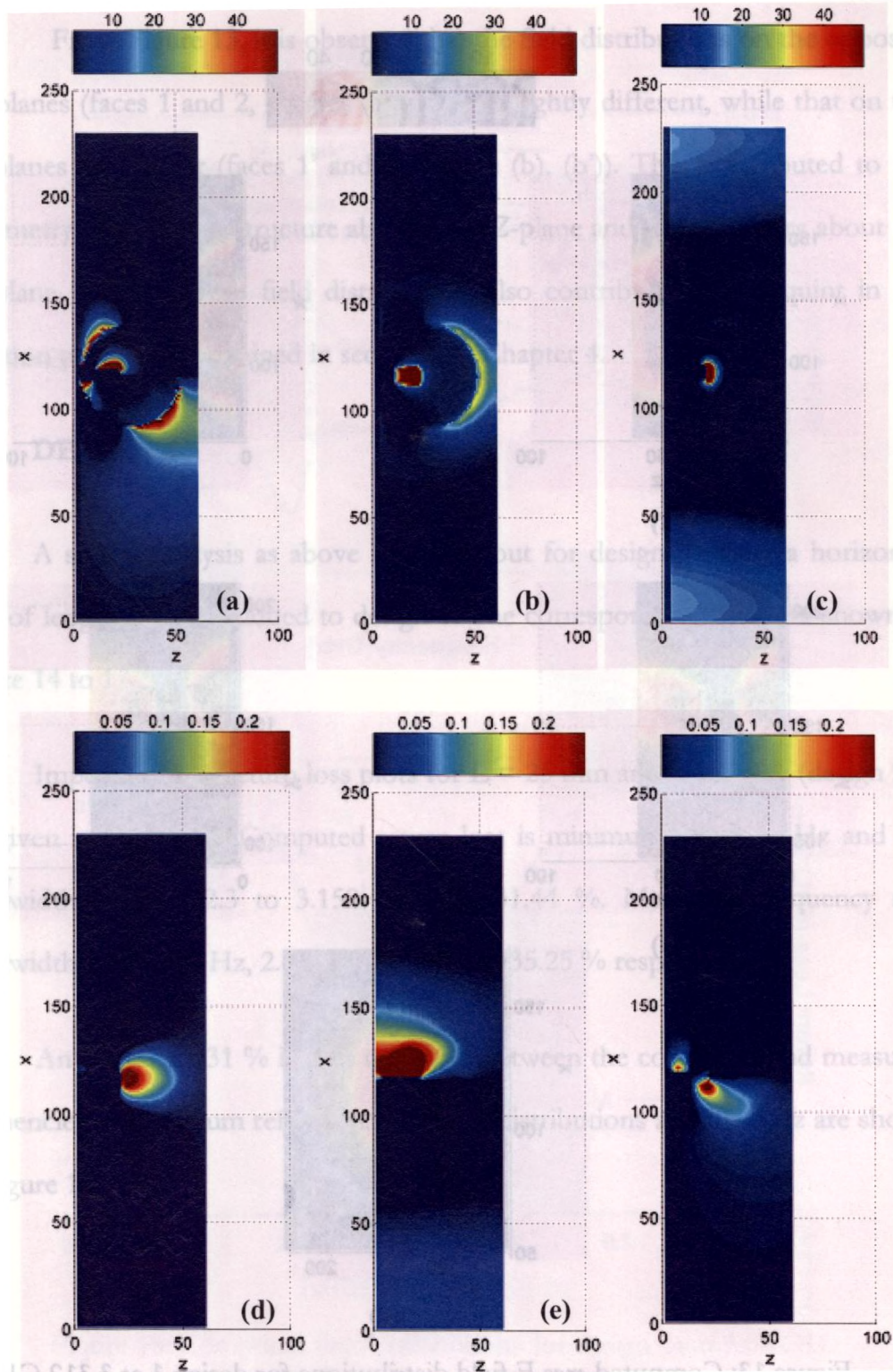


Figure 12: (a) E_x (b) E_y and (c) E_z (d) H_x (e) H_y (f) H_z fields on the face 1 of the DRA for design 1 at 3.312 GHz

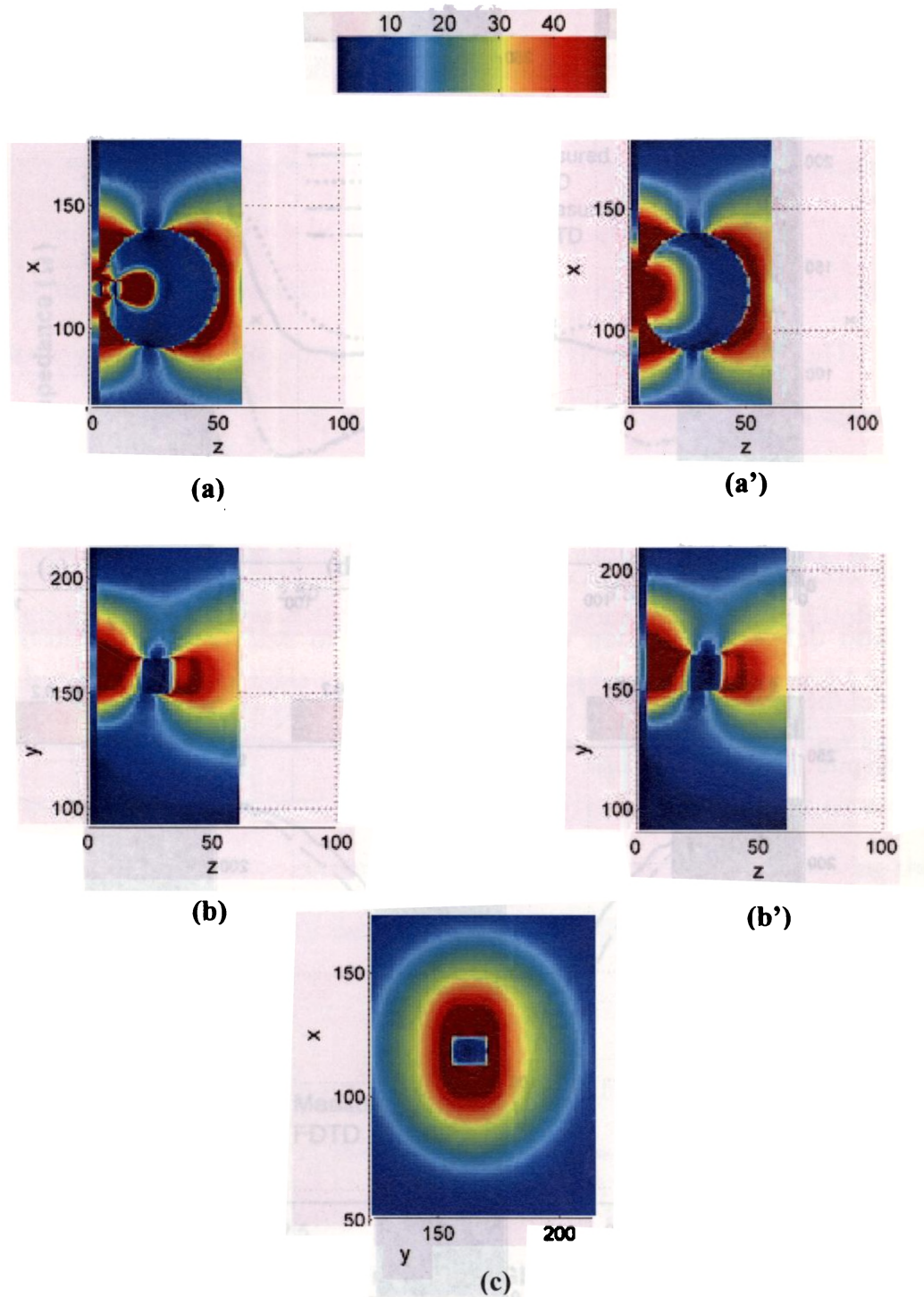


Figure 13: Computed $mag E$ field distributions for design 1 at 3.312 GHz
 XZ-plane (a) face 1 (a') face 2
 YZ-plane (b) face 1' (b') face 2'
 XY-plane (c) Top-face

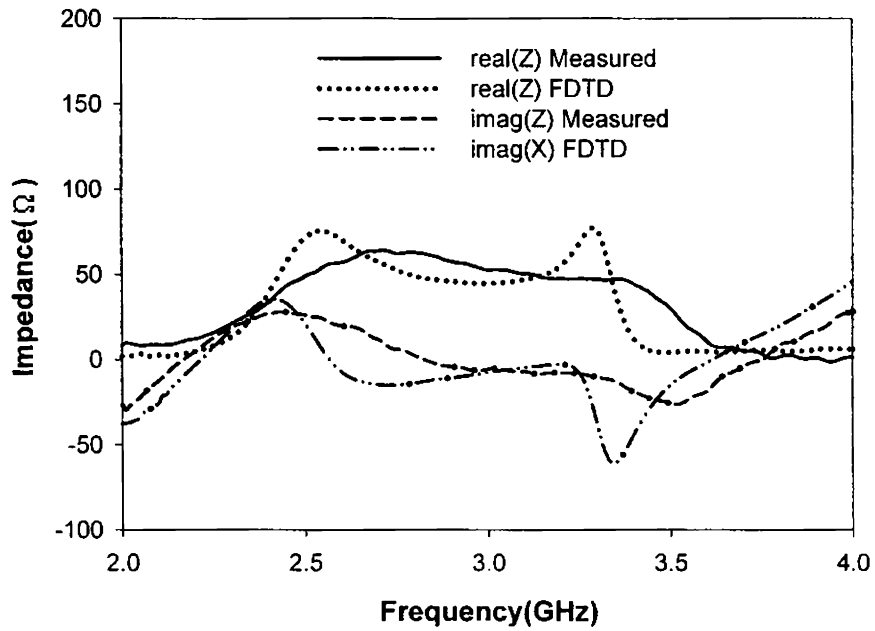
From Figure 13, it is observed that the field distributions on the opposite XZ -planes (faces 1 and 2, Figures (a), (a')) are slightly different, while that on the YZ -planes are similar (faces 1' and 2', Figure (b), (b')). This is attributed to the asymmetry of the DRA structure about the XZ -plane and the symmetry about the YZ -plane. These uneven field distributions also contribute to the squint in the radiation pattern, as explained in section 4.4, Chapter 4.

5.7.2 DESIGN 2

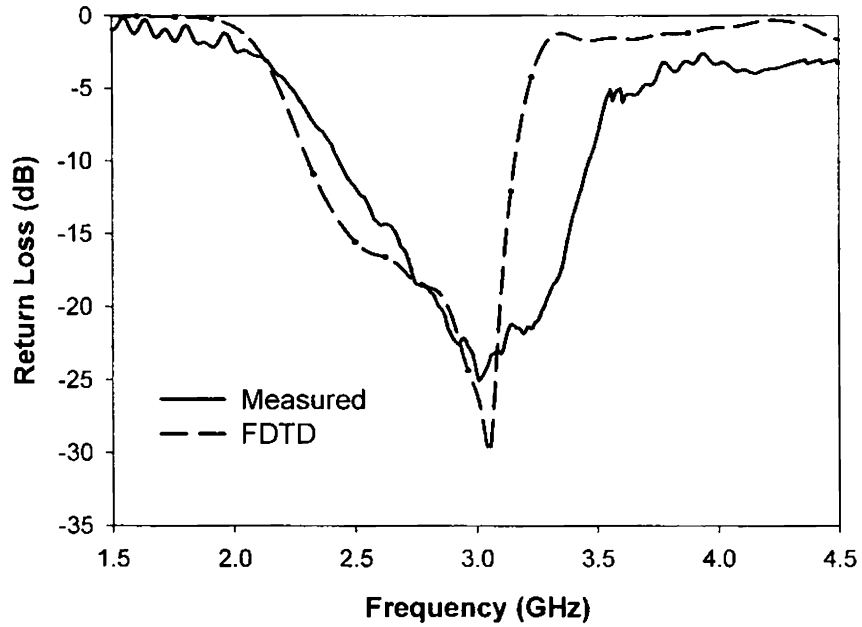
A similar analysis as above is carried out for design 2 where a horizontal stub of length L is also added to design 1. The corresponding plots are shown in Figure 14 to 17.

Impedance and return loss plots for $L = 25$ mm and $h = 7$ mm (design 2a), are given in Figure 14. Computed return loss is minimum at 3.05 GHz and the bandwidth is from 2.3 to 3.158 GHz or 31.44 %. Measured frequency and bandwidth are 3.01 GHz, 2.43 to 3.47 GHz or 35.25 % respectively

An error of 1.31 % is thus observed between the computed and measured frequencies of minimum reflection. The field distributions at 3.05 GHz are shown in Figure 15.



(a)



(b)

Figure 14: Measured and computed (FDTD) (a) Input impedance and (b) Return Loss of the DRA for design 2a

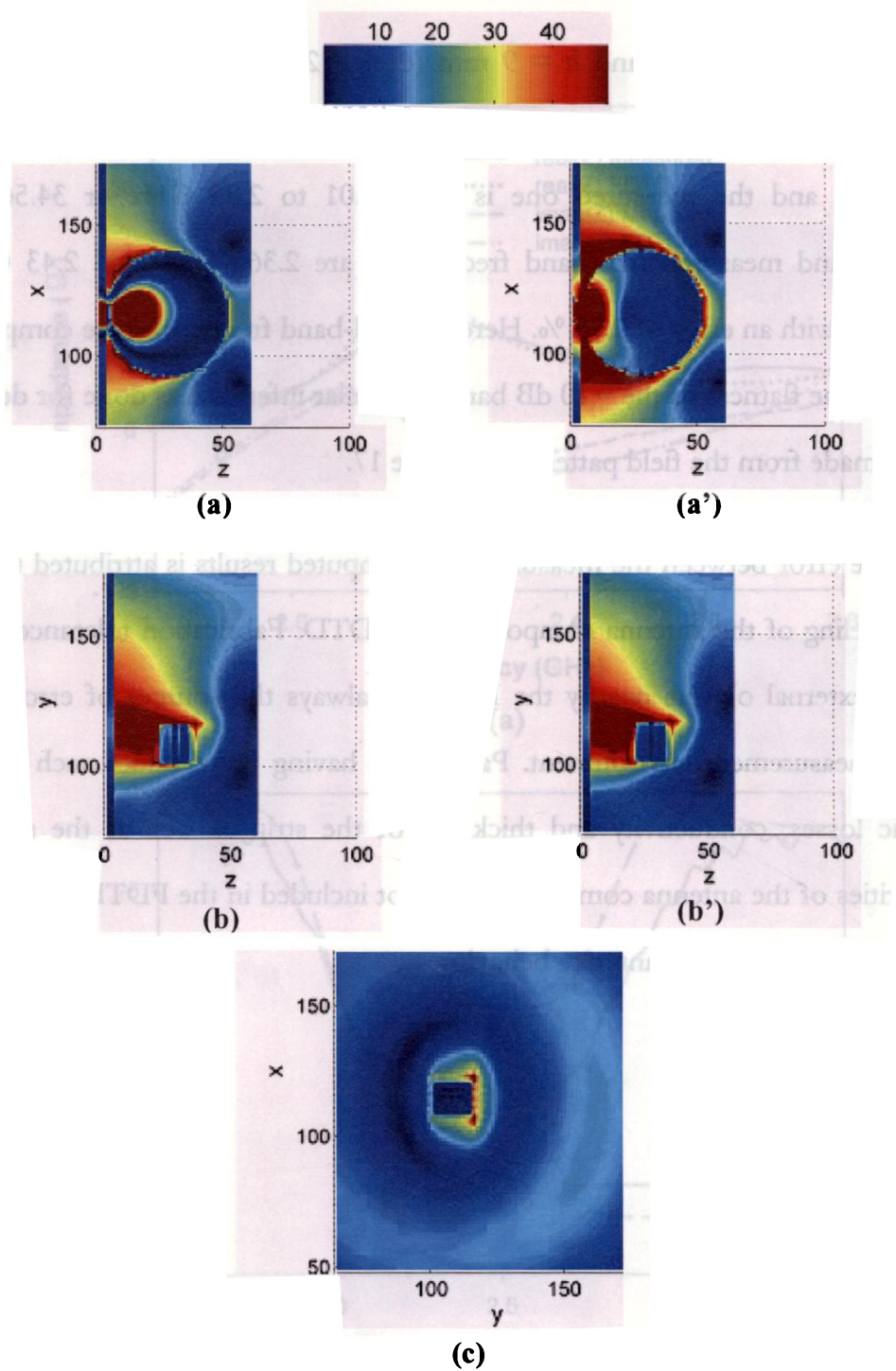
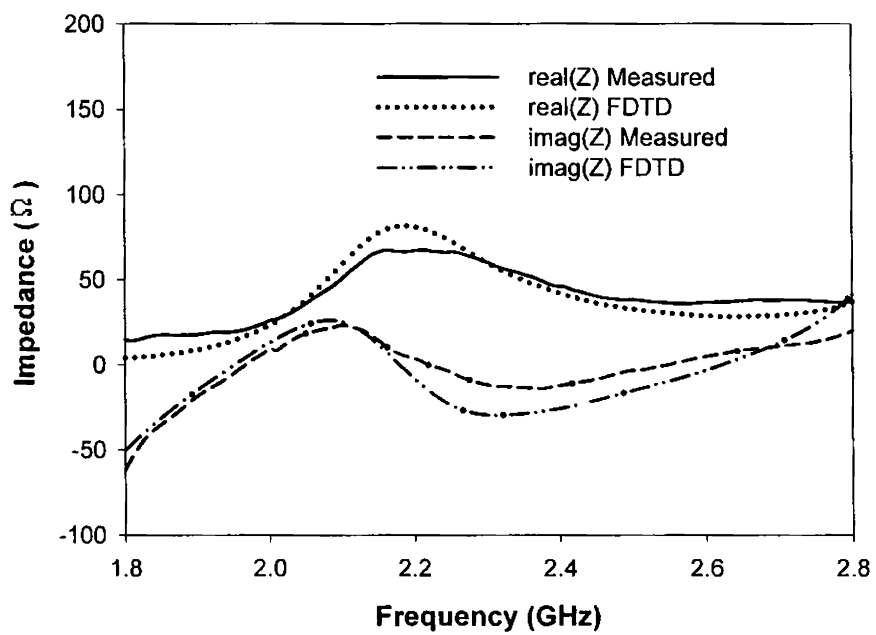


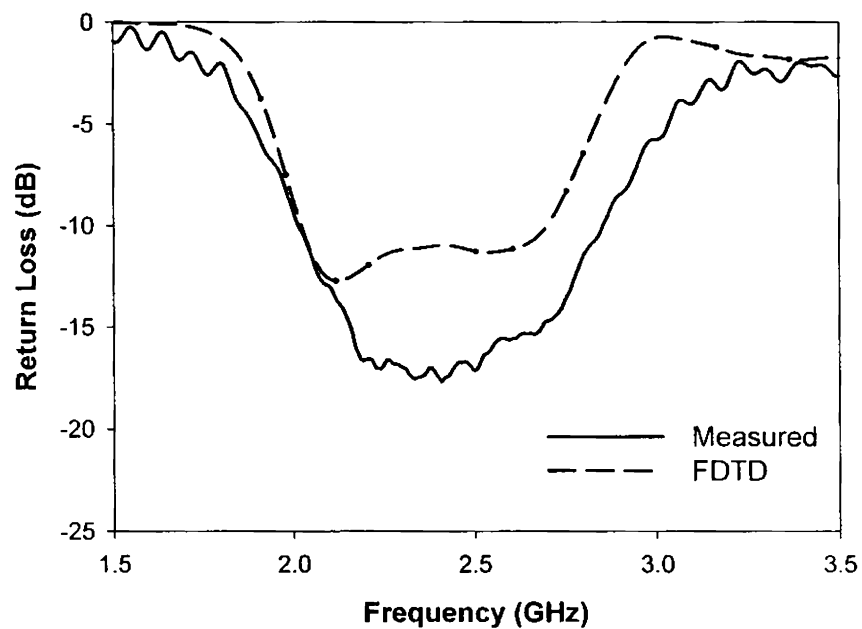
Figure 15: Computed field distributions for design 2a at 3.05 GHz
 XZ-plane (a) face 1 (a') face 2
 YZ-plane (b) face 1' (b') face 2'
 XY-plane (c) Top-face

For $L = 27.5$ mm and $h = 9$ mm (design 2b), corresponding plots are shown in Figures 16 and 17. Computed bandwidth ranges from 2.02 to 2.71 GHz or 29.17 % and the measured one is from 2.01 to 2.85 GHz or 34.56 %. Computed and measured mid-band frequencies are 2.365 GHz and 2.43 GHz respectively with an error of 2.75 %. Here the mid-band frequencies are compared because of the flatness of the -10 dB band. A similar inference as done for design 1 can be made from the field patterns of Figure 17.

The error between the measured and computed results is attributed to the ideal modeling of the antenna components in FDTD. Fabrication tolerances and effect of external objects nearby the DRA are always the sources of error in a practical measurement environment. Parameters having finite values such as the dielectric losses, conductivity and thickness of the strip as well as the surface irregularities of the antenna components are not included in the FDTD modeling, in order to study the ideal antenna behavior.



(a)



(b)

Figure 16: Measured and computed (FDTD) (a) Input impedance and (b) Return Loss of the DRA for design 2b

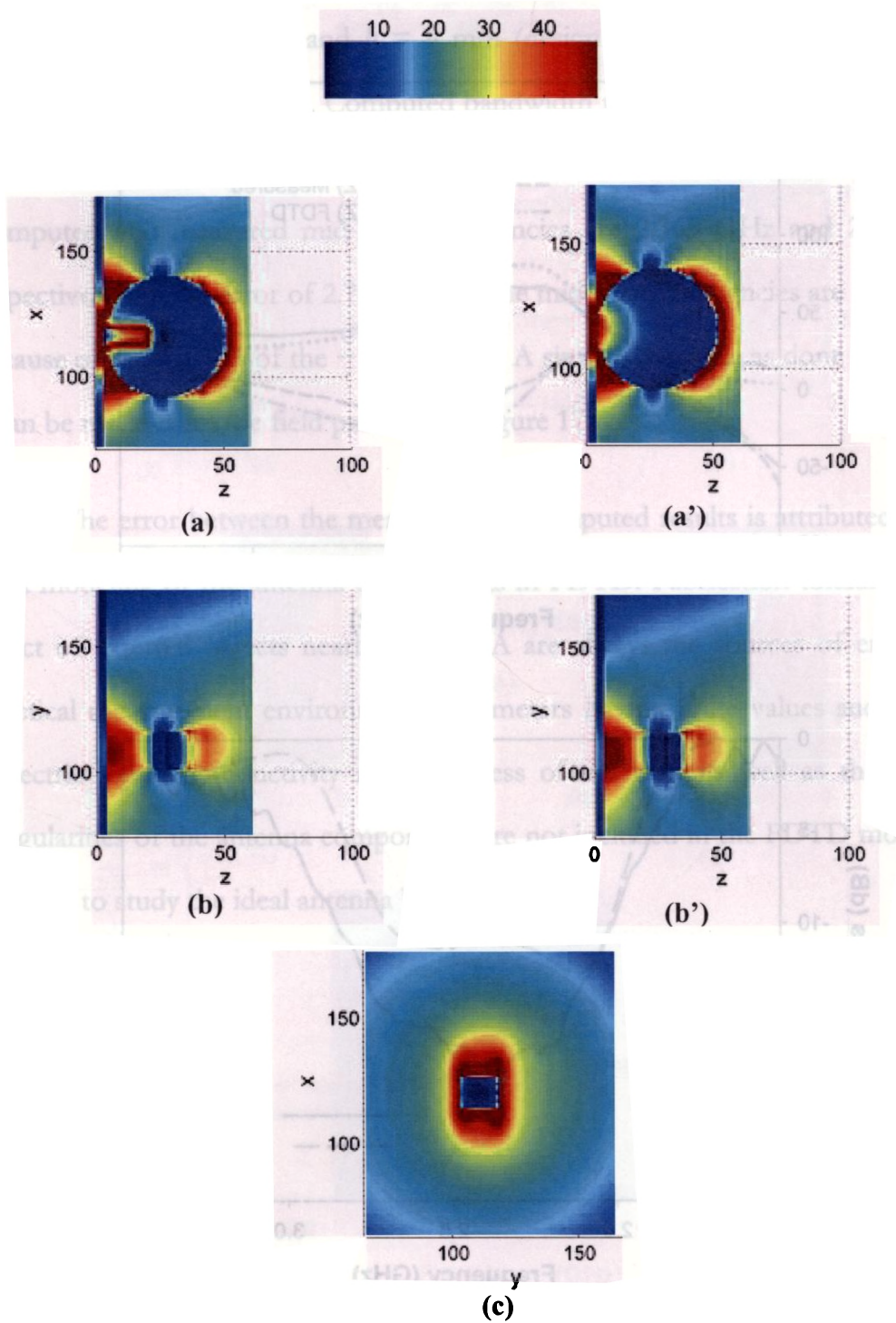


Figure 17: Computed field distributions for design 2b at 2.365 GHz
XZ-plane (a) face 1 (a') face 2
YZ-plane (b) face 1' (b') face 2'
XY-plane (c) Top

CONCLUSION

The numerical technique, FDTD was discussed in this chapter emphasising its application in modeling and analysing antenna problems. Starting with the basic Yee algorithm, the FDTD code for the broadband DRA was developed in MATLAB®. Conformal method was used to model the curved edges of the DR. The input impedance, return loss and near-field patterns of the proposed DRA were computed.

REFERENCES

- [1] K. S. Yee, Numerical Solution of Initial Boundary Value Problems Involving, Maxwell's Equations in Isotropic Media, *IEEE Trans. on Antennas Propag.*, Vol. 14, pp 302–307, May 1966
- [2] T. Uno, Antenna Design Using The Finite Difference Time Domain Method, *IEICE Trans. Commun.*, Vol.E88–B, May 2005
- [3] A. Taflove and M. E. Brodwin, Numerical Solution of Steady-State Electromagnetic Scattering Problems Using the Time-Dependent Maxwell's Equations, *IEEE Microwave Theory Tech*, Vol. 23, pp 623–630, August 1979
- [4] A. Reineix and B. Jecko, Analysis of Microstrip Patch Antennas Using Finite Difference Time Domain Method, *IEEE Trans. on Antennas Propag.*, Vol. 37, pp 1361–1369, November 1980
- [5] A. C. Cangellaris and D. B. Wright, Analysis of the Numerical Error Caused by the Stair-Stepped Approximation of a Conducting Boundary in FDTD Simulations of Electromagnetic Phenomena, *IEEE Trans. Antennas Propagat.*, Vol. 39, pp. 1518–1525, October 1991
- [6] N. Kaneda, B. Houshm, and T. Itoh, FDTD Analysis of Dielectric Resonators with Curved Surfaces, *IEEE Trans. Microwave Theory Tech.*, vol. 45, pp. 1645–1649, September 1997
- [7] S. Dey and R. Mittra, A Conformal Finite-Difference Time-Domain Technique for Modeling Cylindrical Dielectric Resonators, *IEEE Microwave Theory Tech.*, Vol. 47, pp 1737-1739, September 1999

- [8] W. Yu, and R. Mittra, A Conformal Finite Difference Time Domain Technique for Modeling Curved Dielectric Surfaces, *IEEE Microwave Wireless Comp. Lett*, Vol. 11, pp 25-27, January 2001
- [9] X. Zhang and K. K. Mei, Time Domain Finite Difference Approach to the calculation of the Frequency Dependent Characteristics of Microstrip Discontinuities, *IEEE Trans. Microwave Theory Tech.*, Vol. 36, pp 1775-1787, December 1988
- [10] R. J. Luebbers and H. S. Langdon, Simple Feed Model that Reduces Time Steps Needed for FDTD Antenna and Microstrip Calculations, *IEEE Trans. on Antennas Propag.*, Vol. 44, pp 1000-1005 , July 1996
- [11] G. Mur, Absorbing Boundary Conditions for the Finite-Difference Approximation of the Time-Domain Electromagnetic Field Equations, *IEEE Trans. Electromag. Compatibility*, Vol. 23, pp 377–382, November 1981
- [12] J. P. Berenger, A Perfectly Matched Layer for the Absorption of Electromagnetic Waves, *Jour. Comput. Phys.*, Vol. 114, pp185–200, October 1994

The conclusions drawn from the work carried out in this thesis are presented here. In view of the elaborate literature survey carried out, a cylindrical DRA with a novel design was proposed for wideband operation and its characteristics were studied both experimentally and numerically. Existing wideband designs need multiple resonators, additional matching circuits or special DR geometries which are complex in fabrication and/or analysis. Simplicity of the present design owes to the fabrication easiness of the cylindrical DR, its well-defined radiation properties, and the design flexibility. In addition, the present design causes the radiation of a conical beam, unlike the broadside beam as in the case of most of the DRA designs. This is attributed to the DR orientation above the ground plane in requirement of the low-Q design and the conical beam is suited to applications such as vehicular communication and indoor mobile communication, by properly selecting the design parameters for the particular application band.

Main features of the work are:

- **Antenna uses a single cylindrical DR**
- **Main design parameters are the dielectric constant/dimensions of the DR and the height/position of the feed strip**
- **Broad bandwidths higher than 30 % are achieved**

Conclusion

- **Bandwidth tuning is possible for a DR of given parameters, hence operation over multiple application bands is possible**
- **Radiation patterns are conical in shape to be useful in unique applications**
- **Antenna offers high radiation efficiency and good gain suitable for communication applications**

However, the proposed design suffers from a few shortcomings also. Fixing the DR on the substrate is somewhat difficult since no flat surfaces of it are parallel to the substrate. Perspex supports attached to the substrate can fix the DR firmly. Another difficulty of the design is the high surface wave losses associated with the microstrip feed as explained in section 3.7.2, Chapter 3. This can be compacted if low dielectric constant substrate like RT/Duroid ($\epsilon_r = 2.2$) with small thickness is used.

SCOPE FOR FUTURE WORK

Possibility of incorporating components like microwave diodes, inductors, capacitors etc. in the antenna, in order to modify its properties for the purpose of band notching, beam scanning etc. can be sought. A coplanar waveguide feed could be a better alternative to the microstrip feed, when considering the aforesaid device integration. Additional dielectric or microstrip resonators can be incorporated with the present design for achieving ultra wide band (UWB) operation. Also slotted or truncated ground structure can be used for the above

purpose. The effect of material composition of the DR on the antenna properties such as the bandwidth, level of peak/null radiation, antenna gain, efficiency etc. can be studied. The present design can be extended to achieve broadside radiation pattern, by using other low-Q DR geometries that radiate like magnetic dipoles lying parallel to the ground plane.

APPENDIXES

ADDITIONAL COMMENTS

- (1) Q-factor measurement (Pg.66, eq. (3.19)): As per the Khanna-Garault method [10], the displacement 'x' is used to set the bandwidth level in the S_{21} curve, for calculating the Q. If the bandwidth is measured between the points 'x' dB below the maximum S_{21} level (0 dB in fig. 6), on either sides of the resonant frequency, then the resulting $Q=Q_l$. If the points are measured at 'x' dB above the minimum S_{21} point (-40 dB in fig. 6), then $Q=Q_u$. The Q_l and Q_u are related to each other as $Q_u=(1+k)Q_l$, k being the coupling factor between the stripline and the DR. This allows calculation of both Q's from the same S_{21} curve.

- (2) Derivation for radiation efficiency (Pg. 90, eq (3.28)):

The unloaded Q is $Q_u=\omega.E_s/P_{loss}$,

where E_s = energy stored in the DR

P_{loss} =total lost power= $P_{rad}+P_{ohm}$ (radiation+ohmic losses)

Thus, $P_{loss}=\omega.E_s/Q_u$ (1)

Similarly the ohmic loss, $P_{ohm}=\omega.E_s/Q_{ohm}$ (2)

Now, $P_{rad}=P_{loss}-P_{ohm}=(\omega.E_s/Q_u)-(\omega.E_s/Q_{ohm})$ (3)

Putting (1) and (3) in the eqn. $\eta = P_{rad}/(P_{rad}+P_{ohm})$ we get eq. (3.28)

- (3) Radiation patterns (Chapter 4): The radiation of all antennas referred in this chapter are polarised along the direction of the feed strip. The orientations of the 2-D (X, Y, Z) and 3-D (phi, theta, Y) patterns are related to each other as, XZ-plane to phi=0° plane and YZ-plane to phi= -90° plane.

**A CYLINDRICAL DIELECTRIC RESONATOR
ANTENNA FOR DUAL-FREQUENCY OPERATION**

An experimental investigation on a cylindrical dielectric resonator antenna (DRA) for dual-frequency operation is presented. The antenna exhibits linear and identical polarisation characteristics in both frequency bands with broad radiation patterns and good gain.

A.1 INTRODUCTION

Wireless mobile applications demand multi-band antennas, which show efficient radiation characteristics in multiple frequency bands. Different resonator shapes and feed structures have been reported for dual-band operation [Chapter 2]. The present work shows that if properly excited, dual radiating modes with good radiation characteristics can be generated in a simple cylindrical DRA. Antenna measurements are performed with HP 8510C vector network analyser.

A.2 ANTENNA GEOMETRY

A cylindrical dielectric resonator of permittivity $\epsilon_r = 68.5$ is used as the antenna element. The resonator has a diameter $d = 24$ mm and height $h = 11$ mm. A 50Ω microstrip feed line of width 3 mm and length 80 mm is fabricated on a microwave substrate of permittivity $\epsilon_r = 4$ and size 110 mm x 110 mm x 1.6 mm. The proposed antenna geometry is shown in Figure 1.

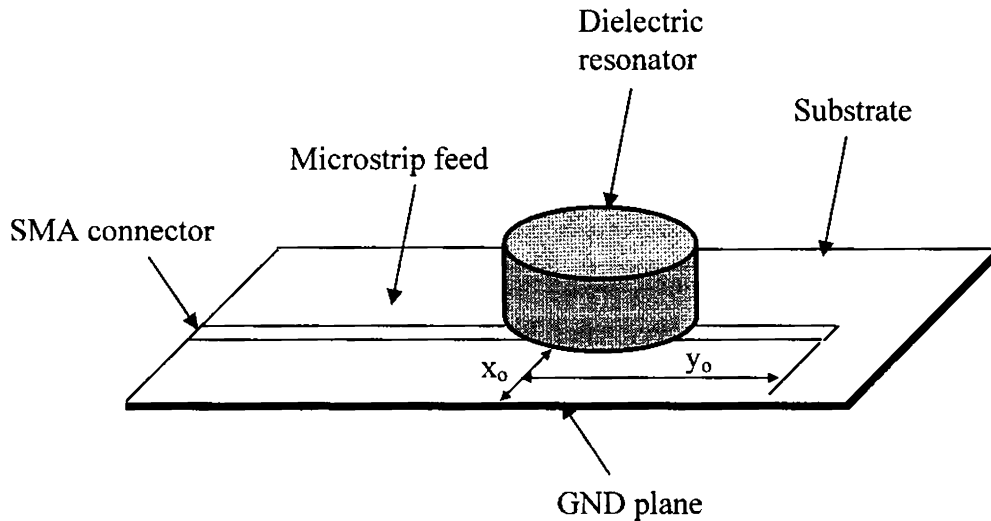


Figure 1: DRA geometry

A.3 RESULTS

The position (x_0, y_0) of the DR is adjusted about the feed line. Different resonant frequencies are observed with varying levels of radiation in the bands. For an optimum feed position $(x_0, y_0) = (70 \text{ mm}, 47.5 \text{ mm})$, dual resonances are obtained as shown in Figure 2. These are at 1.692 GHz and 2.455 GHz, with a frequency separation of 763 MHz. The -10 dB bandwidths are 1.95 % at frequency 1 (1.667 GHz to 1.7 GHz) and 1.67 % at frequency 2 (2.441 GHz to 2.482 GHz).

From the measured transmission coefficients (S_{21}), it is found that the polarisations are linear and are the same in both frequency bands. The measured radiation patterns (E and H - planes) are shown in Figure 3. Patterns are relatively

broad for the two resonant frequencies with cross-polarisation levels less than -15 dB. Measured maximum gain is 7 dBi in band 1 and 5.5 dBi in band 2.

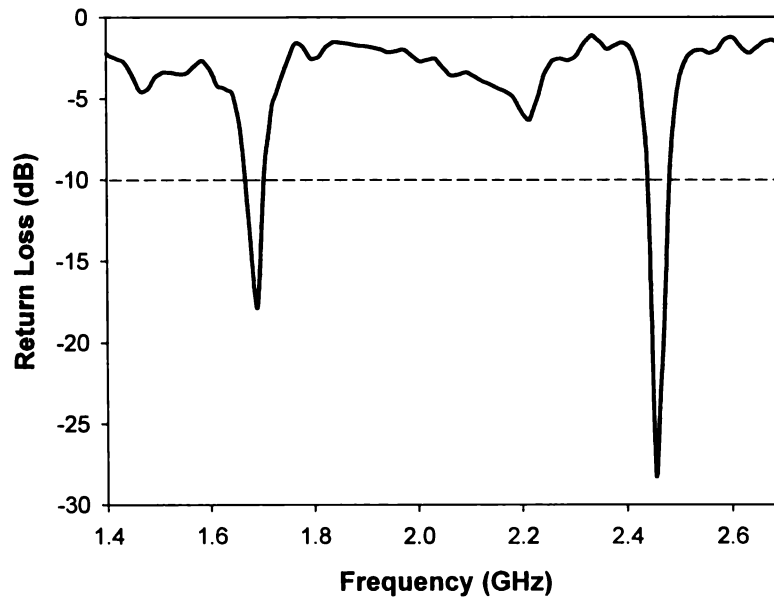


Figure 2: Measured return loss of the DRA

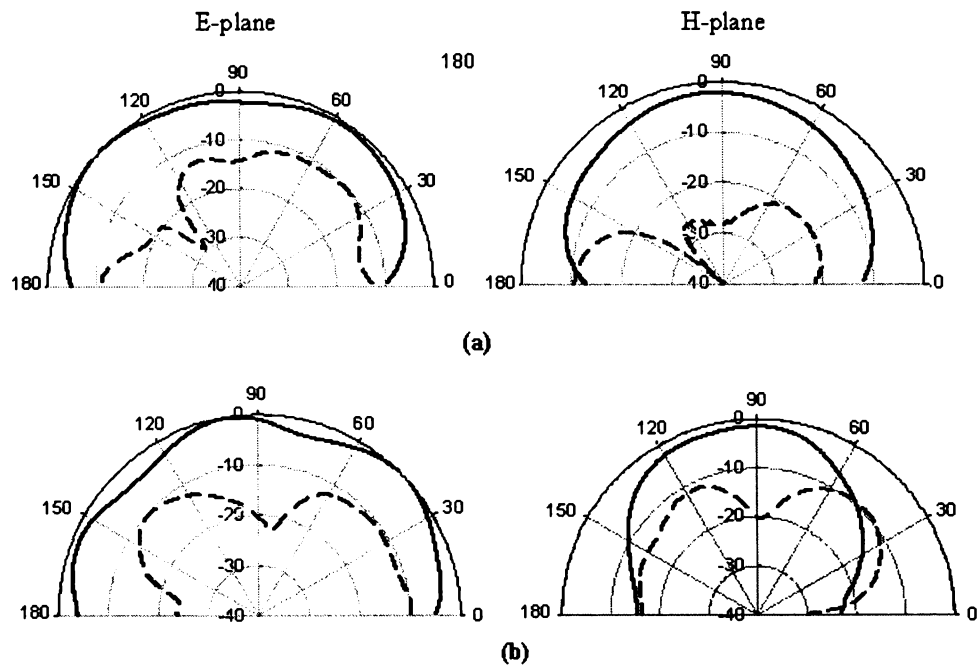


Figure 3: Measured radiation patterns (a) band 1 (b) band2

CONCLUSION

A cylindrical DRA for dual-frequency operation has been demonstrated. The antenna is simple in structure and compact in size. The reflection, impedance, polarisation, and radiation features of the antenna are studied and found suitable for dual-frequency wireless applications.

The work presents the experimental investigation on a cylindrical dielectric resonator antenna (DRA) with a conducting strip loaded on its top surface enabling circular polarisation. The antenna exhibits circular polarisation with an axial ratio (AR) < 3 dB over a bandwidth of 3.14 % and a beam width of 60° .

B.1 INTRODUCTION

The circularly polarised (CP) system, when compared with the linearly polarised (LP) system, allows a more flexible orientation between the transmitting and receiving antennas. In addition, the CP fields of an antenna are less sensitive to the propagation effect than the LP fields. As a result, the CP antennas are widely used in satellite communications. In the present design, two orthogonal modes necessary for CP are excited by loading a metallic strip, diametrically on the top surface of a cylindrical DRA. Strip loading results in a slight downshift of the resonant mode of the DRA and also generates a lower orthogonal mode. The separation between the two modes can be lowered by reducing the strip length and at an optimum length, the two modes merge to give CP.

B.2 ANTENNA GEOMETRY

The antenna geometry is shown in Figure 1. A cylindrical DR of permittivity $\epsilon_{r1} = 20.8$, diameter $2a = 24$ mm and height $h = 7.3$ mm is fed by a 50Ω microstrip transmission line of length 80 mm and width 3 mm, fabricated on a

microwave substrate of permittivity $\epsilon_{r2} = 4$ and size 140 mm (length) x 110 mm (breadth) x 1.6 mm (height) . The DR is placed symmetrically on the feed line with an overlapping distance of $d = 7.5$ mm, as shown in figure which excites the TM_{110} mode at 3.055GHz that radiates in the broadside direction.

A metallic strip of length $L = 2a$ and width $w = 3$ mm is adhered diametrically on the top surface of the DR. Width w is so chosen that the frequency shift of the original DRA mode due to strip loading is minimum . The DR is positioned on the feed in such a way that the metallic strip makes an angle of 45° with the feed strip as shown in Figure 1.

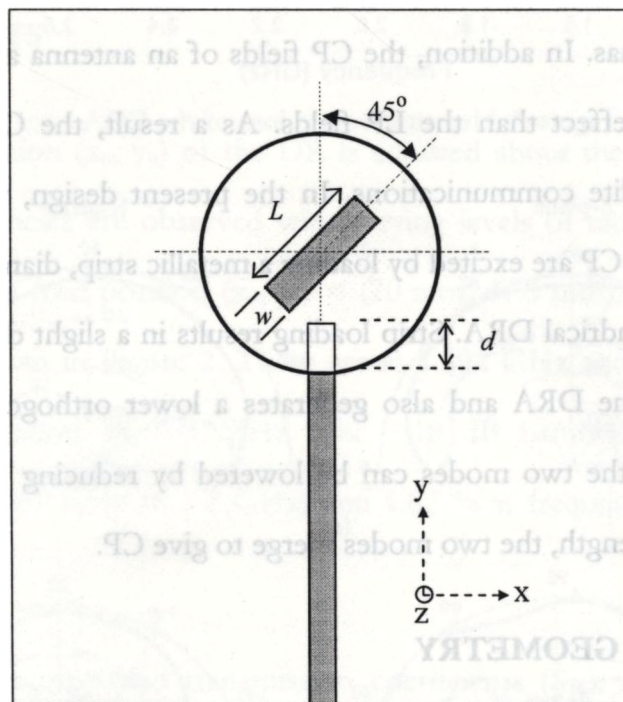


Figure 1: Top view of the cylindrical DRA geometry showing the DR coated with metal strip

B.3 RESULTS

Figure 2 shows the variation in reflection characteristics of the DRA for with variation in L . The original DRA mode (in the absence of strip loading) is indicated by the thin solid curve. It is observed from the figure that, the resonant frequency is reduced from 3.055 to 3.025 GHz, but the impedance matching is improved much on strip loading. In addition, there is a lower resonant mode generated at 1.9 GHz. As the length L is reduced, the lower mode is shifted towards right (higher frequency) considerably while a slight shift of the original mode to the left is observed. At $L = 10$ mm or $\sim 0.1\lambda_0$ where λ_0 is the free space operating wavelength of the DRA, both modes merge to form an impedance band of 2.65 to 3.13 GHz or 16.6 %. The effect of strip width w is also studied and the excitation of the lower-orthogonal mode is observed only when $w = 3$ mm.

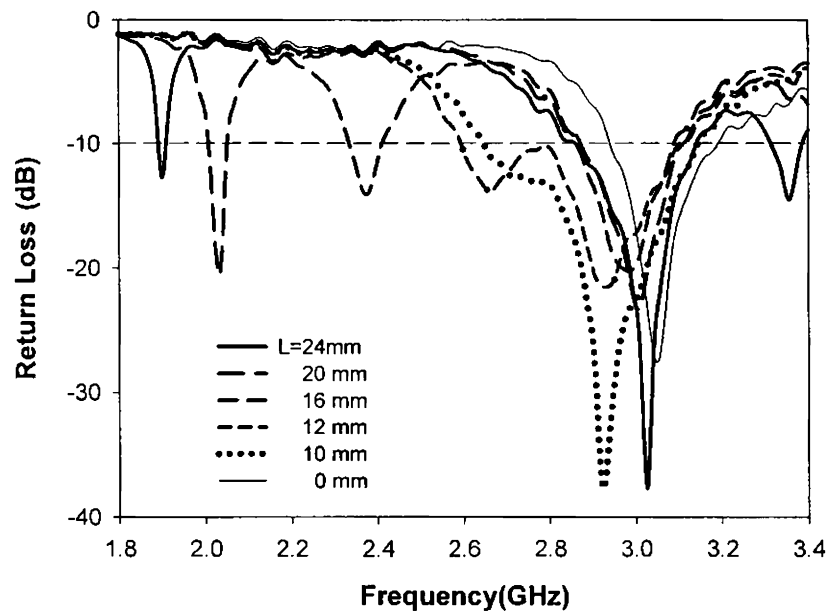


Figure 2: Return loss of the DRA for varying strip length L

The axial ratio in the boresight is measured as shown in Figure 3. An axial ratio bandwidth (AR < 3dB) of 90 MHz or 3.14 % is obtained with minimum AR of 1 dB at 2.87 GHz. Also the axial ratio is found to be below 3 dB over a beam width of $\pm 30^\circ$ from the boresight.

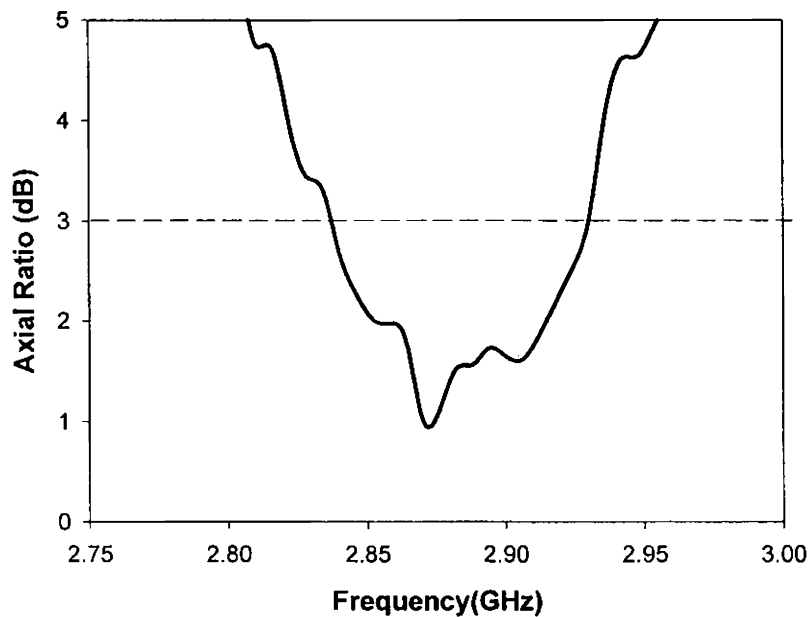


Figure 3: Boresight axial ratio of the DRA for a strip length $L = 10\text{mm}$

Measured radiation patterns at 2.87 GHz for X - Z and Y - Z planes of the DRA are shown in Figure 4. It is clear that the broadside nature of the patterns is unaffected by the strip loading.

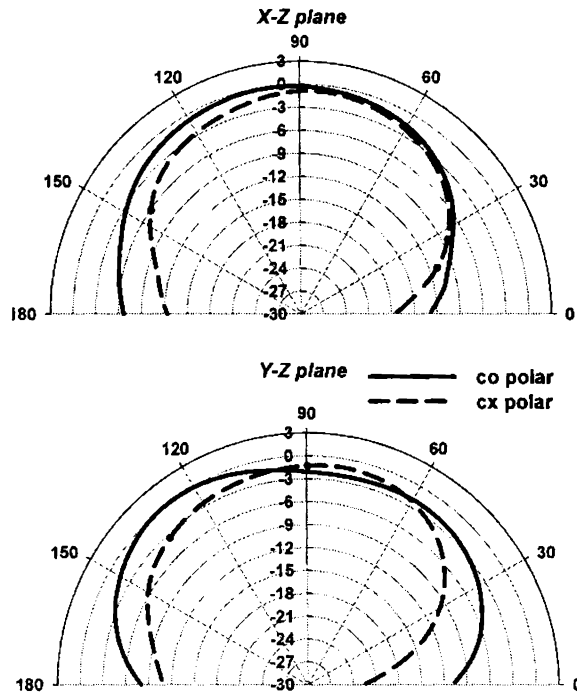


Figure 4: Radiation patterns measured at $f = 2.87$ GHz

CONCLUSION

A cylindrical DRA giving circular polarisation has been presented. The antenna is simple in structure as it comprises only a cylindrical DRA and a loading strip. Measured axial ratio is within 3 dB over a bandwidth of 3.14 % and a beamwidth of 60° .

A cylindrical dielectric resonator antenna with a parasitic conducting strip, loaded coplanar with the 50 Ω microstripline feed has been verified experimentally here. The antenna offers an impedance bandwidth as high as 17.33 % at a centre frequency of 2.77 GHz. The radiation patterns are broad and the low cross-polarisation levels confirm that the antenna is linearly polarised over the entire impedance bandwidth.

C.1 INTRODUCTION

The present design shows how the impedance bandwidth of a cylindrical DRA can be enhanced by adding a parasitic coplanar strip adjacent to the microstrip feed. At an optimum strip position and dimensions, dual radiating modes of similar polarisations are excited in close vicinity to form a linearly polarized and wide impedance band.

C.2 ANTENNA GEOMETRY

The antenna structure is shown in Figure 1. A cylindrical DR of permittivity $\epsilon_{r1} = 20.8$, diameter $2a = 27.3$ mm and height $h = 8.4$ mm is fed with a 50 Ω microstrip transmission line of 80 mm (length) x 3 mm (width), fabricated on a microwave substrate of permittivity $\epsilon_{r2} = 4$ and size 140 mm (length) x 110mm (breadth) x 1.6 mm (thickness). The condition that $\epsilon_{r1} \gg \epsilon_{r2}$, for effective coupling between the feed and the DR is satisfied.

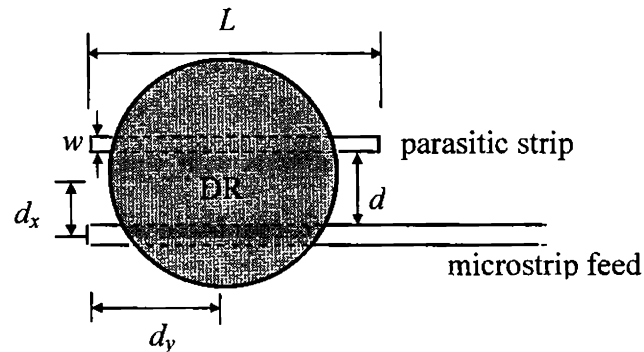


Figure 1: Top view of the DRA geometry

A metallic strip of length L and width w is adhered at a distance of d from the microstripline to modify the feed for the DR as shown in Figure 1. The length of the strip is chosen slightly higher than half the feed strip length i.e. $L = 45$ mm and a width of $w = 1$ mm to start with. The strip length (L), width (w), distance from the feed (d) and the position with respect to the DR (d_x and d_y) are optimized experimentally.

C.3 RESULTS

A maximum bandwidth of 17.33 % obtained for $L = 45$ mm, $w = 2$ mm, $d = 12.5$ mm, $d_x = 2.9$ mm and $d_y = 11.35$ mm. This enhancement in bandwidth is the result of dual radiating modes excited in close vicinity as a result of the strip loading. Depending on the dimensions and the relative position of the parasitic strip, the magnitude and phase of the energy coupled to the strip vary, which excites an additional radiating mode of higher frequency. The return loss and impedance variation at the optimum design parameters are shown in Figure 2, which justify the excitation of dual modes.

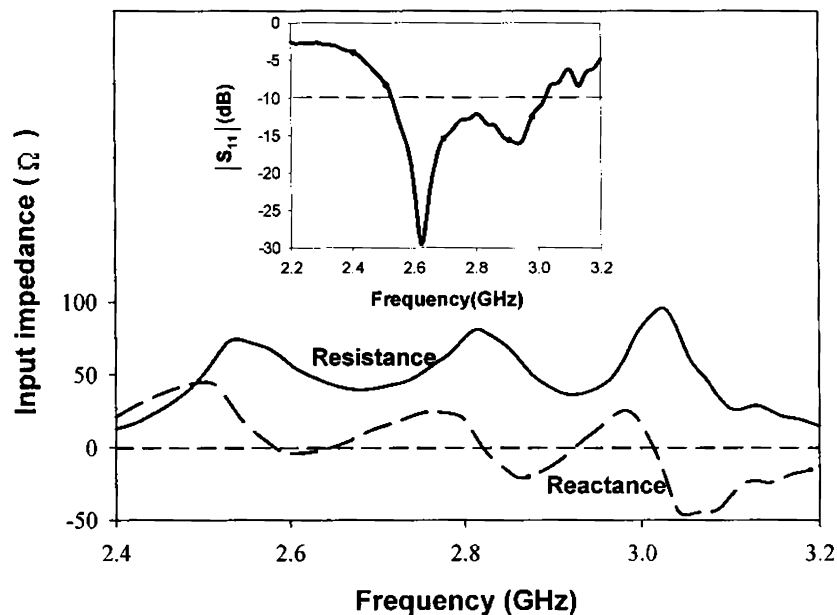


Figure 2: Measured input impedance corresponding to the return loss plot shown in inset for optimum values of $L = 45$ mm, $w = 2$ mm, $d = 12.5$ mm, $d_x = 2.9$ mm and $d_y = 11.35$ mm

Radiation patterns are measured for the two principal planes viz X - Z and Y - Z planes. Figure 3 shows the radiation patterns at 2.62, 2.77 and 2.935 GHz i.e., in the neighbourhood of the lower, centre and upper ends of the operating band respectively. The co-polar patterns are broadsided with good cross-polar levels. At the upper end of the band, the cross-polarisation of the X - Z plane is better than -30 dB. On the other hand, the Y - Z plane shows good cross-polarisation at the lower end of the band. The small degree of asymmetry in the patterns is due to the effects of the SMA connector and feed cable on one side of the antenna. Half power beam widths (HPBW) measured from the radiation patterns are 97°

APPENDIX D

**A HALF-CYLINDRICAL
DIELECTRIC RESONATOR ANTENNA**

A compact half-cylindrical dielectric resonator antenna (DRA) made from a high permittivity ceramic material is investigated. The DRA shows broadside radiation characteristics with good gain across the matching band that covers the 2.4 GHz- WLAN band.

D.1 INTRODUCTION

Many techniques have been proposed to achieve compact DRAs in which the most successful are half volume DRA designs. As the bandwidth of a DRA is limited by the dielectric constant of the DR being used, various feed designs are employed to get the desired impedance bandwidth. A half-cylindrical DR geometry as the one presented here can support multiple radiating modes and if properly excited, impedance bands corresponding to those modes having similar radiation characteristics can be merged to provide the band suitable for a particular application. In this work, a compact half-cylindrical DRA suitable for WLAN application is presented. A resonant mode is excited close to the broadside $TM_{12\delta}$ mode thereby forming the WLAN band of 2.4 to 2.484 GHz.

D.2 ANTENNA GEOMETRY

The antenna geometry is shown in Figure 1. A half-cylindrical dielectric resonator (DR) of permittivity $\epsilon_{r1} = 69$, diameter $2a = 26$ mm and height $d = 12$

mm is fed by a 50Ω microstrip transmission line of length $L = 10$ cm and width $w \sim 3$ mm, fabricated on a microwave substrate of permittivity $\epsilon_{r3} = 4.7$ and size 140 mm x 110 mm x 1.64 mm. The DRA is operated in the broadside TM_{128} mode by properly choosing the feed position. The feed position is optimized experimentally as $(x_o, y_o) = (5$ mm, 40 mm), where x_o and y_o are defined respectively as the vertical and horizontal distances from the stripline to the DR as shown in Fig.1 (b).

For a given TM_{vpm} mode, the resonant frequency is given as

$$f = \frac{c}{2\pi a \sqrt{\epsilon_{r1}}} \sqrt{X_{vp}^2 + \left(\frac{\pi a}{2d}(2m+1)\right)^2} \quad (1)$$

where X_{vp} is the root of the characteristic equation $J'_v(X_{vp}) = 0$, J_v is the v^{th} order Bessel function of the first kind, c is the velocity of light, $v \geq 0$, $p = 1, 2, 3, \dots$ and $m = 0, 1, 2$ etc. For the DRA of the present case, the TM_{128} mode frequency is calculated by (1) as 2.475 GHz.

D.3 RESULTS

Measured return loss of the DRA as a function of frequency is plotted in Figure 2. The antenna has a 2:1 SWR bandwidth ranging from 2.32 to 2.5 GHz (7.45 %) that includes the 2.4 GHz WLAN band of 2.4 to 2.485 GHz. It is noted that the return loss is minimum at the frequency of 2.455 GHz, which agrees reasonably well with the theoretical value calculated above. It is noted that the

bandwidth includes a lower resonance at 2.365 GHz, close to the TM_{128} resonance to form the band of interest. Figure 3 shows the input impedance of the DRA.

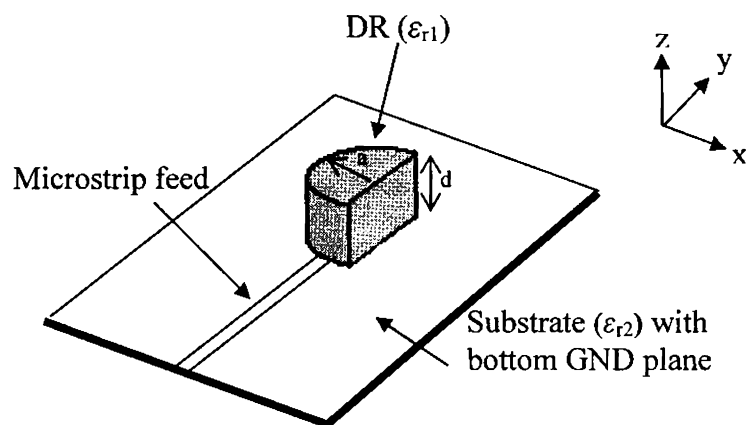


Figure 1: Geometry of the half-cylindrical DRA

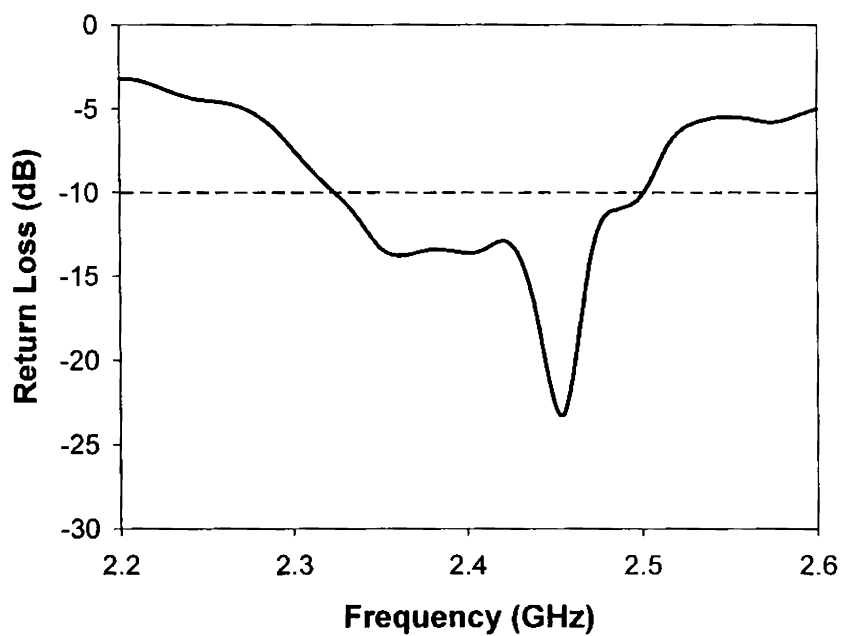


Figure 2: Measured Return Loss of the DRA

Measured radiation patterns at 2.45 GHz are shown in Figure 4. Patterns are relatively broad with good cross-polar levels. The YZ-plane pattern is symmetric because of the symmetry of the DR about that plane.

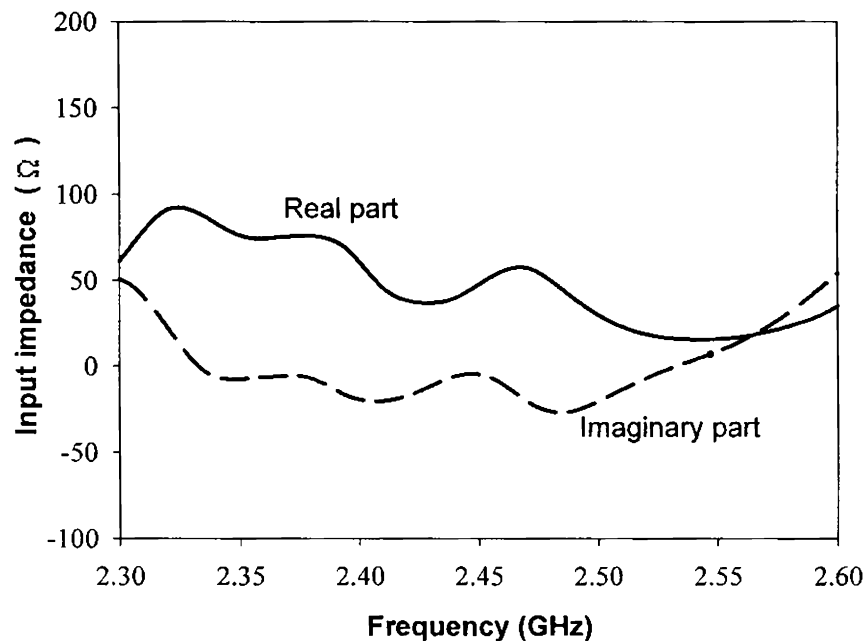


Figure 3: Input impedance of the DRA

But in the XZ-plane, the radiation is stronger at $\theta = 120^\circ$ as shown in the figure. This may be due to the asymmetry of the DR about that plane where its curved surface also contributes to the radiation in that direction. Radiation patterns at other frequencies in the band also show similar characteristics. The antenna offers a peak gain of 4.58 dBi at 2.44 GHz.

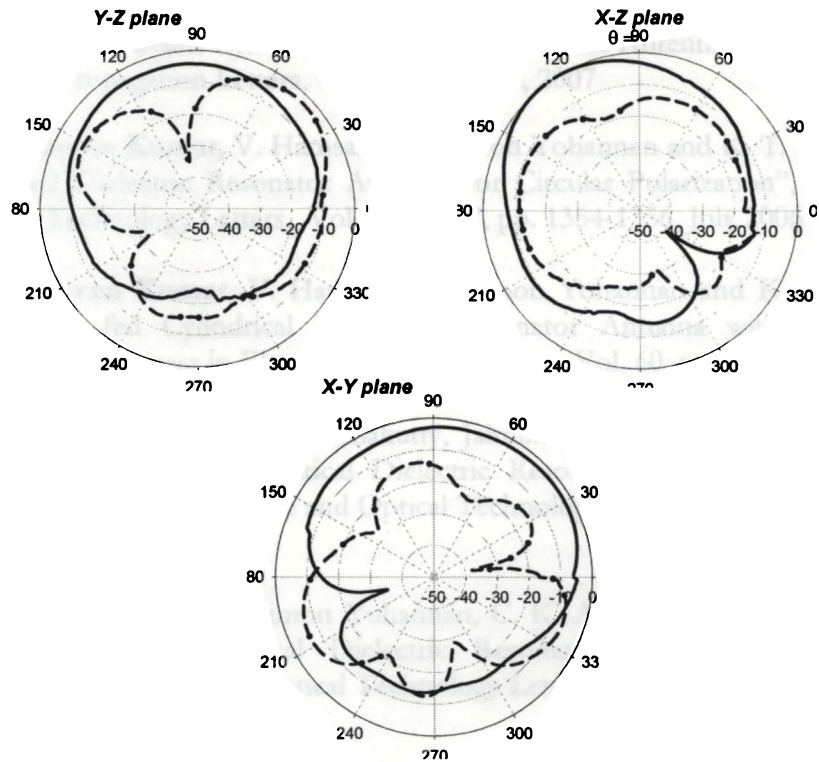


Figure 4: Radiation patterns measured at 2.45 GHz

— Co-polar
- - - Cx-polar

CONCLUSION

A study on microstripline fed half-cylindrical dielectric resonator antenna has been presented. The DRA offers good reflection and radiation characteristics in an impedance band suitable for 2.4 GHz WLAN application.

LIST OF PUBLICATIONS

JOURNALS

1. **A. V. Praveen Kumar**, V. Hamsakutty, Jaimon Yohannan and K. T. Mathew, "A Wideband Conical Beam Cylindrical Dielectric Resonator Antenna", IEEE Antenna and Wireless Propagation Letters, Vol. 6, pp. 15-17, 2007
2. **A. V. Praveen Kumar**, V. Hamsakutty, Jaimon Yohannan and K. T. Mathew, "A Strip Loaded Dielectric Resonator Antenna for Circular Polarization", Microwave and Optical Technology Letters , Vol. 48, No. 7, pp. 1354-1356, July 2006
3. **A. V. Praveen Kumar**, V. Hamsakutty, Jaimon Yohannan and K. T. Mathew, "Microstripline fed Cylindrical Dielectric Resonator Antenna with a Coplanar Parasitic Strip", Progress in Electromagnetic Research, Vol. 60, pp. 143-152, 2006
4. **A. V. Praveen Kumar**, V. Hamsakutty, Jaimon Yohannan and K. T. Mathew "Microstripline fed Half-Cylindrical Dielectric Resonator Antenna for 2.4 GHz WLAN application", Microwave and Optical Technology Letters , Vol. 48, No. 4, pp. 724-726, April 2006
5. **A. V. Praveen Kumar**, Jaimon Yohannan, C. K. Aanandan and K. T. Mathew "Microstripline fed Cylindrical Dielectric Resonator Antenna for Dual-band operation", Microwave and Optical Technology Letters Vol. 47, No. 2, pp. 150-153 October 2005
6. V. Hamsakutty, **A. V. Praveen Kumar**, Jaimon Yohannan and K. T. Mathew, "Hexagonal Dielectric Resonator Antenna for 2.4 GHz WLAN Applications", Microwave and Optical Technology Letters, Vol. 49, No. 1, pp. 162-164, November 2006
7. V. Hamsakutty, **A. V. Praveen Kumar**, Jaimon Yohannan, G. Bindu and K. T. Mathew, "Coaxial Fed Hexagonal Dielectric Resonator Antenna for Multifrequency Operation", Microwave and Optical Technology Letters , Vol. 48, No. 5 , pp. 878 - 880, May 2006.
8. V. Hamsakutty, **A. V. Praveen Kumar**, Jaimon Yohannan and K. T. Mathew, "Coaxial fed Hexagonal Dielectric Resonator Antenna for Circular Polarization", Microwave and Optical Technology Letters , Vol. 48, No. 3 , pp. 581 - 582, March 2006
9. V. Hamsakutty, **A. V. Praveen Kumar**, G. Bindu, Vinu Thomas, Anil Lonappan, Jaimon Yohannan and K. T. Mathew, "A Multifrequency Coaxial Fed Metal Coated Dielectric Resonator Antenna", Microwave and Optical Technology Letters , Vol. 47, No. 6 , pp. 573 - 575, Dec 2005.

10. G. Bindu, Anil Lonappan, Vinu Thomas, **A. V. Praveen Kumar**, V. Hamsakutty, C. K. Aanandan and K.T Mathew, "Two Dimensional Microwave Tomographic Imaging of Low Water Content Tissues", *Microwave and Optical Technology Letters*, Vol. 46, No.6, pp. 599-601 ,Sept 2005

CONFERENCES

1. **A. V. Praveen Kumar** and K. T. Mathew, "Cylindrical Dielectric Resonator Antenna with a Coplanar Parasitic conducting strip", 10th National Symposium on Antennas and Propagation, APSYM-2006, Department of Electronics, Cochin University of Science & Technology, Cochin, India, December 14-16, 2006
2. **A. V. Praveen Kumar**, V. Hamsakutty, Jaimon Yohannan and K. T. Mathew, "Half-Split Cylindrical Dielectric Resonator Antenna for 2.4 GHz WLAN Operation", IEEE AP-S International Symposium on Antennas and Propagation and USNC/URSI National Radio Science Meeting ,Albuquerque, New Mexico, July 9-14, 2006
3. **A. V. Praveen Kumar**, Jaimon Yohannan, Anil Lonappan, Bindu G., Vinu Thomas, V. Hamsakutty and K. T. Mathew, "Microstripline Fed Circular Sector Dielectric Resonator Antenna" -IEEE AP-S International Symposium on Antennas and Propagation and USNC/URSI National Radio Science Meeting ,Washington DC , July 3-8, 2005
4. **A. V. Praveen Kumar**, V. Hamsakutty, Jaimon Yohannan and K. T. Mathew, "Microstripline fed Cylindrical Sector Dielectric Resonator Antenna", APMC- Asia-Pacific Microwave Conference, Suzhou, China, December 4-7, 2005
5. K. T. Mathew, **A. V. Praveen Kumar** and Honey John, "Polyaniline and Polypyrrole with PVC content for effective EMI shielding", IEEE International Symposium on Electromagnetic Compatibility, Portland, USA, August 14 – 18, 2006
6. V. Hamsakutty, **A. V. Praveen Kumar**, Jaimon Yohannan and K. T. Mathew, "Hexagonal Dielectric Resonator Antenna for Multifrequency Operation", IEEE AP-S International Symposium and USNC / URSI National Radio Science meeting, APS/URSI 2006, Alberque, USA, July 9-13, 2006
7. V. Hamsakutty, **A. V. Praveen Kumar**, Jaimon Yohannan and K. T. Mathew, "Coaxial Fed Hexagonal Dielectric Resonator Antenna", APMC- Asia-Pacific Microwave Conference, Suzhou, China, December 4-7, 2005
8. Jaimon Yohannan, **A. V. Praveen Kumar**, Vinu Thomas, V. Hamsakutty, Anil Lonappan, Bindu G. and K. T. Mathew, " Half split Dielectric Resonator Antenna", Ferroelectrics UK International conference , Paisley, UK , April 26-27, 2005

9. Jaimon Yohannan, , V. Hamsakkutty, **A. V. Praveen Kumar**, Vinu Thomas, Bindu G. and K. T. Mathew, “A Rectangular Dielectric Resonator Bandstop Filter”, IEEE AP-S International Symposium and USNC / URSI National Radio Science meeting, APS/URSI 2006, Alberque, USA, July 9-13, 2006.
10. Jaimon Yohannan, **A. V. Praveen Kumar**, Vinu Thomas, V. Hamsakkutty and K. T. Mathew, “Microwave Ceramic Resonator Antenna for Communication Applications” -2005 IEEE AP-S International Symposium on Antennas and Propagation and USNC/URSI National Radio Science Meeting , Washington DC, July 3-8, 2005
11. Jaimon Yohannan, **A. V. Praveen Kumar**, Vinu Thomas, V. Hamsakkutty and K. T. Mathew, “Synthesis of Dielectric Resonators for Microwave Filter Designing”-Progress in Electromagnetics Research Symposium (PIERS 2005) Hangzhou, China, , August 22–26, 2005,
12. G. Bindu, **A. V. Praveen Kumar**, Anil Lonappan, C. K. Aanandan and K. T. Mathew, “Microwave Imaging of Dielectric Wax Cylinders”, 9th National Symposium on Antennas and Propagation, APSYM 2004, Department of Electronics, Cochin University of Science & Technology, Cochin, India, December 21-23, 2004.
13. Jaimon Yohannan, Vinu Thomas, V. Hamsakutty, **A. V. Praveen Kumar** and K.T. Mathew, “Sr_(1-x/2) Na_xNb₂O₆ Ceramic Dielectric Resonator Antennas” 9th National Symposium on Antennas and Propagation, APSYM 2004, Department of Electronics, Cochin University of Science & Technology, Cochin, India, December 21-23, 2004.

ARTICLE CITATIONS

- [1] C. W. Ling, C. Y. Lee, C. L. Tang, and S. J. Chung, “Analysis and Application of an On-Package Planar Inverted-F Antenna”, IEEE Tran. Antennas Propag., Vol. 55, pp. 1774-1780, 2007
- [2] H. Fayad And P. Record, “Multi-Feed Dielectric Resonator Antenna with Reconfigurable Radiation Pattern”, Progress In Electromagnetics Research, PIER 76, 341–356, 2007
- [3] P. Rezaei, M. Hakkak, and K. Forooghi , “Design of Wide-Band Dielectric Resonator Antenna with a Two-Segment Structure”, Progress In Electromagnetics Research, PIER 66, 111–124, 2006

CURRICULUM VITAE

A.V. PRAVEEN KUMAR

RESEARCH FELLOW

Microwave Tomography and Materials Research Laboratory
Department of Electronics
Cochin University of Science and Technology
Cochin- 682-022, India
Phone : +91-484-2576418
Mob : +91-9495161780
Fax : +91-484-2575800
Email : praveenambattu@gmail.com

OBJECTIVE

To secure a challenging position associated with research and development in the field of dielectric resonators, cavity resonators, antennas, microwave materials characterisation or other related fields

ACADEMIC RECORDS

- **Ph.D in Microwave Electronics (2004–2008, Thesis submitted)**
Microwave Tomography and Materials Research Laboratory
Department of Electronics
Cochin University of Science and Technology
Cochin, India
- **M.Sc. in Electronics Science (Microwave specialisation) (2000–2002)**
Department of Electronics
Cochin University of Science and Technology
Cochin, India
CGPA: 8.25/10, First rank
- **B.Sc. in Electronics (1997–2000)**
M.E.S. College
Mahatma Gandhi University
Kottayam, India
Percentage score: 86.45 %, Batch Topper

SUBJECTS STUDIED

Electromagnetic Theory, Wave Guides and Antennas, Microwave Engineering, Radar Communication, Analog and Digital Circuit Design, Digital Signal Processing, Microprocessors and Microcontrollers, Computer Networks

RESEARCH INTERESTS

Microwave Antennas, Dielectric Resonator Antennas, Microwave Materials characterisation, Microwave measurements and Finite Difference Time Domain technique

OTHER INTERESTS

Teaching Electromagnetic Theory, Microwave Engineering, Analog and digital circuit design

RESEARCH EXPERIENCE

- ✦ Fabrication of Dielectric Resonators for antennas and filters through solid state ceramic processing
- ✦ Design and measurement of Dielectric Resonator Antennas for Dual-band, Wideband, Circular polarization and Conical-beam applications
- ✦ Design and measurement of microstrip patch antennas
- ✦ Finite Difference Time Domain analysis of microstrip patch and dielectric resonator antennas
- ✦ Microwave measurement techniques like cavity perturbation, Hakki-Coleman method and Khanna-Garault method for the characterisation of materials like liquids, substrate materials, polymers, ceramics etc
- ✦ Implementation of two-dimensional microwave imaging chamber with transmitting / receiving antennas, interfaced with VNA and workstation as part of the project titled 'Microwave Imaging of Biological Objects for Medical Application Using Freespace Complex Permittivity Measurements', funded by Department of Science and Technology, India
- ✦ Implementation of automated turn-table arrangement interfaced with VNA and workstation for the measurement of antenna radiation pattern as part of the project titled 'Development of Novel Class of Materials for Antenna having Automatic Beam Steering Property' funded by Defense Research and Development Organisation (DRDO), India

- ✦ Anechoic Chamber measurements
- ✦ Co-guided two M.Sc. course projects, one in dielectric resonator antenna and the other in microwave instrumentation for material characterisation.

ACHIEVEMENTS

- ✦ Authored/co-authored 23 research papers in referred journals/conference proceedings
- ✦ Research fellowship from Kerala State Council for Science Technology and Environment (KSCSTE) for the period 2004 - 2007
- ✦ First rank in the M.Sc. Examination
- ✦ Graduate Aptitude Test in Engineering (GATE) scorer – GATE 2003 and GATE 2004 with scores of 90.19 and 93.95 respectively

COMPUTER SKILLS

- ✦ Operating System: Windows 98, Xp, 2k, NT
- ✦ Programming Language: Matlab, C, C++, HPBASIC

ELECTROMAGNETIC SIMULATION TOOLS HANDLED

Ansoft HFSS, CST Microwave Studio

INSTRUMENTS HANDLED

- ✦ Vector Network Analyzers : Agilent 8714 ET, HP 8510 C, Rohde & Schwarz ZVB20 VNAs and HP E8362 B PNA
- ✦ Vacuum thin film coating unit (Hind Hivac Pvt Ltd, India)
- ✦ Muffle Furnace (1200°C)

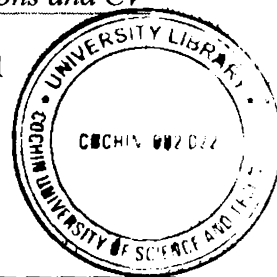
PERSONAL DETAILS

Age and Date of Birth : 27 yrs, 20th May 1980
Sex : Male
Marital Status : Single
Father's Name : A. K. Vijayaraghavan Nair
Nationality : Indian

T338

List of publications and CV

Languages Known : Malayalam, English, Hindi and Tamil
Permanent Address : Ambattu House
Angadikadavu
Angamaly-683 572, Kerala, India



REFERENCES

Dr. K.T. Mathew
Professor Emeritus
Department of Electronics
Cochin University of Science and Technology, Cochin-22, India.
Email: ktm@cusat.ac.in, Ph. +91-484-2576418, Fax: +91-484-2575800

Dr. K. Vasudevan
Professor & Head
Department of Electronics
Cochin University of Science and Technology, Cochin-22, India.
Email: vasudevan@cusat.ac.in, Ph. +91-484-2576418, Fax: +91-484-2575800

Dr. C.K. Anandan
Reader
Department of Electronics
Cochin University of Science and Technology, Cochin-22, India.
Email: anand@cusat.ac.in, Ph. +91-484-2576418, Fax: +91-484-2575800